

# **Micromechanical Analysis of Sheared Granular Materials Using the Discrete Element Method**

Dissertation

Zur Erlangung des Doktorgrades der Naturwissenschaften (Dr. rer. nat.)

Im Fachbereich der Geowissenschaften  
der Universität Bremen

vorgelegt von

Lutz Torbahn

Bremen,

September 2013

1. Gutachter: Frau Prof. Dr. Katrin Huhn
2. Gutachter: Herr Prof. Dr. Tobias Mörz

Datum des Kolloquiums: 05.12.2013



## Preface

This PhD thesis was written at the Department of Geosciences at the University of Bremen in Germany and funded through 'MARUM - Center for Marine Environmental Sciences'. The work was undertaken from May 2009 to September 2013. The data analyzed in this thesis were produced by the author through the application of numerical Discrete Element simulations. Based on this approach, different methods of analyzing the microfabric of granular materials were applied and developed.

This thesis contains five chapters including three research papers that improve the understanding of the effect of the microfabric on the shear strength of granular matter. The introduction gives a general overview of granular matter and its relevance in nature and industry. After that, the focus is on the empirical concepts of friction, strength, and failure as controlling factors for the granular stability. This is followed by a description of the typical physical and mechanical properties of granular matter, such as the composition, the grain size and shape, and the packing and porosity. The introduction also includes a description of the motivation and the main objectives of this research and provides general open scientific questions that will be addressed in the subsequent chapters. The first chapter closes with a detailed description of the different types of model setups and lists all relevant numerical methods applied in this research.

The body of the thesis is represented by three manuscripts (Chapters 2 - 4). Each of them focuses on the coefficient of friction whose behavior is equivalent to the bulk shear stress according to the Mohr-Coulomb criterion. Within the first study, the influence of the model dimensionality, 2D vs. 3D, on shear behavior was investigated. The focus of the second study was the contact formation and evolution of complex particle shape arrangements. Therein, the microfabric of three different basic particle shapes was compared. The third study was designed to examine pore volume changes caused by grain shape variation. The final chapter of the thesis synthesizes the main conclusions from the three manuscripts and presents some future perspectives.

## Table of Contents

Preface .....	2
Table of contents .....	3
Abbreviations .....	5
Abstract .....	6
Kurzfassung.....	8
1 Chapter One Introduction.....	12
1.1 Submarine landslides and slope failure .....	13
1.2 Theory of Friction, Strength and Failure .....	15
1.2.1 Friction .....	15
1.2.2 Strength .....	16
1.2.3 Failure.....	18
1.3 Granular material and sediments.....	19
1.3.1 Sediment composition .....	21
1.3.2 Grain size and shape.....	21
1.3.3 Packing and porosity .....	23
1.3.4 Microfabric .....	24
1.4 Motivation and objectives of this study .....	29
1.5 Methods.....	31
1.5.1 Model setup .....	31
1.5.2 Analyzing methods .....	32
2 Chapter Two .....	40
2.1 Introduction.....	41
2.2 Method .....	42
2.2.1 Discrete Element Method .....	42
2.2.2 Model generation .....	44
2.2.3 Measurement techniques .....	46
2.3 Results .....	47
2.3.1 Overall sample analysis.....	47
2.3.2 Effect of the shear zone localization .....	50
2.4 Discussion .....	51
2.4.1 General .....	51
2.4.2 Measured material properties as a function of dimensionality 2D vs. 3D .....	52
2.4.3 Shear band localization and shear band thickness as a function of dimensionality 2D vs. 3D.....	53

---

2.4.4	Effects of model size or particle number on deformation behavior of granular materials $3D_{\text{small}}$ vs. $3D_{\text{tall}}$ .....	54
2.5	Conclusion.....	55
	Acknowledgements.....	56
3	Chapter Three.....	60
3.1	Introduction.....	60
3.2	Method .....	61
3.3	Results .....	63
3.4	Discussion .....	64
3.5	Conclusion.....	66
	Acknowledgements.....	66
4	Chapter Four.....	70
4.1	Introduction.....	70
4.2	Method .....	71
4.3	Results .....	74
4.4	Discussion .....	76
4.4.1	Interplay: sediment strength and pore volume changes .....	76
4.4.2	Local pore volume changes.....	77
4.5	Conclusion.....	77
	Acknowledgements.....	78
5	Chapter Five Summary .....	80
5.1	Concluding remarks and perspectives.....	80
5.1.1	Conclusions .....	80
5.1.2	Perspectives .....	82
	Danksagung .....	90
	Erklärung .....	95

## Abbreviations

**Table 0-1: Used Abbreviations**

DEM	Discrete Element Method
MC	Measurement circle/ sphere
$F_N$	Normal force
$F_S$	Shear force
R	Radius
$V_S$	Shear velocity
$\sigma_N$	Normal stress
$\sigma_N'$	Effective normal stress
$\tau$	Shear stress
$\tau'$	Effective shear stress
$\tau_{max}$	Shear strength
$\mu$	Coefficient of internal friction
$\mu_{(P)}$	Particle coefficient of friction
$\mu_{peak}$	Peak coefficient of friction
$\mu_{crit}$	Coefficient of friction at critical state
c	Cohesion
$c'$	Effective Cohesion
$\phi$	Friction angle/ slope angle
$\sigma_1$	Largest principal stress
$\sigma_3$	Lowest principal stress
$\varepsilon$	Strain
$k_N$	Normal particle stiffness
$k_S$	Shear particle stiffness
D	Bulk density
e	Void ratio
$\eta$	Porosity
$N_C$	Number of contacts
$C_N$	Coordination number
$V_C$	Volume of particle overlapping
$V_P$	Particle Volume
$N_P$	Number of particles
$d_P$	Particle displacement vector
$d_{50\%}$	Mean particle diameter
EE	Edge-to-edge particle contact
EF	Edge-to-face particle contact
FF	Face-to-face particle contact
$V^{meas}$	Volume of measurement circle (2D)/ sphere (3D)
$V^{void}$	Volume of voids/ pore space
$V^{mat}$	Volume of particle s
p	Pore pressure

## Abstract

The significance of deformation processes within granular matter is known. This is particularly the case with respect to the micromechanics and the associated processes of shear zones, and especially basal shear zones, which occur at submarine landslides. In order to describe the shear zone processes, the knowledge of the material shear strength is important. The current understanding is that the shear strength and the failure plane localization depend on multiple properties. The relevant properties are microfabric with structure and texture, changes in effective pore pressure, and mineral composition. It is a fact that shear strength is influenced by these factors and, as a part of this research; some of these characteristics are analyzed.

For the purpose of measuring the mechanical strength of different materials, the approach of material destruction is used meaning that the experiment is run until the internal material structure is destroyed. For granular matter, such as sediment samples and fault gouges, geotechnical shear experiments are generally used. With that, the samples are prepared by loading and further deformed by shearing. The material strength is ensured as long as the outer applied forces do not exceed the internal deformation resistance of the material. During the shear experiments, many important material parameters can be determined, such as friction coefficient or porosity.

For the investigation of the micromechanics during shearing, however, geotechnical laboratory experiments are limited. Measuring the behavior of individual grains during the shear process is difficult because most particles hide inside the sample or they are too small to detect by sensors. Hence, for this study traditional geotechnical apparatuses were not applied. Here, investigation of the micromechanics was undertaken using the Discrete Element Method (DEM). This numerical approach allows for investigations of granular matter during the shear deformation in a microscale. It is based on simple physical contact and motion laws that allow for the definition of individual grain behavior that result in the complex bulk behavior. In recent years, this numerical approach has been frequently applied to simulate granular processes in multiple scales.

In this study, the DEM was used to construct several numerical shear experiments that are derived from geotechnical ring shear and direct shear experiments. The ring shear test uses two rings on top of each other filled with the sample. For shearing both rings rotate against one another to apply the shear movement. The advantage of such an approach lies in the large strain, which can be conducted. In contrast, the advantage of the direct shear test lies in the very simple construction to apply the shear deformation. It is a six sided box where the upper part can moved relative to the lower part. Samples of the direct shear test varied based on the grain shape. Thus, many different microfabrics were investigated with the numerical experiments. With detailed microfabric information, contact topology, contact size and type, and the illustration of the associated pore volumes can be derived. Furthermore, additional features, such as the particle motion, the coefficient of friction, and sample dilation were investigated.

A few features influencing the deformation behavior were investigated in this study. For that reason, the manuscripts were focused on the following aspects:

1. dimensionality – the particle dimension (2D, 3D) seems to have an influence on the deformation behavior and geotechnical experiments show at least an effect on the physical properties of spherical, disc, and rod-like particles; and
2. grain shape – according to geotechnical experiments, the grain shape significantly affects the deformation behavior and they essentially influence the microfabric. Two individual studies investigate:

- a. the effect on the contact behavior of interacting grains which is not possible in laboratory investigations; and
- b. the development of pore volumes in – laboratory measurements show that pore water saturated samples strongly react to pore volume changes, which cause a variation in the pore pressure behavior. It is generally known that transient pore pressure variation significantly affects the stability, and hence, the deformation behavior of granular matter.

In Chapter 2, different deformation behaviors between 2D and 3D ring shear models were determined. It has been shown that significant variations occurred regarding the physical parameters, such as friction coefficient, porosity, and shear zone geometry. In the 3D experiments the peak coefficient of friction and the porosity showed larger values. Furthermore, differences in the dimension are transferrable to the failure plane localization. In the 2D simulation, the failure plane mostly developed at the fixed wall, whereas in the 3D simulations, the failure plane often developed at the moved wall.

In the following chapter (Chapter 3), direct shear tests were applied to analyze the impact of particle shape on the contact evolution during the shear process. While shearing the samples, changes in the microfabric are reflected by the changes in the contact configuration where point contacts are transformed into edge contacts and edge contacts into face contacts. The analyses of contacts point out that even the microfabric of rod-like and plate-like grains predominantly consists of simple point contacts, whereas the edge and face contacts played only a minor role in frequency. In contrast to the rod-like shapes the plate-like shapes offer additionally an increase in the face contacts. This transformation leads to similar alignment of particles up to parallel alignment and, hence, reflects changes to the microfabric.

In Chapter 4, the consequences of grain shape variation regarding the pore volume development is demonstrated. The stronger the deviations from an ideal spherical shape, the larger were the evolving pore volumes. The microfabric, and hence, the arrangement of particles to one another is destroyed during the shear process and exhibited a decrease in pore volumes, simultaneously, based on the stronger particle densification, an increase in the friction coefficient. Hence, a densification and stabilization of the microfabric of rod-like and plate-like particles occurred.

The main aim of this research was to investigate the micromechanics of sheared granular materials. It was shown that aspects of dimensionality, contact behavior, and pore volumes highlighted the importance of an improved understanding of the microfabric. This research is significant because past studies were limited in determining such grain scale details due to laboratory limitations and applicable numerical analyzing methods. In the context of this research, several possibilities for further research on microfabric were identified: complex flocculated and dispersed particle associations, development of transient pore pressure during the collapse of the microfabric, a cyclic loading of different microfabrics, composites of particle shapes within the sample, and observing the strain behavior complex particle shapes during large deformation.



## Kurzfassung

Die Bedeutung von Deformationsprozessen innerhalb granularer Materialien ist weitreichend bekannt. Dies gilt vor allem für die mikromechanische Betrachtung der damit verbundenen Prozesse von Störungszonen und besonders basalen Störungszonen, die an submarinen Hangrutschungen auftreten. Als ein wichtiger Bestandteil zur Beschreibung der Vorgänge innerhalb von Störungszonen wird die Scherfestigkeit des Materials angesehen. Bisher ist bekannt, dass die Scherfestigkeit sowie die örtliche Bestimmung von Scherflächen durch eine Vielzahl von Faktoren beeinflusst werden. Zu den wichtigsten Faktoren zählen das Mikrogefüge mit entsprechender Struktur und Textur, Veränderungen im effektiven Porendruck und die mineralogische Zusammensetzung. Der Einfluss auf die Scherfestigkeit durch diese Faktoren ist bekannt und wird als Teil dieser Arbeit weiter vertieft.

Ein etablierter Ansatz zur Messung der mechanischen Festigkeit von unterschiedlichen Materialien bieten Experimente die das Verhalten bis zur Zerstörung der inneren Materialstruktur untersuchen. Bei granularem Material wie Sedimentproben und Störungsletten verwendet man in der Regel geotechnische Scherexperimente. Generell werden dazu die Proben eingespannt und durch Scherung deformiert. Die Festigkeit des Materials ist dabei solange gewährleistet wie der äußere Kräfteinfluss geringer ist als der interne Materialwiderstand. Durch die Scher-Experimente lassen sich viele wichtige Materialkenngrößen wie zum Beispiel Reibungskoeffizienten und Porosität bestimmen.

Für die Untersuchung der Mikromechanik bei fortlaufender Verscherung lassen sich die geotechnischen Labor-Scherversuche nur begrenzt einsetzen. In der Regel ist es nicht möglich das Verhalten einzelner Sedimentkörner innerhalb der Probe während des Scherprozesses zu ermitteln, weil sich die Körner im inneren der Probe der Beobachtung durch Sensoren entziehen oder diese zu klein sind um durch Sensoren wahrgenommen zu werden. Daher wurde in dieser Studie auf die Anwendung von geotechnischen Apparaturen verzichtet. Eine weitere Möglichkeit mikromechanische Untersuchungen vorzunehmen bietet die Methode der Diskreten Elemente (DEM). Es handelt sich dabei um einen numerischen Ansatz der es ermöglicht eine Analyse im Kornmaßstab durchzuführen. Dabei basiert diese Methode auf einfachen physikalischen Kontakt- und Bewegungsgesetzen und erlaubt die Festlegung von einfachem Verhalten einzelner Körner welches hin zu komplexen Verhalten einer großen Masse führt. In den letzten Jahren diese Methode wurde häufig für die Simulation von granularen Prozessen in unterschiedlich großen Maßstäben eingesetzt.

In dieser Arbeit wurde durch Verwendung der DEM mehrere numerische Scherzellen konstruiert die den geotechnischen Ringscher- oder Direktscher-Apparaten im Labor nachempfunden wurden. Ringscherversuche verwenden zwei übereinander angeordnete Ringe die mit einer Probe gefüllt werden. Für die Verscherung werden beide Ringe gegeneinander rotiert. Der Vorteil einer solchen Apparatur liegt in den großen Verformungen, die damit durchgeführt werden können. Im Gegensatz dazu liegt der große Vorteil der direkten Scherversuche in deren Einfachheit im Aufbau. Es handelt sich dabei um eine sechs-seitige Box deren oberer Teil sich gegenüber dem unteren Teil verschieben lässt. In den direkten Scherversuchen wurden die Proben in ihrer Kornform variiert. Daraus resultiert eine Vielzahl unterschiedlicher Gefügeformen die im Verlauf der numerischen Experimente untersucht wurden. Eine detaillierte Beschreibung des Mikrogefüges wurde durch die Verwendung der Partikel-Nachbarschaftsbeziehungen, Kontaktgröße bzw. Kontaktarten, und der Darstellung dazugehöriger Porenräume erreicht. Neben dem Mikrogefüge wurden weitere mikromechanische Parameter wie zum Beispiel die Bewegungen der Partikel analysiert. Ebenfalls wurden auch typische geotechnische Parameter wie etwa Reibungskoeffizient und Volumenausdehnung der Probe untersucht.

Folgende Auswahl an Faktoren die das Deformationsverhalten beeinflussen konnten in dieser Studie untersucht werden. Daher liegt der Fokus der Manuskripte auf den folgenden Aspekten:

1. Dimension: Die Dimension der Partikel scheint einen Einfluss auf die Deformation zu haben. Geotechnische Untersuchungen von 2D und 3D legen einen starken Einfluss auf die physikalischen Parameter von Kugeln, Scheiben und Stäbchenförmigen Partikeln nahe.
2. Kornform: Entsprechend von geotechnischen Experimenten hat die Kornform einen erheblichen Einfluss auf das Deformationsverhalten, in dem sie maßgeblich den Aufbau des Mikrogefüges mitbestimmt. In den zwei Studien wird:
  - a. die Auswirkung auf das Kontaktverhalten untersucht, da es in Laboruntersuchungen während der Verscherung nicht möglich ist die Kontaktinformation an interagierenden Körnern zu analysieren und
  - b. die Untersuchung von Porenräumen zeigen im Labor, dass mit Porenwasser gesättigte Proben stark auf Porenraumänderungen reagieren. Diese Änderungen führen zu Porendruckänderungen. Bekanntlich haben sich schnell ändernde Porendrücke einen großen Einfluss auf die Stabilität und somit auf das Deformationsverhalten von granularen Materialien.

In Kapitel 2 konnte ein unterschiedliches Deformationsverhalten zwischen den 2D und den 3D Ringscher-Modellen ermittelt werden. Deutliche Unterschiede wurden in den physikalischen Parametern des Reibungskoeffizienten, der Porosität und der Scherzonengeometrie während der Verscherung beobachtet. So zeigt der Spitzenwert des Reibungskoeffizienten für 3D Simulationen höhere Werte an. Auch für die Entwicklung der Porositäten werden in den 3D Versuchen generell höhere Werte beobachtet. Dieser Unterschied zwischen den Dimensionen führt sich fort bei der Lokalisation der Scherflächen. Bei den 2D Modellen entsteht die Scherzone immer an der festen Wand während in den 3D Modellen die Scherzone meistens an der bewegten Wand herausgebildet wird.

Im darauf folgenden Kapitel (Kapitel 3) wurden Direktscherversuche verwendet, um den Einfluss der Partikelkonform auf das Kontaktverhalten während der Verformung zu analysieren. Veränderungen des Mikrogefüges während der Verscherung werden durch die Veränderungen in den Kontaktkonfigurationen wiedergespiegelt, wobei Punktkontakte in Kantenkontakte und Kantenkontakte zu Flächenkontakten umgewandelt werden, welche eine Parallelisierung der plättchen-förmigen Partikel und somit eine Veränderung des Mikrogefüges zur Folge hat. Dabei zeigte sich, dass das Mikrogefüge auch von stäbchen- und plättchen-förmigen Partikeln hauptsächlich durch einfache Punktkontakte dominiert wird und Kanten- bzw. Flächenkontakte eine untergeordnete Rolle in der Häufigkeit spielen.

Im Kapitel 4 wird die Auswirkung der Kornformänderung auf das Porenvolumen aufgezeigt. Je mehr sich die Kornformen von den idealen runden ballförmigen Partikeln entfernen desto größer wird das Porenraumvolumen der Partikelmenge. Die Zerstörung des Mikrogefüges durch Verscherung und somit eine Änderung der Partikelanordnung zeigt eine Abnahme des Porenvolumens und gleichzeitig eine stärkere Verdichtung der Partikel, welche eine Zunahme des Reibungskoeffizienten bewirkt. Somit wurde eine Verdichtung und Stabilisierung des Mikrogefüges bei den komplexeren Kornformen während der Verscherung erreicht.

Das Hauptziel dieser Studie war die Untersuchung der Mikromechanik von granularen Materialien während der Verscherung. Der Einfluss der Dimensionalität, das Kontaktverhalten und das Verhalten des Porenvolumens führten zu einem verbesserten Verständnis in Bezug zur Rolle des Mikrogefüges gegenüber Deformationen. Diese Forschungsarbeit ist daher bedeutsam, weil vorige Studien viel stärker eingeschränkt waren in ihren labortechnischen Möglichkeiten und anwendbaren numerischen Analyse-Methoden. Verschiedene Möglichkeiten für eine weitere Untersuchung des Mikrogefüges wurden in dieser Studie aufgezeigt: komplexe geflockte und zerstreute Partikelanordnungen, schnelle Veränderungen von Porendrücken während des Zerfalls des Mikrogefüges, Mischungen von Partikelformen und Beobachtung des Verhaltens komplexer Kornformen während längerer Deformationen zählen dazu.



## 1 Chapter One Introduction

A system composed of a large number of solid entities, grains or particles is called granular matter [Ristow, 2000; Herrmann, 2002; Ausloos *et al.*, 2005]. Although sand is the most well-known and classical representative of a granular matter, many different natural types exist, e.g., dust powder, pebbles, and rocks [Ristow, 2000; Herrmann, 2002; Ausloos *et al.*, 2005]. Actually, granulates are ubiquitous in our life and there is almost no area where they do not occur. For instance, in the food industry we encounter them in a huge variety of products, e.g., salt, sugar, coffee (beans and powder), rice, or pasta. For the industrial application of granular matter, a wide field has developed, e.g., coal and ore mining, pills and granulates in pharmaceutical industries, high resistant ceramics, railroad ballast, and catalyzers and powders in chemical industries [Herrmann, 2002]. Another important field of application is in civil engineering and geophysics dealing with geological processes of granulates, such as erosion and large scale tectonics or the prediction of natural hazards, such as landslides, rock avalanches, or pyroclastic flows [Jaeger and Nagel, 1992; Jaeger *et al.*, 1996; Nicot *et al.*, 2005; Forterre and Pouliquen, 2008].

The nature of granular matter is extremely divers. Although we have an idea of some of the granular features, it is still not possible to anticipate accurately many of the phenomena associated with them (Figure 1-1). Scientific attention attracted granular matter due to its exceptional features, such as self-organizing, fragile, and non-homogeneous flow behavior, however, current theories are limited in some ideal states, such as quasi-static flow, rapid flow, and non-adhesion contact mechanics [Sun *et al.*, 2009]. A unique aspect of granular behavior is that it can exhibit phase behavior similar to solids, fluids, or gaseous materials [Jaeger *et al.*, 1996; Forterre and Pouliquen, 2008]. For a solid-like response, static or quasi-static conditions are necessary, whereas for fluid or dense gaseous behavior, granular flow or rapid granular flow is required [Campbell, 1990; Jaeger *et al.*, 1996; Forterre and Pouliquen, 2008]. Therefore, the driving factor for the specific granular behavior is the mechanical condition that influences the flow properties [Herrmann, 2002; Pouliquen and Chevoir, 2002; Forterre and Pouliquen, 2008]. A granular solid phase behavior is desirable for applications of storage such as in silos and granular piles [Jaeger *et al.*, 1996]. However, the convenience of the granular fluid phase lies in the moving features and is preferred for granular transport and processing, such as in agriculture and industry [Jaeger *et al.*, 1996]. Often the transition from solid to fluid phase and vice versa is intended and desired, but sometimes immediate and unwanted phase transitions can end in disaster. For example, unforeseen stress fluctuations of granulates in a silo can lead to a collapse of the silo [Ristow, 2000]. In another case, the sudden transition from the solid to the fluid phase on a granular slope leads to slope destabilization and, therewith, forms the basis for the initiation of dangerous landslides and rock avalanches [Jaeger and Nagel, 1992; Jaeger *et al.*, 1996]. This can happen, if for instance, the sand pile is inclined above a critical angle and starts to flow where the onset of the flow is given by a friction criterion [Jaeger and Nagel, 1992]. This macroscopic criterion is a result of the stress state and uses the ratio of shear stress to normal stress for frictional materials, which is simply the tangent of the slope [Jaeger and Nagel, 1992; Forterre and Pouliquen, 2008].

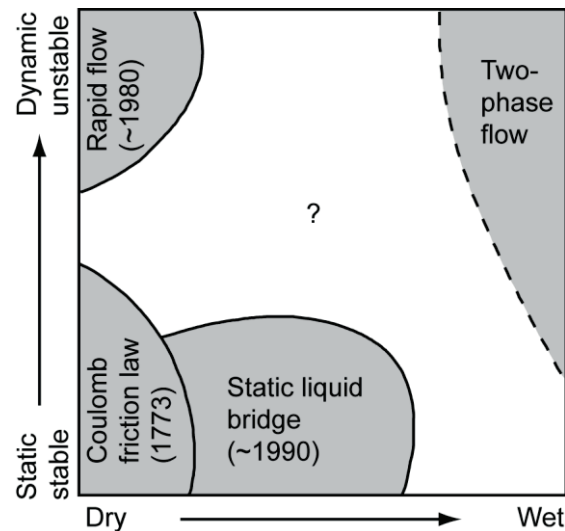


Figure 1-1: Present theories of granular matter [Sun et al., 2009].

On the basis of the stress state the two-faced micro-macro behavior of granulates is obvious. The macroscopic granular response including a large number of particles behaves as a continuum and can be described by the continuum mechanical approach, in which the macroscopic stress is the average stress of the participating particles, whereas the individual particles and their interaction in the microscopic scale can be described with the discrete mechanical approach, in which the stress is the result of the particle forces at sharing frictional contacts [Mitchell, 1976; Jaeger et al., 1996; Mitchell and Soga, 2005]. A relation between micromechanical behavior of discrete particles and the macroscopic granular response exist [e.g., Lambe and Whitman, 1969; Tessier et al., 1992; Mitchell and Soga, 2005; Andrade et al., 2011]. In that respect, the macroscopic mechanical behavior of granular matter is regulated primarily by their structure and the applied effective stresses [Mitchell and Soga, 2005]. Furthermore, the structure depends on the particle features, such as arrangement, density, anisotropy, and microfabric, whereas the microfabric comprises particle sizes, shapes, and distributions along with the arrangement of grain packings and grain contacts [Mitchell and Soga, 2005].

### 1.1 Submarine landslides and slope failure

With regard to submarine landslides, which occur as a consequence of slope failure [e.g., Hampton et al., 1996; Locat and Lee, 2002], the previous mentioned micro-macro relation of granular matter is relevant for investigation of landslide processes. On the macroscopic view, landslides are a downward movement, along a frictional failure plane, driven by gravitational forces [Hampton et al., 1996]. They often occur on inclined areas, such as on continental slopes (active and passive margins), fjords, active river deltas, oceanic volcanic islands and ridges [e.g., Hampton et al., 1978; Farrow et al., 1983; Moore et al., 1994; Watts and Masson, 1995; Hampton et al., 1996; Urgeles et al., 1997; Masson et al., 1998; Urgeles et al., 1999; McAdoo et al., 2000; Locat and Lee, 2002; Hafliðason et al., 2004; Kvalstad et al., 2005; Strozyk et al., 2009]. From the microscopic perspective, the submarine slope material and failure plane is composed of a granular sediment matrix that is influenced by the frictional behavior at the grain contacts and the pore pressure, which build up by the fluid-filled pore space [e.g., Goren et al., 2010].

Nearly always the gravitational force is not sufficient to initiate a landslide [Hampton *et al.*, 1996]. However, a large number of submarine landslides exist whose occurrence is related to additional factors, known as trigger mechanisms, which influence the slope stability. In the last decades, many potential landslide trigger-mechanisms were identified (Figure 1-2), e.g., oversteepening, seismic loading, rapid sediment accumulation, gas charging, depositional loading, sea-level fluctuation, tectonics, and gas-hydrate dissociation, which have since been assigned to a variety of past landslide events [e.g., Morgenstern, 1967; Hampton *et al.*, 1996; Laberg and Vorren, 2000; Locat and Lee, 2002; Canals *et al.*, 2004; McAdoo *et al.*, 2004; Sultan *et al.*, 2004; Fine *et al.*, 2005; Mienert, 2005; Masson *et al.*, 2006; Strozyk *et al.*, 2009; Mienert *et al.*, 2010]. Most of the trigger-mechanisms have in common that they affected the sediment strength either by exceeding the frictional strength or by transient pore pressure variations [e.g., Hampton *et al.*, 1996; Locat and Lee, 2002]. A buildup of pore pressure in fine-grained sediment, which is caused by loading, can partially support the weight of grains, and therefore, decreases the frictional resistance at grain contacts that in turn decreases the sediment strength [Hampton *et al.*, 1996].

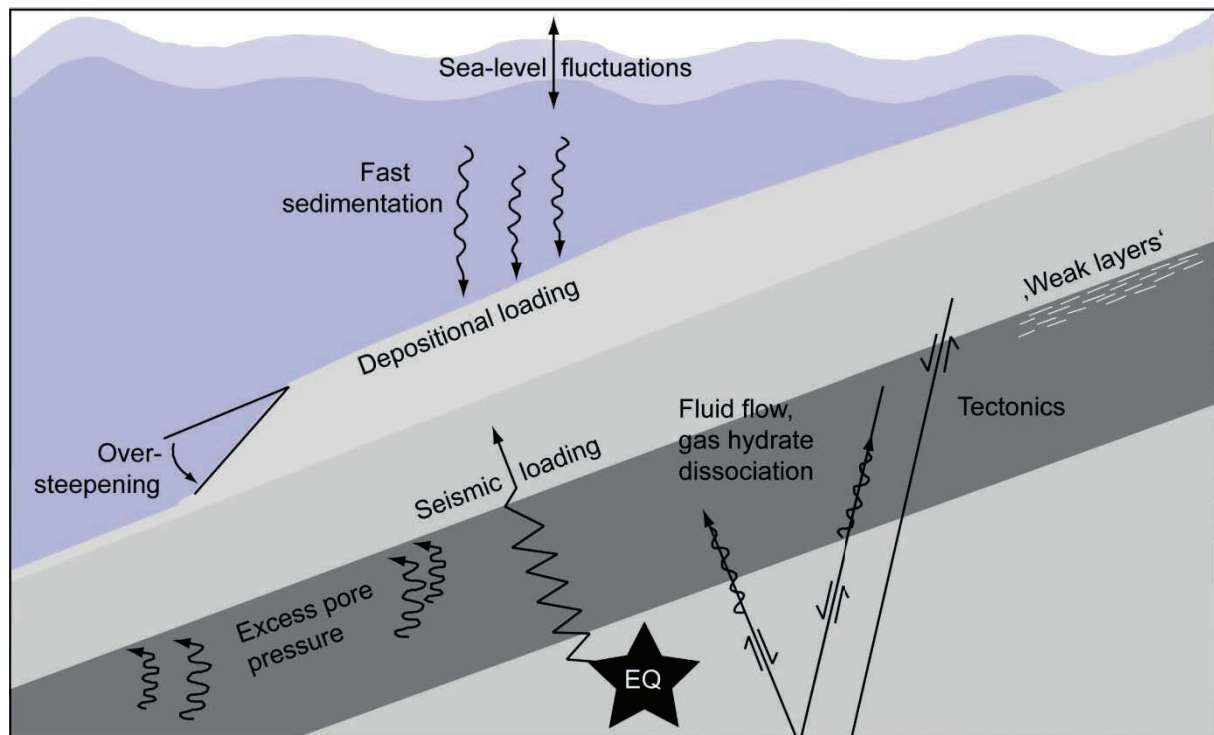


Figure 1-2: Schematic interaction of trigger mechanisms for submarine landslides [modified from Strozyk, 2009].

Often, slope failure occurs in areas in which the sediment strength is reduced compared to the surrounding material. In the literature, such areas are described as 'weak layers' [e.g., Trincardi *et al.*, 2004; Masson *et al.*, 2006]. Weak layers can be attributable to regional changes in sedimentation style caused by climatic changes of glacial and interglacial conditions [Bryn, 2005] and changes in mineral composition and texture [e.g., Marone, 1998; Kopf and Brown, 2003; Saffer and Marone, 2003; Ask and Kopf, 2004; Huhn *et al.*, 2006]. However, the fundamental failure behavior of the interplay between weak layers and potential trigger events is not yet fully understood. In particular, many questions about the micromechanical processes within the weak layer microfabric still remain unanswered. In recent years, properties that affected the microfabric, e.g., sediment composition, packing, grain size, and grain shape were investigated in laboratory [Frye and Marone, 2002; Mair *et al.*, 2002].

*al.*, 2002; *Saffer and Marone*, 2003; *Anthony and Marone*, 2005] and in numerical DEM simulations [*Jensen et al.*, 1999; *Abe et al.*, 2002; *Guo and Morgan*, 2004; *Huhn et al.*, 2006; *Kock and Huhn*, 2007a; b; *Abe and Mair*, 2009; *Schöpfer et al.*, 2009; *Szarf et al.*, 2011]. A crucial parameter for material strength, and hence, for slope failure that is also controlled by the microfabric is the material friction [*Mitchell and Soga*, 2005].

## 1.2 Theory of Friction, Strength and Failure

### 1.2.1 Friction

Friction is a term that describes the resistance to sliding if two bodies move relative to each other at jointed contacts, the resistance to volume change (dilatancy), grain rearrangement, and grain crushing [e.g., *Beeler et al.*, 1996; *Lockner and Beeler*, 2002; *Gao et al.*, 2004; *Mitchell and Soga*, 2005]. That means, the exceedance of the shear resistance is required to cause a relative movement between solid bodies [*Lambe and Whitman*, 1969; *Hazzard and Mair*, 2003]. According to Gao et al. [2004], two basic empirical relationships regarding friction were first observed by Leonardo da Vinci (~1500) and Amonton [1699]. First, the shear resistance is proportional to the normal force  $\sigma_N$  between two bodies, and second, the shear resistance is independent of the dimensions of the two bodies.

Consequently, macroscopic sliding motion of a brick along a wall (Figure 1-3) has the same features as the sliding motion of minerals at microscopic grain to grain contacts [e.g., *Lambe and Whitman*, 1969; *Smith*, 1998; *Mitchell and Soga*, 2005].

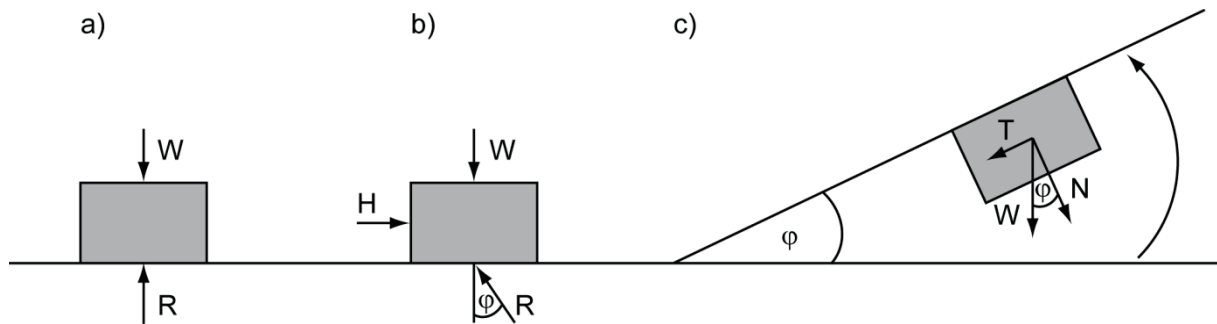


**Figure 1-3: Derivation of frictional is derived from the stress states of normal and shear stresses [modified from Smith, 1998].**

A geometrical derivation of the frictional resistance (Figure 1-3) is given by Smith [1998]. If a block of weight  $W$  rests on a horizontal plane (Figure 1-3a), then the vertical reaction  $R$  is equal to  $W$ , and consequently, the block is not moving. Moreover, if a horizontal force  $H$  is added to the block (Figure 1-3b) and the magnitude of  $H$  is large enough, so that the block is starting to move, then the reaction  $R$  is no longer vertical aligned but become an inclined angle  $\phi$  to the vertical. Furthermore, if the horizontal plane is inclined (Figure 1-3c) until the block begins to move, and then the inclined angle is also equal to  $\phi$ . This angle  $\phi$  is described as the friction angle and can be calculated by:

$$\tan \phi = \frac{H}{W} = \frac{R \sin(\phi)}{R \cos(\phi)} = \frac{T \sin(\phi)}{N \cos(\phi)} = \frac{\tau}{\sigma_N} = \mu \quad (\text{Eq. 1-1})$$

$T$  is the force parallel to the inclined angle,  $N$  is the normal and perpendicular aligned, and  $\mu$  is the coefficient of friction that is derived from the stress components of shear stress  $\tau$  and normal stress  $\sigma_N$ . Both parameters  $\mu$  and  $\phi$  can be used to describe the frictional resistance.



Friction is also considered as an inner force inside bodies acting contrary to the externally applied forces, and thus, against the interior body deformation [Mitchell and Soga, 2005]. In this case, the deformation of a body, such as a sediment packing, consists of an assembly of single sediment grains and is defined by the mean frictional behavior of the single grains [Mitchell and Soga, 2005].

### 1.2.2 Strength

All aspects of granular stability and slope stability depend on the strength of the granular matter [Mitchell and Soga, 2005]. The shear strength is defined by the maximum shear stress  $\tau_{max}$  that a material is able to sustain before failure occurs [e.g., Lambe and Whitman, 1969; Smith, 1998; Mitchell and Soga, 2005; Atkinson, 2007]. The Mohr-Coulomb criterion describes the dependency of shear strength on the friction coefficient, the normal stress, and the cohesion [Handin, 1969; Heyman, 1972; Smith, 1998; Atkinson, 2007]:

$$\tau_{max} = \mu \sigma_N + c \quad (\text{Eq. 1-2})$$

For cohesionless materials a similarity to Eq. 1-1 cannot be hidden. In cohesive materials a cohesive strength can be observed even if the normal stress tends to zero [Mitchell, 1976; Mitchell and Soga, 2005].

For a saturated granular material filled with a fluid the shear strength is dependent on the effective and not on the total stress [Terzaghi, 1925]. Thereby, the pore fluid pressure counteracts the total stress. As a result the effective stress  $\sigma'_N$  is the total stress reduced by the pore pressure  $p$ :

$$\sigma'_N = \sigma_N - p \quad (\text{Eq. 1-3})$$

$$\tau_{max} = \mu \sigma'_N + c' \quad (\text{Eq. 1-4})$$

This implies that the total stress and cohesion is replaced with the effective stress and the effective cohesion  $c'$  [Terzaghi, 1925].

A shear strength calculation of a granular sample is generally achieved via deformation tests. Therefore, geotechnical shear devices are used to deform the sample and to obtain the stresses. Commonly applied are the direct shear device and the ring shear device. A simple setup offer the direct shear test that consists of a box filled with the sample, whereas the upper box part is able to move relative to the lower part in order to deform the sample. However, the ring shear test (Figure 1-4a) uses two cylindrical walls, whereas one can rotate. With a ring shear device large sample strain can be achieved. Figure 1-4b schematically shows the deformation pattern of a passive strain marker according to typical ring shear deformation [Schulze, 2009].

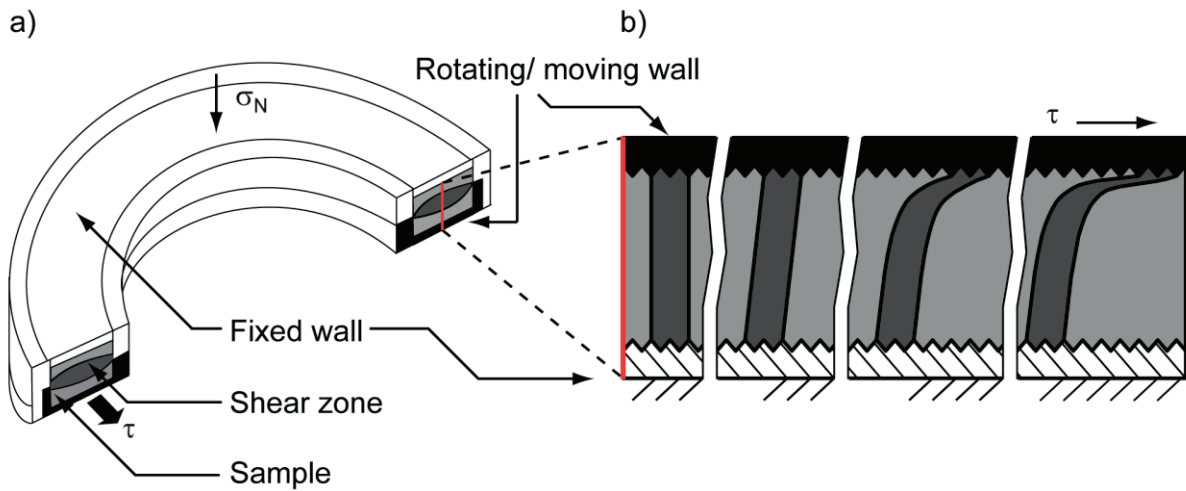


Figure 1-4: a) Schematic ring shear device [modified from Iverson *et al.*, 2010] and b) a simplified slice through the sample [modified from Schulze, 2009]. The shear deformation is indicated by the dark grey passive marker.

An exemplary log of stresses versus strain is illustrated for dense and loose granular matter with corresponding volume strain (Figure 1-5). The differently packed material shows different typical stress response for densely (representative of a solid state) and loosely (representative of a fluid state) packed material [Herrmann, 2002]. At the initial shear deformation the loose and dense packed matter is hardened indicated by the negative volume strain and an increase in the shear stresses. Then, the loose granular matter achieved the peak state that is also the critical state and represents the material strength. Differently behaves the dense granular matter that also achieves the peak state with the material strength, with appearing of incipient Riedel shears [Tchalenko, 1970; Marone, 1998], and then the stresses reduces and material softening occurs accompanied by dilative volume strain and ended in the critical state. The basic concept of critical state is that under sustained uniform shearing at failure, a unique combination of porosity mean pressure and deviator stress exist [Mitchell and Soga, 2005].

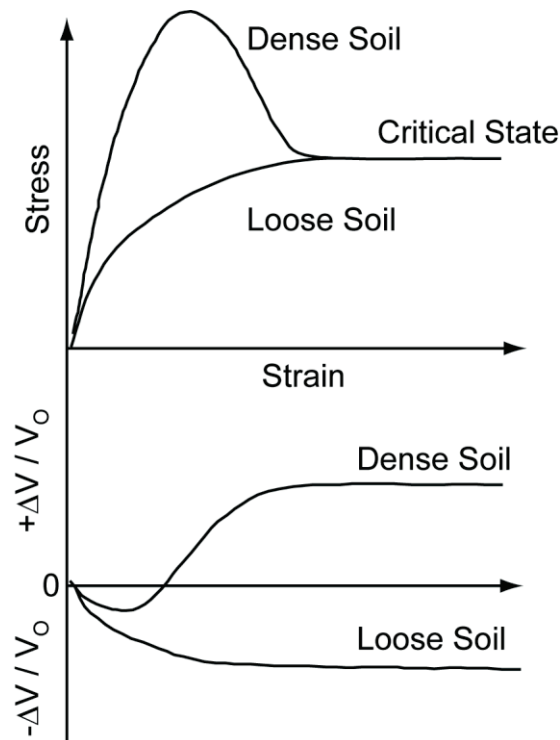


Figure 1-5: Stress-strain behavior and volumetric strain of dense and loose soils [Mitchell and Soga, 2005].

### 1.2.3 Failure

In the previous section the shear strength is described by the Mohr-Coulomb failure criterion (Eq. 1-2) and indicates the maximum shear stress a material can sustain. Alternatively, the same criterion can be applied to calculate the shear stress that leads to material failure [e.g., Handin, 1969; Lambe and Whitman, 1969; Heyman, 1972; Smith, 1998; Mitchell and Soga, 2005]. For engineering problems this failure criterion has successfully and widely applied for soil and rock mechanics of the shallow crust [Handin, 1969].

A geometrical and simple approach to solve a failure problem is the Mohr-Coulomb envelope (Figure 1-6). The envelope is defined by the material strength at several normal stresses [Smith, 1998; Atkinson, 2007]. In the simplest case the envelope is linear and for cohesionless material it crosses the diagram origin [Handin, 1969]. Moreover, the slope of the Mohr envelope is represented by the coefficient of friction. The basic ideas of the Mohr envelope is as follows [Lambe and Whitman, 1969; Smith, 1998]:

- A) if the Mohr circle is located completely within the envelopes, then the material state will be stable;
- B) if the Mohr circle is tangent to the Mohr envelope, then full strength is achieved and incipient failure will occur; and
- C) for a granular material, it is impossible to archive a stress state where the Mohr circle intersects the envelope.

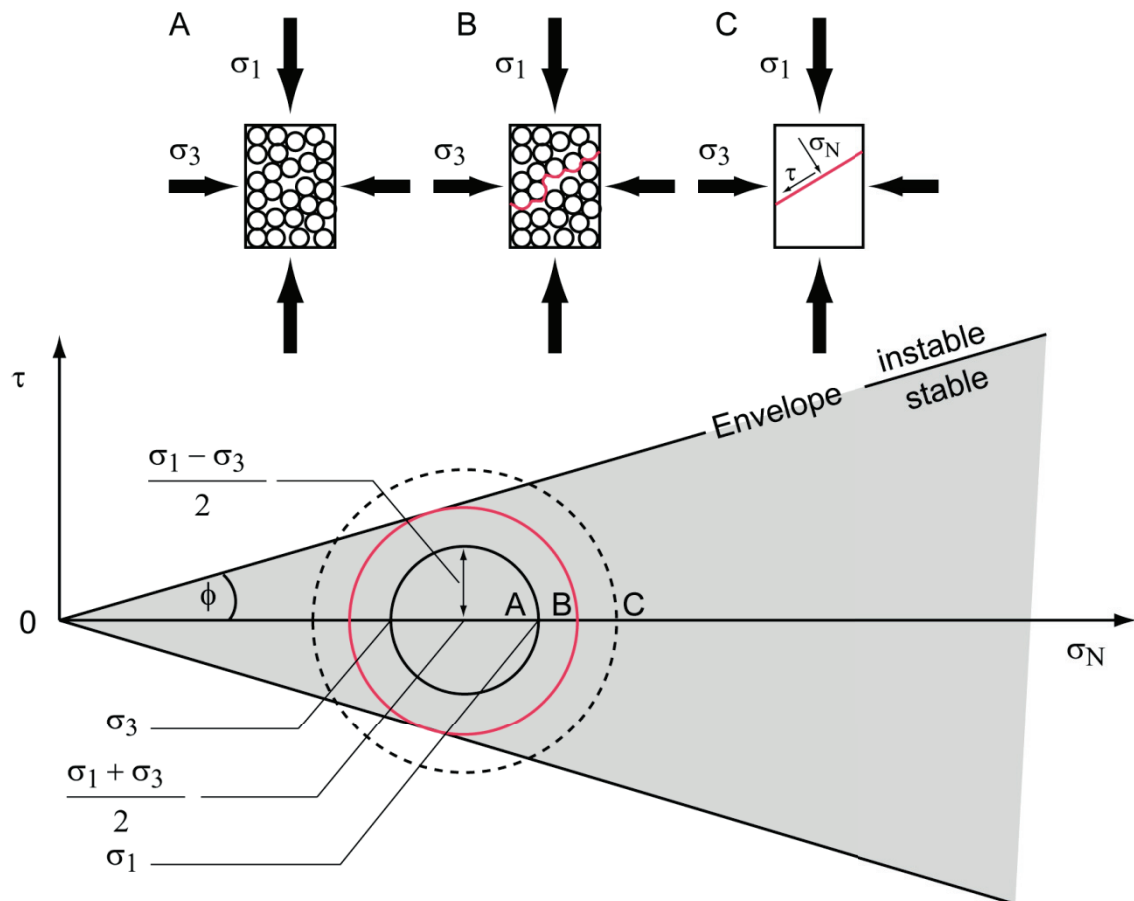
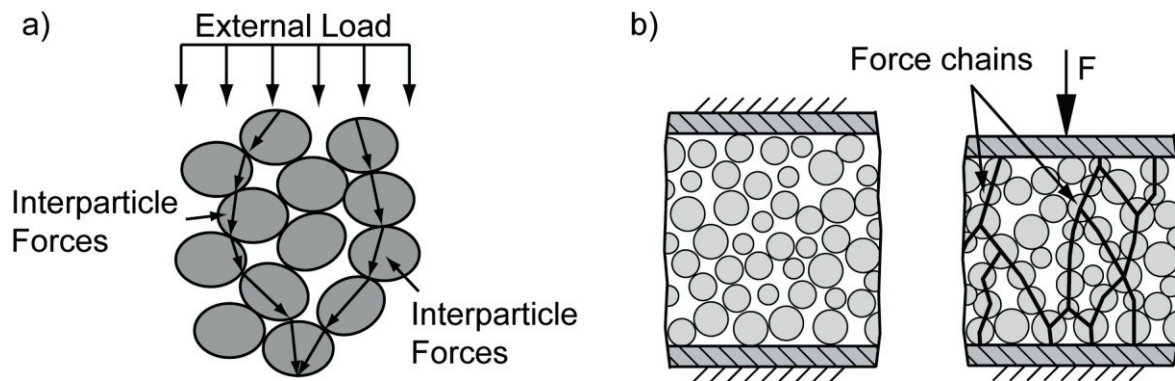


Figure 1-6: Illustration of the Mohr-Coulomb envelope for cohesionless material. A Material is stable B material is critical when the Mohr-circle touches the envelope and C material is unstable (impossible for granular matter) [modified after *Smith, 1998*] The external load is applied by the principal stresses termed as  $\sigma_1$  and  $\sigma_3$ .

### 1.3 Granular material and sediments

Granular material refers to a large range of macroscopic particles subject to the classical laws of mechanics [*Herrmann, 2002*]. Due to the fact that single particles act as distinct grains, the particle assembly behaves like a continuum [*Jaeger and Nagel, 1992; Jaeger et al., 1996; Nicot et al., 2005*]. Single particles represent solids whose surfaces may be shaped arbitrarily. The configuration of these irregularly formed particles leads to heterogeneous structures [*Pohlman et al., 2006*]. Particle size ranges from powders to rocks [*Ausloos et al., 2005*]. However, the behavior of all particles as a bulk material cannot exclusively be described by well-known physical laws for solids, fluids, and gases. Granular material can also behave like all of these physical aggregate states [*Jaeger et al., 1996*]. This is due to the large number of the degrees of freedom for a single grain as well as for granular aggregates leading to irreversible and high-grade nonlinear particle or aggregate interactions [*Mitchell and Soga, 2005*].

A typical volume element of granular material consists of many single particles in frictional contact with each other [*Roux and Combe, 2002*]. Each particle interaction, such as force transmission between particles, requires a direct contact [*Lambe and Whitman, 1969*]. Consequently, the transmission of forces only passed on by frictional and/or inelastic collisions (Figure 1-7a).



**Figure 1-7:** a) *Schematic illustration of external load transfer through particles in contact by interparticle forces [Mitchell and Soga, 2005].* b) *Forming of force chains applying an external load ( $F$ ) [modified from Schulze, 2009].*

While the hydrostatic pressure in a box filled with a fluid increases exponentially with depth, the mean pressure in a box filled with granular material is constant [Forterre and Pouliquen, 2008]. This phenomenon also describes the non-varying flow velocity of granular materials, such as sand in an hour glass, and shows the specific force transmission in a pile of sand which takes place at the grain contacts [Jaeger *et al.*, 1996]. In a densely packed granular material, these contacts form a network by building arc-shaped contact bridges that dissipate stresses (Figure 1-7b) [Schulze, 2009]. That also means that within a static densely packed granular packing, no homogenous or continuous stress distribution exists, but rather a complex contact network that distributes the stresses inside the granular system [Herrmann, 2002; Nicot *et al.*, 2005; Schulze, 2009]. Within this contact network, there are contacts that transmit a multiple of the mean stress as well as a fractional amount of the particle weight force [Kock and Huhn, 2007a]. This shows that the stress distribution inside a granular material is highly heterogeneous [Mitchell and Soga, 2005; Schulze, 2009].

In a dynamic system, where energy is externally supplied, granular material shows liquid properties and a so-called liquefaction of the granular material occurs [Jaeger *et al.*, 1996; Forterre and Pouliquen, 2008]. A previously stable slope can dissolve as a result of vibrations in the underground [Pöschel, 2000]. Well-known examples of dynamic granular systems are hour glasses or rock and snow avalanches. A typical dynamic effect is the dilatancy of granular materials. The dilatancy describes the behavior of granular material with a large packing density that have to change their volume in order to deform (Figure 1-8) [Schulze, 2009]. Hence, dense grain packages respond with loosening of the grain structure during deformation [Lambe and Whitman, 1969; Mitchell and Soga, 2005].

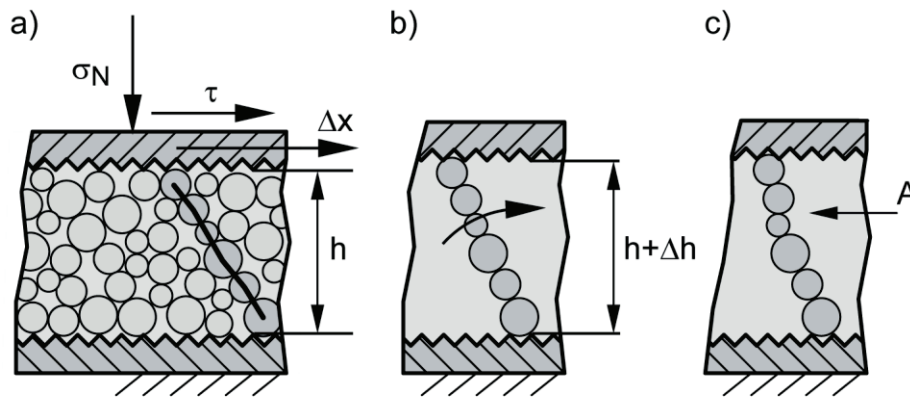


Figure 1-8: Principle of dilatancy [modified after Schulze, 2009]. a) The line of particles is not able to perform the shear movement. b) Through a sample extension of  $\Delta h$  the shear movement can be conducted. c) Thereby, the particle arrangement is changed at the point A.

### 1.3.1 Sediment composition

After Mitchell and Soga [2005], the study of sediment composition in relation to its sediment properties can be realized in two ways. First of all, natural sediments are used to analyze the sediment composition and the corresponding engineering properties. Applying this method, the measured properties are directly related to natural conditions. Otherwise, the compositional analysis is difficult and time-consuming, and in soils containing several minerals, the influence of one particular mineral is difficult to isolate.

In the second approach, the engineering properties of synthetic soils are investigated. It is the primary objective to prepare the sediment samples of known composition. This method is much easier to handle but it unfortunately has the side-effect that the properties of the pure minerals may not be the same as those of the natural sediments [Mitchell and Soga, 2005].

### 1.3.2 Grain size and shape

#### Grain size

One simple approach characterizing sediments is to classify them according to their grain sizes [e.g., Mitchell and Soga, 2005; Atkinson, 2007]. The grain size also gives an indication of how the sediment was formed during transport and deposition because a close relationship between the size and the acting stresses with respect to grains exist [e.g., Lambe and Whitman, 1969; Mitchell and Soga, 2005]. It is therefore possible to interpret from a single grain the transported medium, the distance, and the transport mechanism. A typical range of classification for sand to clay grain sizes is illustrated in Figure 1-9.

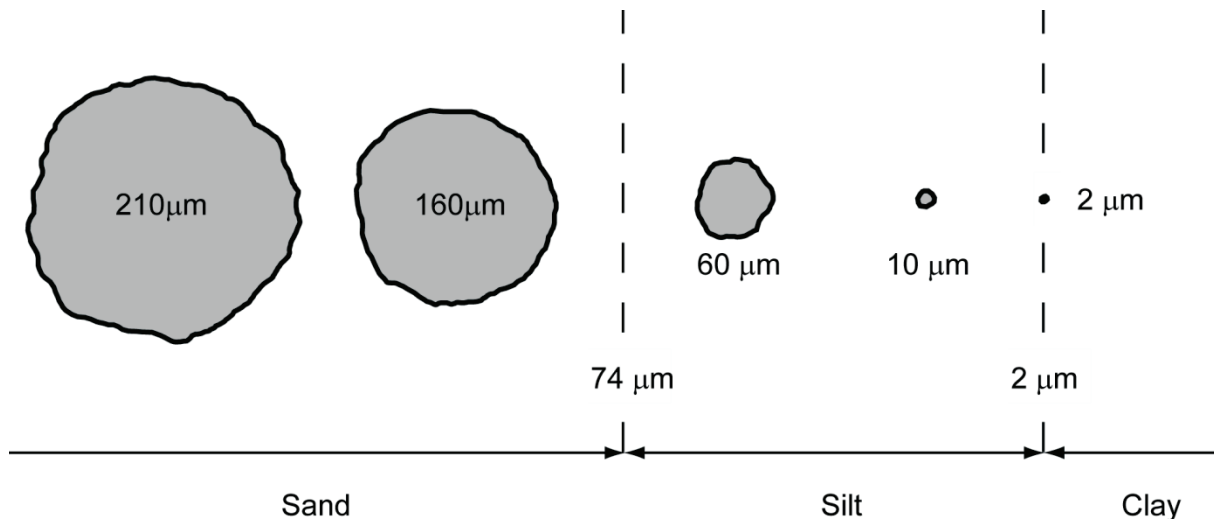


Figure 1-9: Different sediment grain sizes [modified after Mitchell and Soga, 2005].

### Grain size distribution

The grain size distribution is another factor that describes the granular microfabric. Similar to the grain size, the distribution of grain sizes provide additional information about the history of sediment transport and the sediment behavior during the deformation [Mitchell and Soga, 2005]. Furthermore, the grain size distribution significantly contributes to the stress distribution within a granular packing [Mitchell and Soga, 2005]. Moreover, the grain size distribution is an indicator for the grade of particle sorting. If the sediment consists only of one dominant grain size then it is well-sorted. In contrast, a mixture of more grain sizes is typical for poorly-sorted sediments [Mitchell and Soga, 2005]. Well-sorted sediments are typically deposited by wind or flowing water, whereas poorly-sorted sediments are deposited by gravity, such as during debris flows or glacial processes [Lambe and Whitman, 1969]. Often, natural sediments are characterized by a log-normal distributed grain size distribution [e.g., Spencer, 1963; Tucker, 1981; Füchtbauer, 1988].

### Grain shape

The grain shape, roundness, and sphericity are factors that influence the grain morphology [Mitchell and Soga, 2005]. The shape depends on the mineralogical composition, the grade of weathering and abrasion, as well as on diagenetic processes after deposition [Tucker, 1991]. For silt and sand material the grain shape is characterized by different grades of angularity (Figure 1-10) [e.g., Krumbein, 1941; Powers, 1953; Mitchell and Soga, 2005]. However, many clayey minerals often have a plate-like shape, such as smectite, kaolin, illite, and muscovite [Lafeber, 1966; Bennett et al., 1991b] or a rod-like or tubular shape, such as attapulgite and halloysite, respectively [Oakley and Jennings, 1982; Wen and Aydin, 2003].

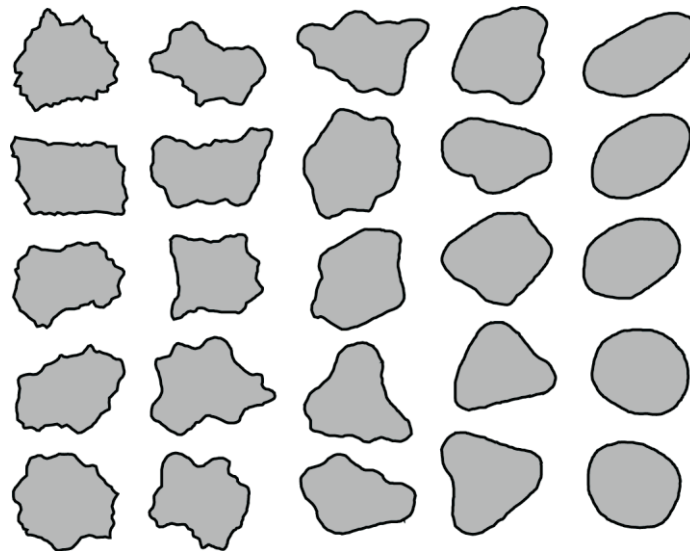


Figure 1-10: Different contour shapes of sand and silt grains regarding roundness and angularity [Mitchell and Soga, 2005].

For the deformation behavior of a granular matter with respect to granular flow the factor of grain shape is significant. Many studies show that surface roughness, angularity, roundness, and sphericity have a strong influence on the bulk stress or bulk frictional behavior [e.g., Mair et al., 2002; Guo and Morgan, 2004; Anthony and Marone, 2005; Kock and Huhn, 2007b; Yan, 2009; Härtl and Ooi, 2011; Szarf et al., 2011].

### 1.3.3 Packing and porosity

The granular packing can be defined as the arrangement of solid units in which each unit is in contact with its neighbors [Graton and Fraser, 1935]. Furthermore, the number of the neighbors in contact defines the coordination number, which is an indicator for the grain packing. In addition to the coordination number different parameter are suitable for describing the packing. The bulk density ( $D$ ), porosity ( $\eta$ ), and void ratio ( $e$ ) are commonly used as a measurement of packing. They are related to one another by the following relationship [Panayiotopoulos, 1989]:

$$\eta = \frac{e}{1+e} = 1 - D \quad (\text{Eq. 1-5})$$

In general, the packing depends on already mentioned parameters of previous sections, such as grain shape, grain size, and grain size distribution and sorting that also affect the porosity [Lambe and Whitman, 1969; Mitchell and Soga, 2005]. For uniform spherical particles of the same size a relation between the granular packing and the porosity exist in which a loose packed granular assembly is associated with a high porosity and densely packed particles results in low porosity (Figure 1-11; Table 1-1) [Panayiotopoulos, 1989].

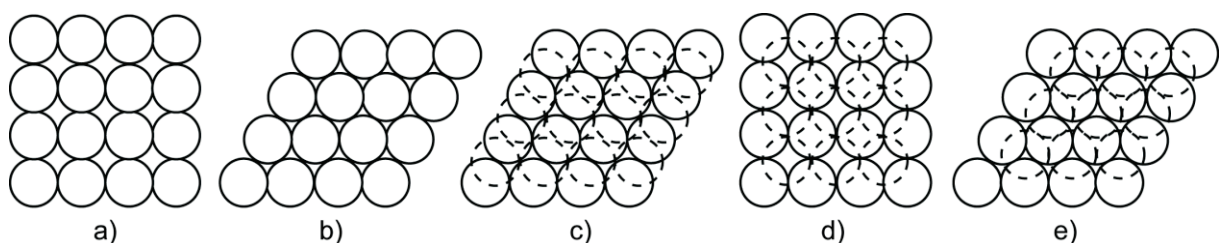


Figure 1-11: Different packing of uniform sized spherical particles [Panayiotopoulos, 1989].



Table 1-1: Packing features of coordination number and porosity according to Figure 1-11

Type of packing	Porosity [%]	Coordination Number
Simple-cubic (a)	47.64	6
Cubical-tetrahedral (b)	39.54	8
Tetragonal-sphenoidal (c)	30.19	10
Pyramidal (d)	25.95	12
Tetrahedral (e)	25.95	12

In Figure 1-12, the basic principle of a granular packing is demonstrated with an identical set of grains for a dense and loose packed particle assembly between fix walls [Rietema, 1991]. In contrast to the dense packed sample, the loose packed particles show larger pore spaces, and hence, a higher porosity, whereas a fewer number of neighbor contacts occur that results in a lower coordination number. The change in the particle arrangement with the corresponding variation in the pore spaces results in a modification of the granular microfabric [Mitchell and Soga, 2005].

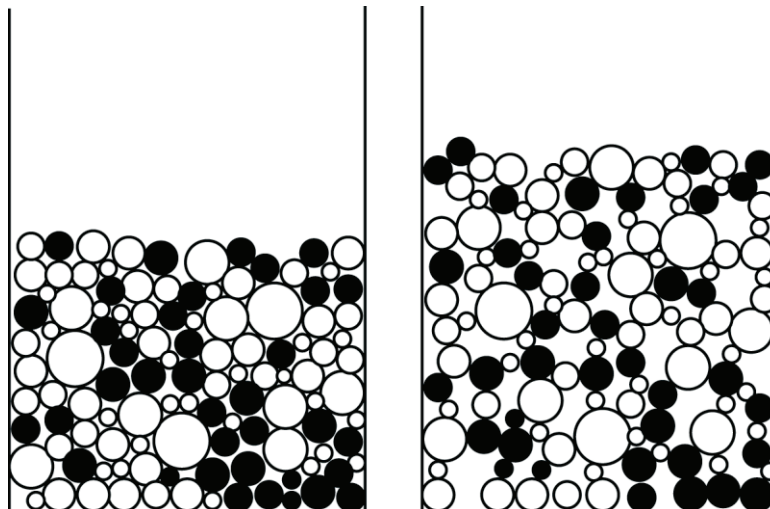
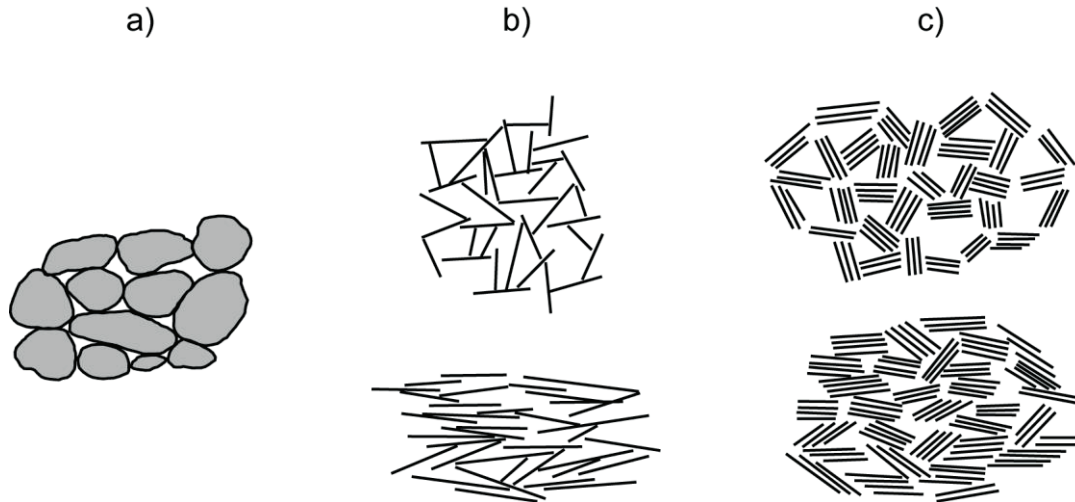


Figure 1-12: Different packing of the same set of particles [Rietema, 1991].

### 1.3.4 Microfabric

The microfabric refers to the arrangement of particles, particle groups, and the corresponding pore spaces inside the granular matter and strongly affected the mechanical behavior of granular matter [Mitchell and Soga, 2005]. Parameters mentioned in the previous sections, such as grain size, grain shape, and packing and porosity have an effect on the microfabric. Furthermore, grain orientation and contact orientation characterizes the microfabrics [Lafeber, 1966; Oda, 1972; Mahmood and Mitchell, 1974; Mitchell, 1976]. The preferred orientation of contacts in a grain structure can be geometrically described with the fabric tensor [Oda, 1972], which is also an indicator for the internal texture [de Gennes, 1999].

Three primary elements can be used to describe the microfabric of particles [Collins and McGown, 1974]. First, the elementary particles composed of individual clay, silt, and sand particles (Figure 1-13a, b). Second, the particle assemblages consist of elementary particle arrangements in which own mechanical attributes and definable physical boundaries appear (Figure 1-13c). The last one is the pore space that describes the voids filled with gas and fluids. Although granular matter can have the same porosity the sediment fabric, and hence, the particle arrangement can be different [Panayiotopoulos, 1989; Mitchell and Soga, 2005].



**Figure 1-13: Particle arrangements a) individual silt or sand interaction, b) individual clay platelet interaction and c) clay platelet group interaction [modified from Collins and McGown, 1974].**

Usually, fabrics of sand and silt reveal single particle arrangements, whereas for clayey material often particle aggregations are observed [e.g., Moon, 1972; Mitchell, 1976; Moon and Hurst, 1984; Panayiotopoulos, 1989; Bennett et al., 1991b; Mitchell and Soga, 2005]. The particle association can be described by the following modes (Figure 1-14) [van Olphen, 1977; Mitchell and Soga, 2005]: dispersed, flocculated, deflocculated, and aggregated. Dispersed assemblages signify that no face-to-face (FF) associations of clay particles exist. For flocculated particle assemblages, edge-to-edge (EE) or edge-to-face (EF) associations appear, whereas for deflocculated particles no associations between the particles occur. However, aggregated assemblages indicate FF associations of multiple clay particles.

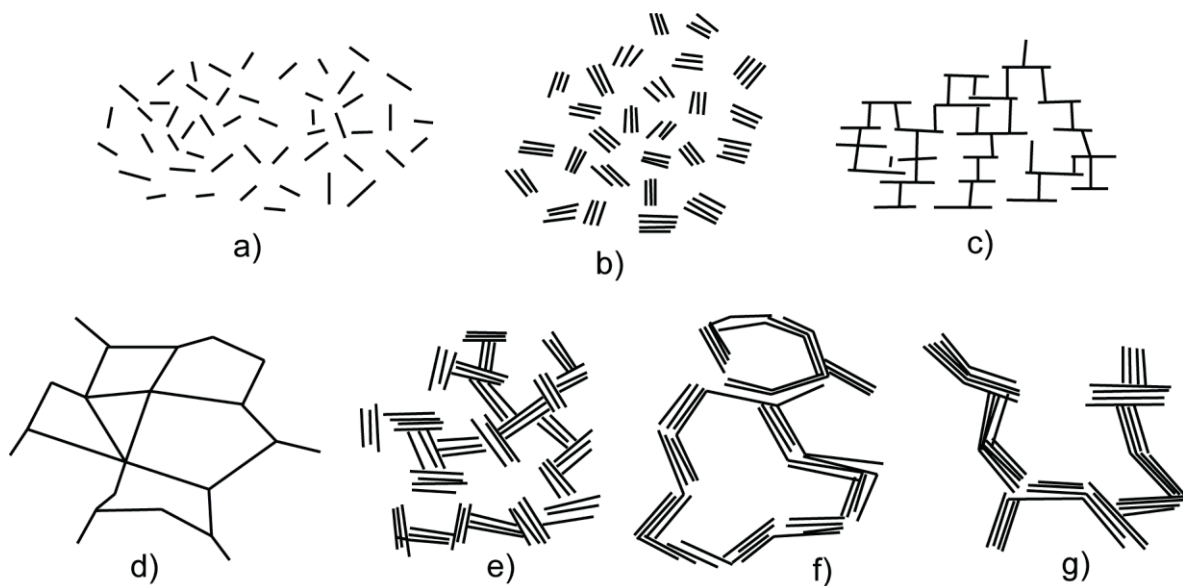


**Figure 1-14: Several arrangements of plate-like particles: a) Dispersed and deflocculated, b) aggregated but deflocculated (parallel aggregation or FF association), c) EF flocculated but dispersed, d) EE flocculated but dispersed, e) EF flocculated and aggregated, f) EE flocculated and aggregated and g) EF and EE flocculated and aggregated [van Olphen, 1977].**

From these basic arrangements more complex associations can be formed. The *cardhouse* (Figure 1-14c) is an open EF arrangement that usually occurs with the flocculated, but dispersed particle arrangement [Mitchell and Soga, 2005]. Furthermore, the arrangement of parallel oriented clay particles with FF contacts refers to a *domain* or *book* arrangement (Figure 1-15a) [Aylmore and Quirk, 1960; Sloane and Kell, 1966] and stepped FF contacts (Figure 1-15b, c) [Smalley and Cabrera, 1969]. The EF composition of books is termed as *bookhouse* (Figure 1-14e). Moreover, larger fabric units containing groups of particles or aggregates are termed as a *cluster* [Olsen, 1960].

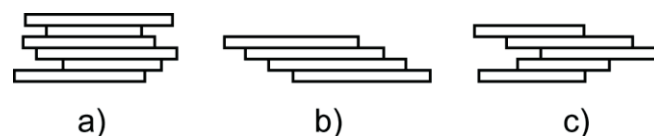


**Figure 1-15: Forming of a) a book structure illustrated by Moon [1972] according to laboratory observations [Sloane and Kell, 1966], and b) and c) “stepped FF” contacts [Smalley and Cabrera, 1969].**

A loose packed assembly for silt is described by the honeycomb structure which was introduced by Terzaghi [1925] (Figure 1-16a). This fabric is based on very fine grains that are small enough for molecular forces to persuade them to adhere each other [Sloane and Kell, 1966]. With respect to plate-like particles a similar structure is proposed for electrolyte-rich marine clay sediments (Figure 1-16b) [Engelhardt and Gaida, 1963]. Moreover, the relation between open clay microfabrics and large pore spaces, and hence, large ranges in porosity within the clayey material is schematically demonstrated in Figure 1-17 [Bennett et al., 1981].

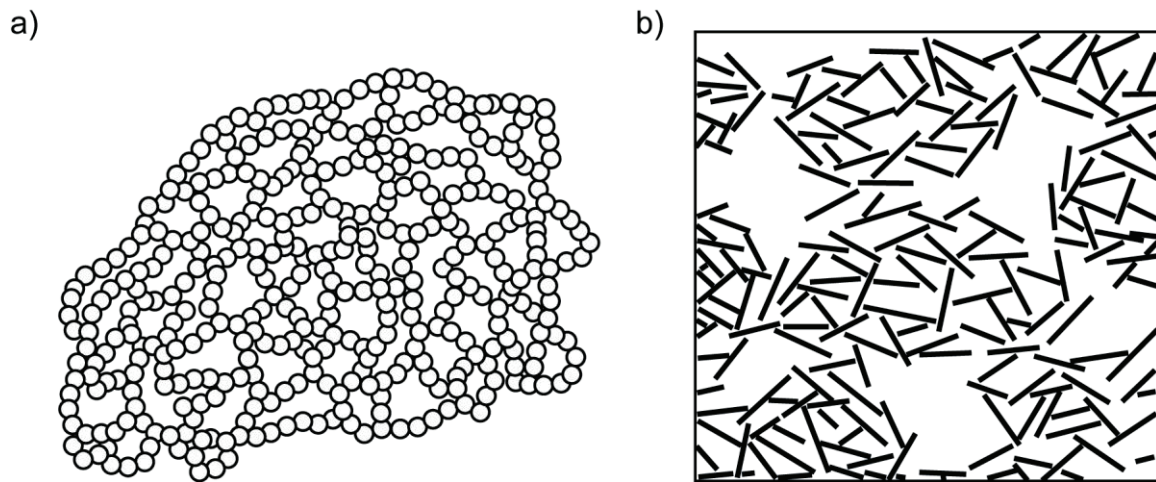


Figure 1-16: a) *Honeycomb structures of silt particles [Mitchell and Soga, 2005]. b) Proposed clay aggregate structure for marine environments with edge-to-face contacts [Engelhardt and Gaida, 1963].*

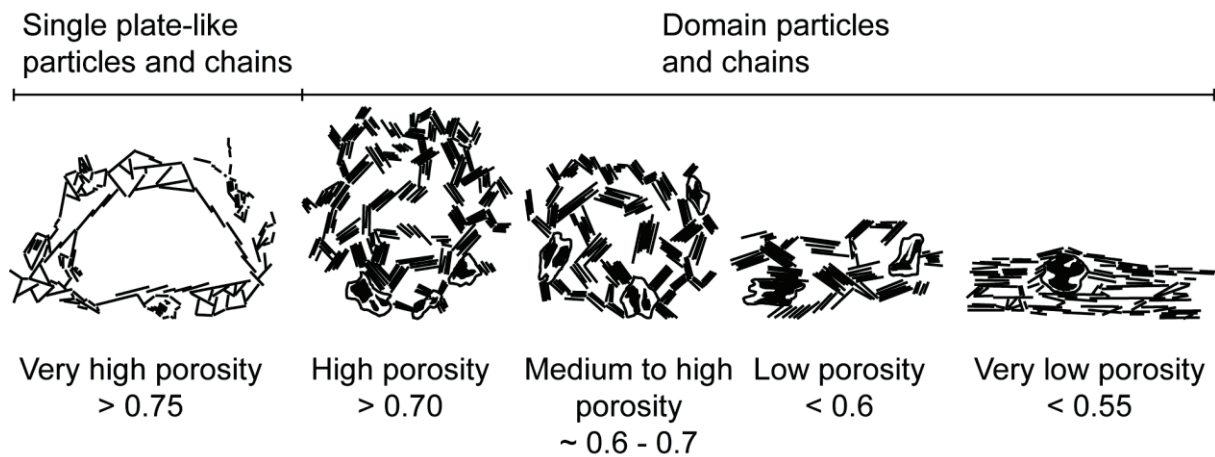


Figure 1-17: *Several porosity states of plate-like particle microfabrics [modified from Bennett et al., 1981].*

Many studies reveal a change in the microfabric during the deformation of a granular matter [e.g., Saffer and Marone, 2003; Abe and Mair, 2005; Kock and Huhn, 2007b; Abe and Mair, 2009; Yan, 2009]. A comprehensive study of microstructural changes in kaolin containing material caused by direct shearing is presented by Morgenstern and Tchalenko [1967]. They recognized oriented domains along shear surfaces (Figure 1-18). Moreover, they found two bands of domains oriented parallel to the shear plane. For deformed plate-like clay particles, a parallel alignment of particles is usually observable [e.g., Sloane and Kell, 1966; Moon and Hurst, 1984; Wen and Aydin, 2003; Mitchell and Soga, 2005].

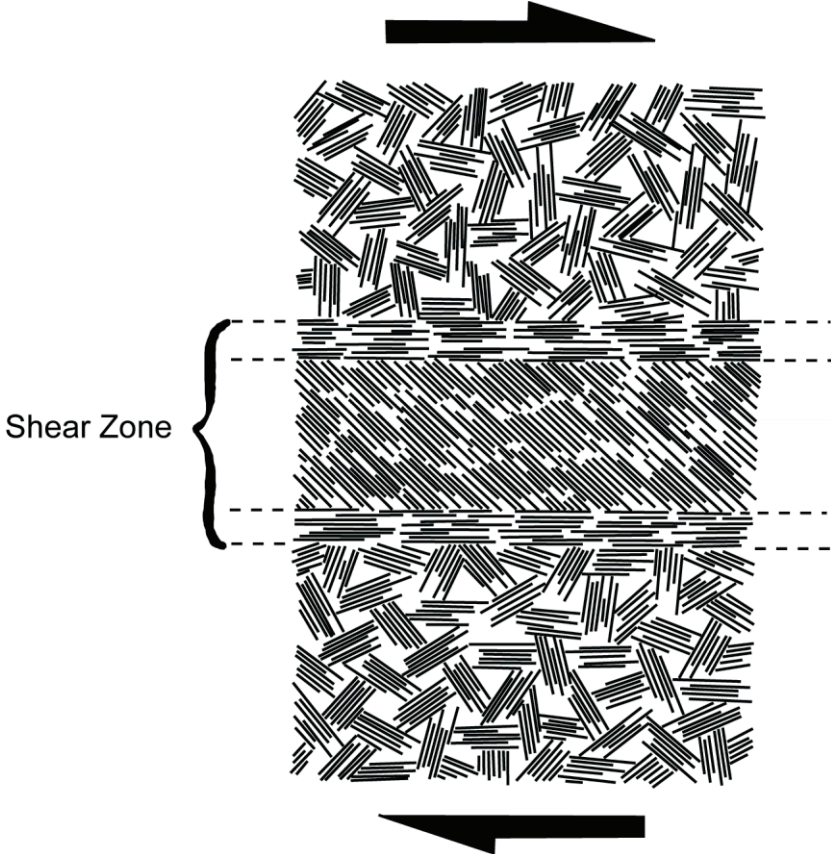


Figure 1-18: Parallel alignment of plate-like particles within a shear zone during shear deformation [Morgenstern and Tchalenko, 1967].

## 1.4 Motivation and objectives of this study

The primary objective of this study is to investigate the influence of the granular microfabrics on their micromechanical properties, using the DEM. It is already known that the microfabric with its large variety of particle arrangements differently affect the deformation processes of a granular matter. For instance, a high porous layer of granular particles behave in another way than a compacted granular material. This is particularly apparent for the macroscopic behavior of friction and porosity. Although, the macroscopic behavior is often investigated in laboratory the responsible microscopic processes are generally not very well known.

Having such knowledge is crucial in order to assess and predict the behavior of granular matter with respect to external factors. It will be helpful, for example, for the investigation of phase transitions, and hence, for the stability of the current granular phase. This affects a wide range of granular applications, e.g., construction of footings and foundations, stabilizing and destabilizing of slopes.

Therefore, many studies investigated the microfabric and the corresponding mechanical properties. But in laboratory experiments an investigation of the microfabric and the micromechanical properties is not possible during the deformation processes inside the deformed sample. However, this is of particular interest because during deformation changes in the microfabric occur that in turn influence the granular properties. Thus, an investigation with numerical models is unavoidable.

Many numerical DEM studies have been conducted in the last twenty years. Most of them are based on 2D models. Especially in the last years more and more 3D numerical models were published. It was noticed that a discrepancy exist between both types of dimensionality (2D- 3D) for the same problems. That aspect is insufficiently investigated by the community and forms the first research part of this study. Furthermore, the effect of grain shape and corresponding particle arrangements, which define the microfabric, forms the second part of this study.

### (I) Dimensionality

The dimensionality is known to affect the deformation behavior. In the laboratory, in-plane (2D) and spatial (3D) investigations are difficult to compare during shear deformation on a microscale. So, a deeper examination of shear strength and localization has not been done. For that reason the effect of dimensionality is the first major objective of this study. The following specific questions are addressed:

- (1) What is the effect of dimensionality on the physical properties of the:
  - frictional strength (coefficient of friction) and the
  - pore volume (porosity)?
- (2) What is the effect of dimensionality on shear zones regarding:
  - localization within the sample and the
  - shear zone characteristics (thickness)?

### (II) Grain shape

Laboratory studies show that the grain shape strongly influences the deformation behavior of granular matter. Nevertheless, identical grain shapes are difficult to achieve in laboratory shear experiments. Elongated grains tend to form different types of microfabrics. On a microscaled level, these microfabrics are poorly investigated and their consequences regarding deformation are not adequate investigated during the shear processes. That is why the parameter of grain shape is investigated in detail concerning the frictional strength with

respect to (a) the contact configurations and (b) the pore volume evolution. For that reason, the effect of grain shape is (a) the second and (b) the third major objective of this study. The following specific questions are addressed:

(a)

- (1) What is the effect of grain shape on the frictional strength?
- (2) How does the microfabric evolve with respect to:
  - contact distribution between the different grain shapes and
  - evolution of contact types during the deformation?

(b)

- (1) Is there any relation between the frictional strength and the pore volume?
- (2) What is the behavior of local pore volume changes:
  - as an indication for microfabric changes and
  - regarding the shear plane development?

## 1.5 Methods

The DEM is a numerical granular based model approach that allows for multiscale simulation from grain-to-grain to macroscale. A detailed description is given by many studies [e.g., *Cundall and Strack, 1978; 1979; Potyondy and Cundall, 2004*]. The DEM fundamentals consist of particles in contact (Figure 1-19). Certain characteristics defined the individual particles, such as particle friction coefficient, particle stiffness, and density. The interaction of single particles is based on simple physical motion and contact laws. For this study, the DEM code of Particle Flow Code (PFC2D, PFC3D) in two- and three-dimensions is applied. In addition to the basic algorithms, the code provides a C++ user-interface for the implementation of user-designed functions. This feature was used to optimize the time of simulation and to implement routines to simplify post-processing analyses.

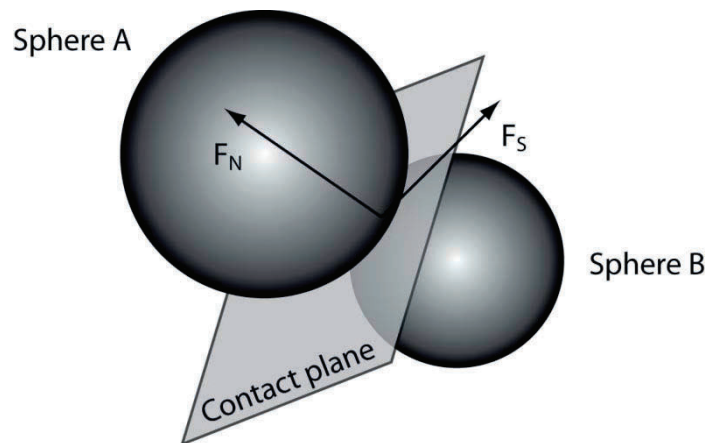


Figure 1-19: Two particles in contact [modified from *Belheine et al., 2009*].

The convenience of numerical modeling lies in the control regarding the initial and boundary conditions, which can be easily reproduced, in contrast to laboratory experiments. This aspect allows for isolating parameters in detailed studies to qualify and quantify their behavior. This method offers all the available particle data, such as position, velocity, rotation, and acting forces at high resolution in space and time and, furthermore, allows for continuous monitoring during the simulation. For the modification of particle shape, individual particles can be combined to simulate clumps of arbitrary shape (Figure 1-20). In this study, this technique is used to form the fixed shaped rod-like and plate-like particles consisting of single particles.

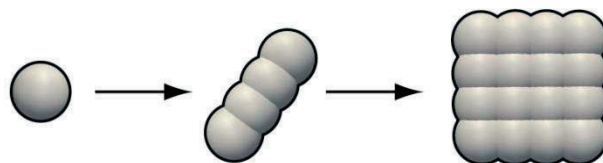


Figure 1-20: Applied grain shapes in direct shear experiments, which increase the shape complexity from ideal spherical shape to rod-like shape to plate-like shape.

### 1.5.1 Model setup

Different kinds of geotechnical shear experiments were adapted according to ring shear tests (Figure 1-21; see Chapter 2) or direct shear tests (Figure 1-22; Chapter 3 and 4). The direct



shear test is a very simple set-up consisting of walls at the boundaries, whereas the ring shear test allows for shearing of large strain rates by using periodic walls as boundary conditions. That means the particles that escape one side of the boundary are simultaneously recreated on the opposite side. In this way, the behavior of a large sample can be simulated using only a small number of particles.

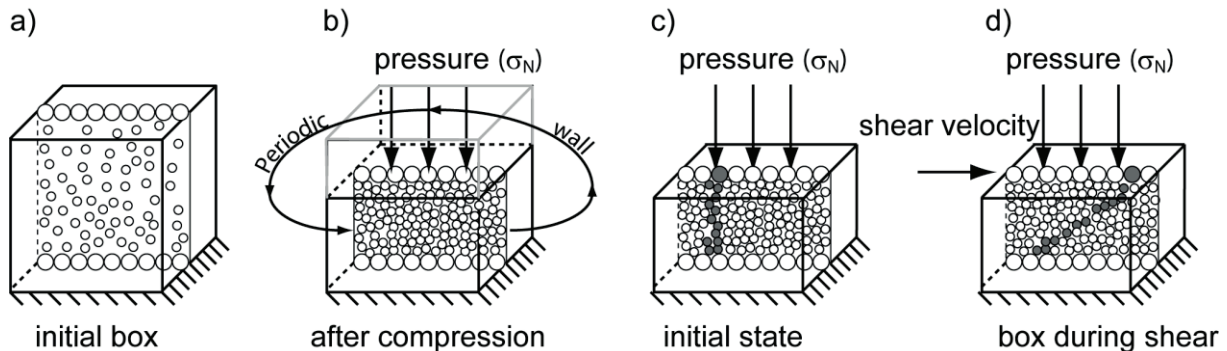


Figure 1-21: Schematic illustration of the ring shear processes. Box sidewalls are defined as periodic.

In general, the shear tests consist of a fixed bottom part and a sheared upper part. A shear velocity of  $1\mu\text{m/s}$ , comparable to laboratory experiments, was applied. For the ring shear test, 5 MPa on the sheared upper wall was applied to load the sample. The loading was constant during all the simulations. The loading conditions were chosen based on laboratory experiments, which showed this specific value to be a minimum for observed grain fracture processes [Mair *et al.*, 2002]. In the direct shear tests, the microstructure was varied by changing the applied particle shapes according to Figure 1-20.

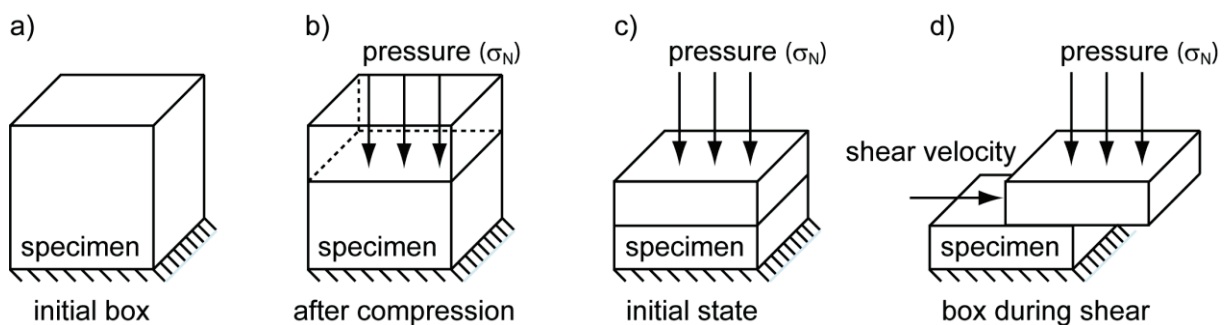


Figure 1-22: Schematic illustration of the direct shear processes.

At this point, it is crucial to note and keep in mind that the particle properties described by the DEM, and which are predefined by the modeler himself, are distinct from the bulk properties of the particle assembly, which are similar to the measurements obtained in lab experiments.

### 1.5.2 Analyzing methods

While the shear processes were performed, many analyzing methods were applied, running and logging data in the background, for investigating the material response. In that regard, some methods were derived from the laboratory approaches, such as friction coefficient and pore volume investigations. On the other hand, several specific numerical methods were used or especially developed as a part of this study. Both methods of investigation allowed for a detailed study of the micromechanics on a grain scale. In this study, the following analyzing methods were applied (briefly illustrated in Figure 1-23).

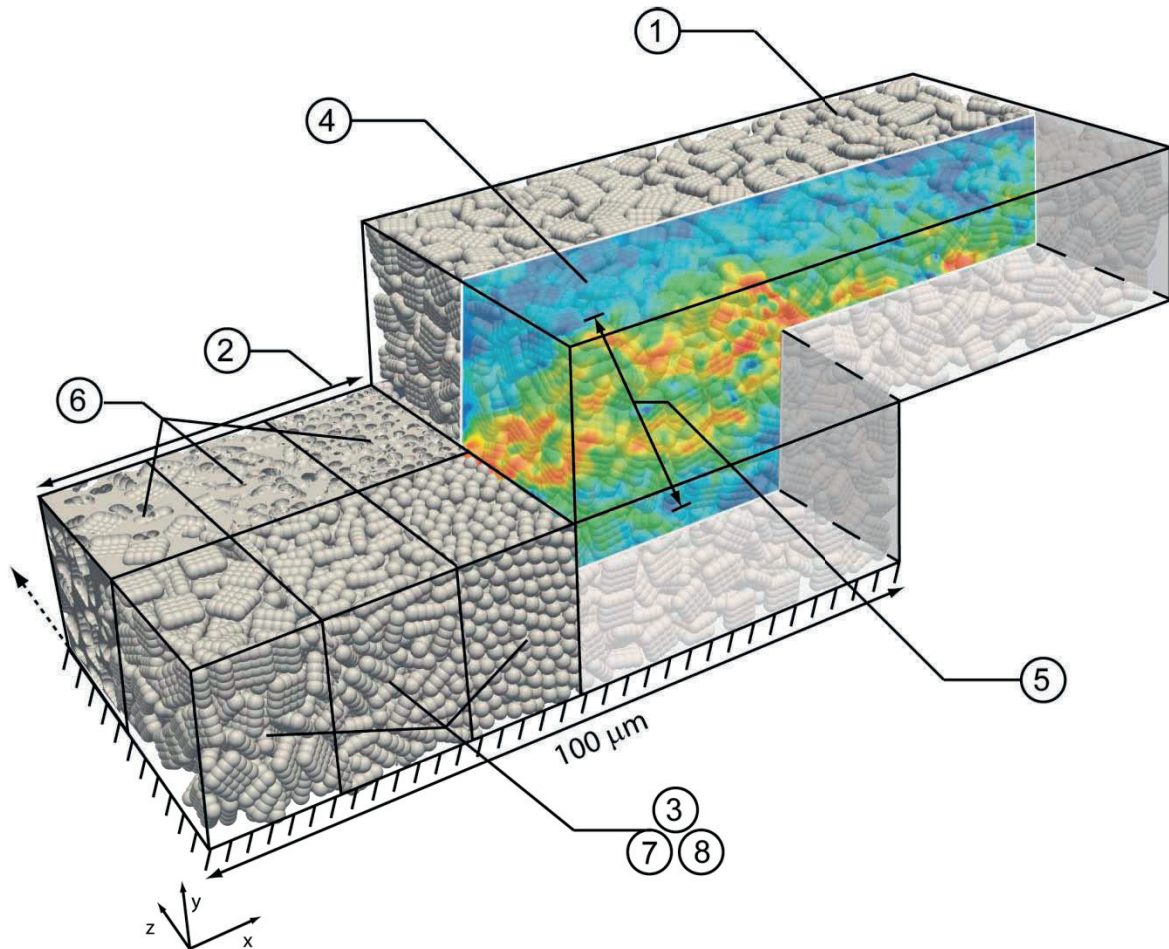


Figure 1-23: Summarized illustration of analyzing methods represented for the direct shear test. Methods comprises: (1) Visualization, (2) Strain and displacement, (3) friction, (4) particle slip and localization, (5) Shear zone thickness, (6) pore volume and porosity, (7) coordination number, (8) contact size and type of contact.

### (1) Visualization:

Different techniques for particle visualization were used. For the rendering process, the data of the particle geometries, virtual light, and virtual camera were used to create an image. Simple particle rendering occurred during the simulations by PFC2D or PFC3D. It also made vertical lines of colored particles possible acting as passive strain markers to indicate the different stages of deformation.

In contrast, for a high-level particle rendering the PARAVIEW software has been used. It is based on the Visualization Toolkit (VTK) [Schroeder *et al.*, 2004]. The VTK library contains a huge amount of techniques and algorithms for the computational graphical data visualization, modification, and analyses. After the simulations, the high-level particle rendering was applied as a post-processing step for the direct shear experiments. Therefore, the sample reconstruction was achieved necessarily by logging particle positions and radii during the shearing process.

### (2) Strain and displacement:

The deformation behavior of the shear boxes was logged continuously. For the ring shear experiments, the strain ( $\epsilon$ ) was monitored as the ratio of the amount of the displaced wall and the initial shear box height. This deformation was described by a dimensionless analysis [%] and allowed for a comparison between the results independent of the shear box size.

$$\varepsilon = \frac{\text{horizontal displacement } [\mu\text{m}]}{\text{shear box height } [\mu\text{m}]} \quad (\text{Ring-shear test}) \quad (\text{Eq. 1-6})$$

In contrast, the deformation during the direct shear test was described by the absolute values [ $\mu\text{m}$ ] of the wall displacement. Nevertheless, a general dimensionless analysis for direct shear experiments uses, instead of the initial shear box height, the initial shear box width:

$$\varepsilon = \frac{\text{horizontal displacement } [\mu\text{m}]}{\text{shear box length } [\mu\text{m}]} \quad (\text{Direct-shear test}) \quad (\text{Eq. 1-7})$$

While the direct shear box width is equal to 100  $\mu\text{m}$ , the magnitudes of the absolute values and the dimensionless values correspond to each other. Thus, 40  $\mu\text{m}$  displacement correlates with 40 % strain.

During the ring shear experiments, the shear deformation were performed at least until the critical state was reached, whereas the maximum grade of deformation for the direct shear experiments was 40  $\mu\text{m}$ . The primary reason is that at larger grade of deformation, boundary effects and the walls of the upper and lower shear box would influence the measurable sample area.

### (3) Friction:

The friction is a material property that characterizes the resistance to the material deformation behavior. According to the Mohr-Coulomb criterion, the friction coefficient for cohesionless material is derived from the ratio of shear stress and normal stress. At a grain-to-grain contact, the frictional resistance acts as long as the ratio does not overcome a threshold. In this case, the threshold is exceeded then stable sliding between the involved particles occurs. For a particle assembly, the behavior at the single particle contacts is summed. The corresponding mean value represents the frictional behavior of the particle assembly. Compared to laboratory conditions, the numerical approach allows for determination of the friction coefficient inside the sample and not only at the area where wall and sample are in close contact. In this way, it is also possible to define areas of special interest for a detailed investigation regarding the frictional behavior. Therefore, the applied software PFC2D and PFC3D allows for definition of spherical measurement areas in which the mean stress tensor was obtained, and thus, provides the stress state of the particle assembly.

$$\mu = \frac{\tau}{\sigma_N} \quad (\text{Eq. 1-8})$$

### (4) Particle slipp and detection of localization features:

The behavior of the interacting particles in contact is based on the frictional strength. If the frictional resistance is overcome, then single particles slide relative to each other. This relative particle movement as an indication for slipp behavior can be logged as changes in the particle positions. Therefore, particle properties, such as position, displacement, and the radius are logged with the beginning of the shear process. Further, these data are used for post-processing with the GMT software [Wessel and Smith, 1991]. A two-dimensional crop from inside the sheared sample was created to generate a vector field with the particle displacements as the input parameter. Subsequently, normalized gradients were determined based on the displacement vector fields. The illustrations of the normalized gradients

highlighted localized areas of large displacement and signify areas of slip planes or shear bands (Figure 1-24).

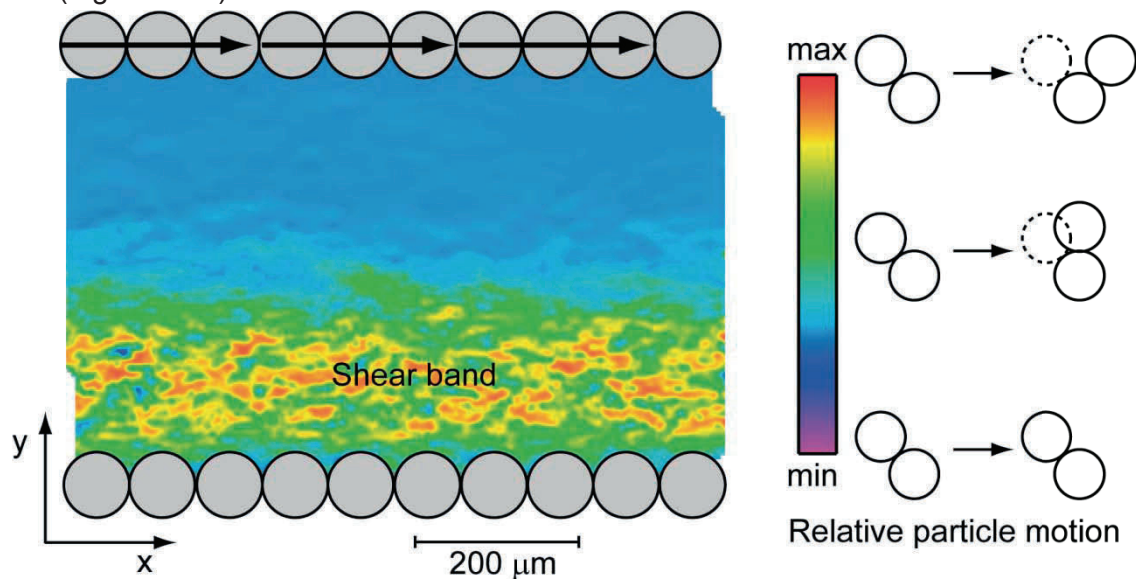


Figure 1-24: Localization of particle slip and shear band formation by illustrating the relative particle motion in a ring shear experiment.

**(5) Shear zone thickness:**

The thickness of the localized shear bands was determined by using the normalized gradients, which reflect the areas of large slip and large relative particle movement. The illustrations obtained from the GMT software allow for a direct measurement of the thicknesses (Figure 1-25).

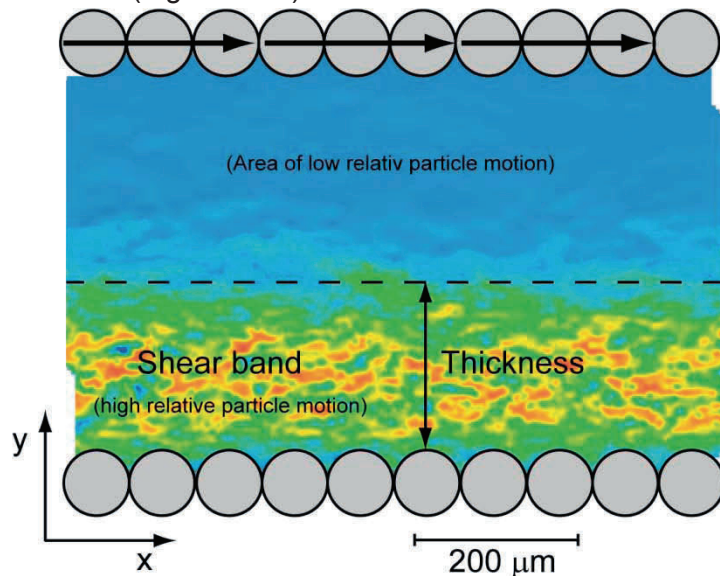


Figure 1-25: Determination of the shear band thickness based on the relative particle motion in a ring shear experiment.

**(6) Pore volume and porosity:**

In this study, the term pore volume and pore space describes the sample area that is not filled with particles. The applied methods to determine the pore volume differ significantly from the laboratory investigations.

The method that is provided by the PFC2D and PFC3D software determines the analytical solution of the porosity ( $\eta$ ):

$$\eta = \frac{V^{void}}{V^{meas}} = \frac{V^{meas} - V^{mat}}{V^{meas}} = 1 - \frac{V^{mat}}{V^{meas}} \quad (\text{Eq. 1-9})$$

$V^{void}$  describes the void area and therewith the pore space,  $V^{meas}$  is the measured volume, and  $V^{mat}$  is the volume of the particles:

$$V^{mat} = \sum_{N_P} V_P - \sum_{N_C} V_C \quad (\text{Eq. 1-10})$$

$V^{mat}$  is the result of the sum of single particle volumes ( $V_P$ ) and the subtracted sum of the volumes of particle overlap ( $V_C$ ). The particle volume ( $V_P$ ) is calculated using the radius ( $R$ ) according to:

$$V_P = \begin{cases} \pi R^2 t, & 2D (t = 1) \\ \frac{4}{3} \pi R^3, & 3D \end{cases} \quad (\text{Eq. 1-11})$$

Another approach uses the VTK software package [Schroeder *et al.*, 2004] for the pore volume calculation. In this approach, a three-dimensional grid of the pore space is created (Figure 1-26).

That grid can be seen as a negative (comparable to a photo negative in photography) to the particle assembly. Based on that grid, a volume calculation algorithm is applied [Alyassin *et al.*, 1994]. That implies, the finer the applied grid, the more accurate is the pore volume calculation.

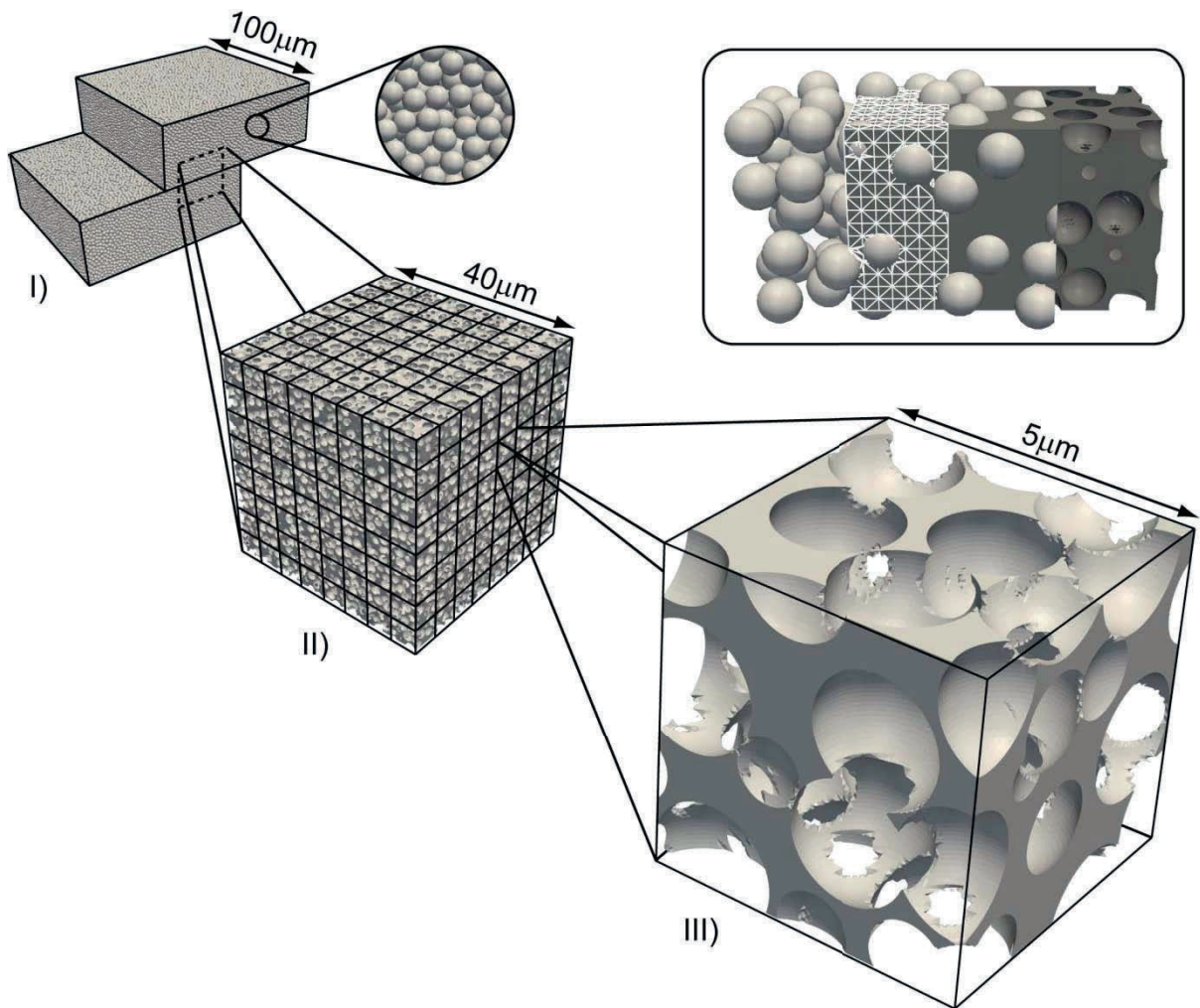


Figure 1-26: Steps of pore volume calculation from I) the sample to II) the pore volume cube to III) a single sub-cube. The rounded box represents the single stages of pore space determination from particles to pure pore space.

**(7) Coordination number:**

The coordination number is an element of the microfabric description. It is also an indicator for the particle packing. In Figure 1-27, the basic principle of the coordination number is illustrated. Every particle has a number of contacting neighbor particles.

$$C_N = \frac{\sum N_B n_C^{(B)}}{N_B} \tag{Eq. 1-12}$$

$C_N$  is the coordination number,  $N_B$  is the number of balls, and  $n_C^{(B)}$  is the number of contacts per particle.

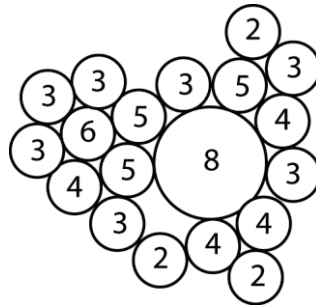
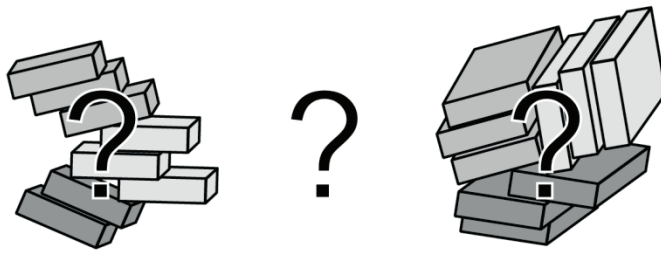


Figure 1-27: Spherical particles with corresponding coordination number in 2D.

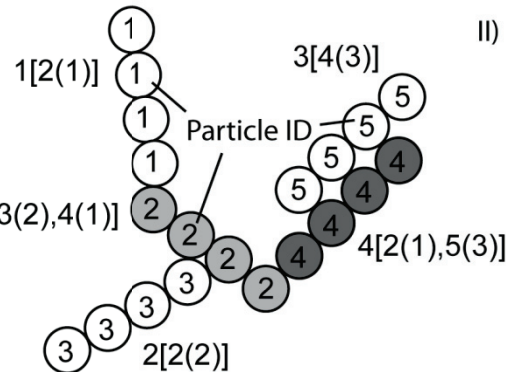
### (8) Contact size and type of contact:

A new method to describe the contact behavior of a particle assembly was developed as a part of this study. The general contact relations were analyzed and evaluated to a topological data structure. This data structure allows for a detailed analysis of contacts of single or arbitrary shaped particles (composed of single particles). Thus, it is possible to describe the contact area as a sum of single contacts between two particles. On the basis of this information, it is possible to derive the topological structure of the contacts. This helps to identify the microfabric structure of particles and their contacts consisting of point, edge, or face contacts (Figure 1-28).

I)



Number of contacts  
ID of neighbour particle  
Coordination number



III)

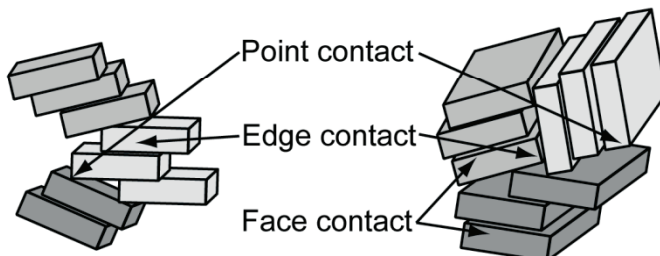


Figure 1-28: Scheme of contact size and contact type determination I) Assembly of particles of unknown contact structure. II) Simplification of the method to determine the contact topology. III) Step that attributes the contact topology to the particle assembly.





## 2 Chapter Two

### (Manuscript 1)

Prepared to submit to

**International Journal for Numerical and Analytical Methods in Geomechanics**

## Impact of model dimensionality on numerical shear test experiments

Lutz Torbahn<sup>1,\*</sup>, Katrin Huhn<sup>1</sup>

<sup>1</sup> MARUM – Center for Marine Environmental Sciences and Faculty of Geosciences, University of Bremen, Leobener Str., D-28359 Bremen, Germany

\* Corresponding author: Phone +49(0)421 218 65866 Fax +49(0)421 218 65872

E-mail: ltorbahn@marum.de

### Abstract

This study describes numerical experiments, which were used to examine the effects of dimensionality on the shear processes in granular materials. For this purpose one 2D and two 3D numerical shear setups were developed with identical configurations except of the number of the applied particles in order to isolate the pure effect of the dimensionality. It became apparent that the physical properties of friction coefficient, porosity and shear band features such as localization and thicknesses were influenced by the factor of dimensionality. Although the same material was used for all the samples, the peak shear strength was larger in the 3D experiments. The same was observed for the 3D porosity measurements. Further differences exist with regard to the shear band localization and thicknesses while in the 2D experiments the development of the shear bands occurred always close to the fixed wall and those of the 3D experiments appeared all, except of one special case ( $3D_{\text{tall}^*}$ ), close to the moving wall. Moreover, for the 3D experiments it has been found that all the shear bands, excluding the  $3D_{\text{tall}^*}$ , have formed with a lower thickness compared to the 2D experiments. Another aspect investigated in this study examined the vertical model size based on the different number of applied particles regarding the physical properties. It was shown that the changes in the vertical size affected the frictional softening behavior until the steady state was achieved and the thickness of the formed shear bands.

**Keywords:** DEM, ring shear, granular matter, 2D, 3D, friction, porosity

### 2.1 Introduction

The physical characterization of granular matter has been a focus of geoscientific research for decades. In contribution to this theme, the major aim of this study was to gain a deeper insight into the deformation behavior and, particularly, the failure behavior of granular materials. Many studies have previously dealt with the destabilization processes of granular material to identify and, if possible, to quantify the key role of the different material properties. These laboratory and numerical studies confirmed the influence of the coefficient of friction [Biegel *et al.*, 1989; Marone and Scholz, 1989; Mair and Marone, 1999; Mair *et al.*, 2002; Saffer and Marone, 2003; Anthony and Marone, 2005; Kock and Huhn, 2007a; Abe and Mair, 2009], porosity [Marone and Scholz, 1989; Aharonov and Sparks, 2002], and internal structure [Kopf and Brown, 2003; Guo and Morgan, 2004; Kock and Huhn, 2007a; Abe and Mair, 2009] on the shear resistance of fault gouge and sediments.

In general, laboratory derived information on material behavior and physical parameters, such as material friction or porosity, can only be determined based on the entire specimen [Marone and Scholz, 1989]. A closer look inside the sample during shearing is severely limited by measurement techniques and sensor resolution in the laboratory, and hence, it is difficult to obtain detailed information about the physical processes on a grain scaled level. Current possibilities for examining grain processes include the use of X-rays, which can be used for internal sample investigation of shear bands; however, this technique can be successfully applied only on sands [Oda *et al.*, 1998; Oda and Iwashita, 2000]. Another technique involves the use of digital camera sensors to obtain information about the grain movements during shearing, but this method is restricted to the shear box boundaries and can only be utilized to investigate large grain size classes, such as sand [Rechenmacher, 2006]. At the present state of this research field, numerical experiments, such as granular shear tests, allow for a deeper insight into the material behavior and the physical processes that occur on a micro-scaled level inside the sample during the shearing.

In recent years, the Discrete Element Method (DEM) [Cundall and Strack, 1979; Potyondy and Cundall, 2004] has been successfully used to simulate failure processes in granular material [Aharonov and Sparks, 1999; Mora and Place, 1999; Morgan, 1999; Place and Mora, 2000; Mair and Hazzard, 2007]. This technique allows for simulation of 2D and 3D numerical 'lab' experiments such as numerical shear tests, to investigate physical properties of numerical 'sediments'. Herein, DEM model simulations [Morgan and Boettcher, 1999; Hazzard and Mair, 2003; Mair and Abe, 2011] of granular material were undertaken with the adopted settings of geotechnical shear experiments to allow for comparisons and, thus, model validation.

Previous 2D studies, using smooth particles, have investigated, the aspects of frictional strength, porosity, and dilation of numerical 'sediments' and 'fault gouge' on a micro-scaled level utilizing numerical shear experiments [Morgan, 1999; Aharonov and Sparks, 2002; Hazzard and Mair, 2003; Guo and Morgan, 2007]. These allowed for a deeper insight into grain behavior and the micro-mechanical physics and represent a remarkable improvement in the understanding compared to laboratory measurements. However, the frictional strength and porosity values of the numerical samples described in those studies were significantly lower than those of natural materials [Morgan, 1999; Aharonov and Sparks, 2002; Hazzard and Mair, 2003; Guo and Morgan, 2004]. The lower values derived from 2D can be explained by the necessary simplification involved in a 2D numerical model compared to a 3D analogue

experiment, which includes a significant limitation regarding all aspects of textural and structural micro-mechanics. The discrepancies between numerical studies of granular materials and analogue lab experiments [e.g., *Frye and Marone, 2002*] can be reduced by extending 2-D numerical experiments into the third dimension [*Hazzard and Mair, 2003*]. In that, an additional dimension directly influences the material strength and the number of adjacent particle interactions, which reduces the discrepancy between laboratory and numerical model results [*Hazzard and Mair, 2003*].

However, as the application of 3D models requires higher computer capacity due to increases in calculation time and increases with the numbers of particles, 3D numerical models are rarely used. Furthermore, the influences of model dimensionality (2D vs. 3D) are inadequately investigated with respect to the geomechanical issues in the case of laboratory and numerical shear experiments [*Frye and Marone, 2002; Hazzard and Mair, 2003*]. The study of *Hazzard and Mair [2003]* showed a significant influence of the third dimension on the frictional behavior. Moreover they investigated the relationship between parameter fluctuation and grain reorganization. However, in total, there has been little discussion about the effect of dimensionality in literature regarding the aspects of frictional strength, porosity, dilation, particle movement, and internal structure. In that context, there is an urgent need to clarify whether special emphasis needs to be placed on either simplification or precision. Accordingly, it is necessary to observe whether processes are sufficiently reproduced in models of varying dimensionality.

The aim of this study was to evaluate and validate the factor of dimensionality on numerical 'geotechnical' shear experiments. For this purpose, numerical 'ring shear experiments' were designed in 2D and 3D which were congruent with the model properties and boundary conditions of lab experiments. Therein, the two 3D model approaches were a simple extension of the 2D experiment by adding a model depth. The only distinguishing criterion between both 3D experiments and the 2D setup was the number of implemented particles that also define the different model heights. Next to these differences, all the three experimental setups consisted of the same model parameters which allow for a direct comparison regarding the pure influences of the dimensionality and the influences of the different number of implemented particles. We showed that adding a third dimension and varying the model height caused differences in the physical parameters considering friction coefficient, porosity and variations in the deformation behavior, especially in shear band initiation and their geometrical development during shearing of larger displacements.

## 2.2 Method

### 2.2.1 Discrete Element Method

The Discrete Element Method (DEM) as a granular numerical approach has been applied successfully to investigate failure processes, especially the formation and the on-going propagation of faults in granular materials in 2D [*Morgan, 1999; Kock and Huhn, 2007a*] and in 3D [*Abe and Mair, 2009; Kuhn, 2010*]. A characteristic feature of this discrete approach, in both 2D and 3D experiments (Figure 2-1), is that microscopic particle and contact properties (e.g., coefficient of particle friction  $\mu_P$ , and particle normal and shear stiffnesses  $k_N$ ,  $k_S$ ) must be prescribed to simulate the resultant macroscopic response (e.g., coefficient of friction  $\mu$ , porosity  $\eta$ ) in accordance with natural conditions [e.g., *Morgan, 1999*]. These macroscopic properties allow for a comparison to laboratory experiments [*Hazzard and Mair, 2003*]. Details of the DEM have been described by other [*Cundall and Strack, 1978; 1979; Itasca, 2004*;

2005]. For the experiments presented in this paper, the DEM application of Particle Flow Code 2D and 3D (PFC2D, PFC3D; ITASCA®) was applied.

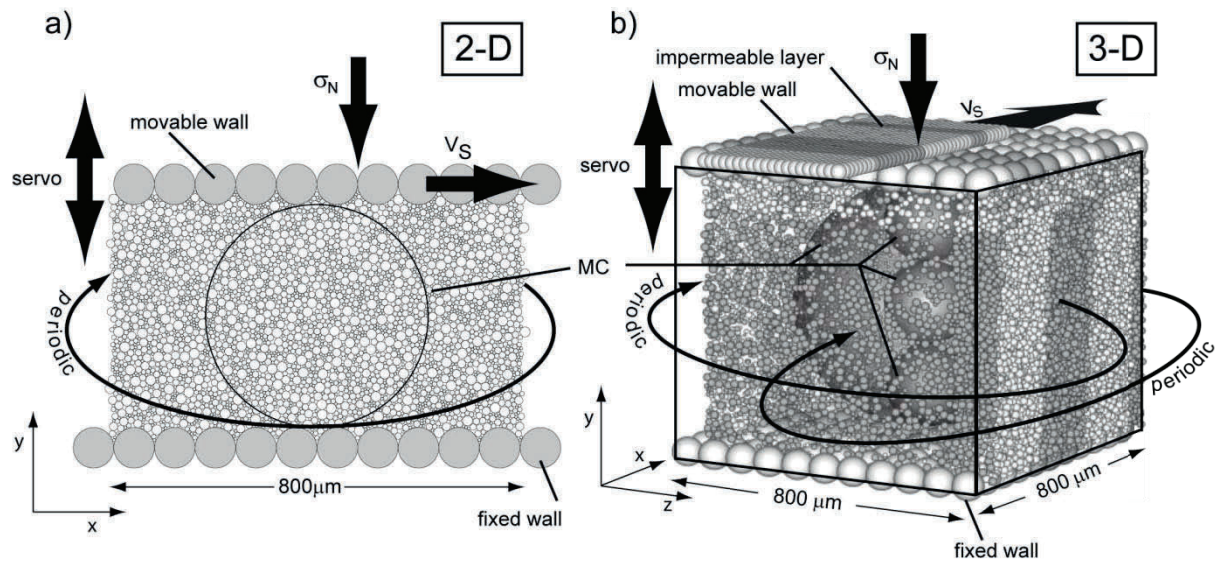


**Figure 2-1: (a) The 2D numerical shear box experiment with 3,895 particles and (b) the 3D<sub>tail</sub> numerical model with 180,000 particles. The top and bottom boundary walls consist of a double layer structure to avoid particle escape in the vertical direction. Thick black arrows mark the applied boundary conditions. Material properties such as friction coefficient and porosity were measured within the measurement spheres (MC).**

During one calculation step, forces acting on the particles ensure that the particles interact at contact points with each other. Thereby, the contact behavior is described by a contact law using the microscopic material properties. In these simulations a linear contact law was applied that is defined by the normal and shear stiffnesses acting in series for the interacting particles. Based on the particle forces acting at the contacts, the particle motion is calculated by using the second Newtonian law which updates all particle positions and contacts. Consequently, the particle motions are used to update the forces at each contact [Itasca, 2004; 2005].

Furthermore, the coefficient of particle friction defines the limit of the shear force at contact points. As long as the shear force overcomes this limit, stable sliding is initiated [Hazzard and Mair, 2003]. The normal and shear stiffnesses are defined by the ratios of contact forces and the resulting displacements.

These force-displacement calculations of particle interactions allow for the simulation of a Mohr-Coulomb material with material hardening and softening and a, subsequent, irreversible deformation (Figure 2-2). Both hardening and softening behaviors are represented as irreversible deformation effects that produce a peak and critical state friction in dense particle assemblies [Mitchell and Soga, 2005].

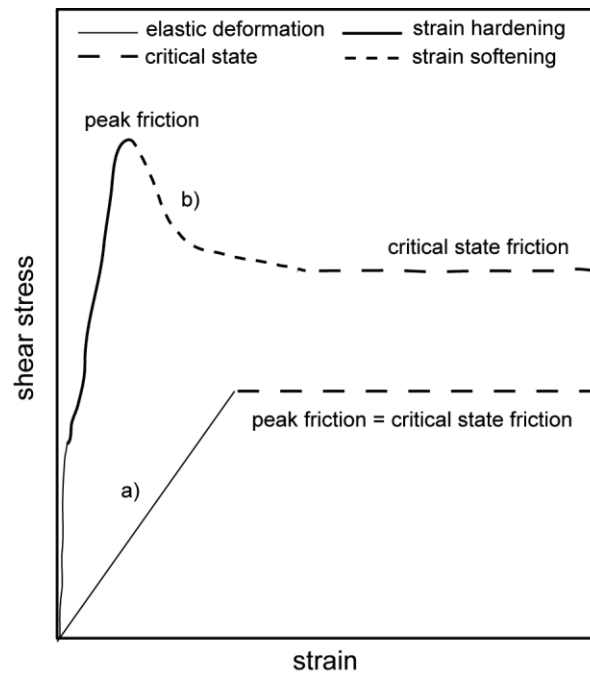


Figure 2-2: Material behavior or shear stress vs. strain curves measured in laboratory experiments are shown for (a) ideal Coulomb materials [e.g. Mandl, 1988] and (b) natural granular materials with strain hardening and softening (e.g., dry quartz sands) [Lohrmann et al., 2003].

## 2.2.2 Model generation

### 2D

We constructed a rectangular 2D numerical shear box (Figure 2-1a) based on the general settings of laboratory ring shear tests. This 2D box was constructed with stiff top and bottom walls consisting of ideal spherical particles. Similar to the rough structure of laboratory boundaries these particle arrangements simulated a comparable boundary roughness. Unbreakable bonds between these boundary particles formed rigid walls. The horizontal extension of the box was  $800\ \mu\text{m}$ , while the box height is equal to  $520\ \mu\text{m}$  and was not predefined, but rather depended on the sample size or particle number, as well as the confining stress. Opposite to the bottom wall, which remained absolutely fixed at any time, the top wall was moved in the x- and y-directions during each simulation. Both sides of the box were designated as ‘periodic walls’, where particles passing by one side were, subsequently, recreated on the opposite side (Figure 2-1a). Hence, an infinite sample, similar to a ring shear sample, was simulated without boundary effects, which allow for the simulation of large strain rates. Using this approach, the sample sizes and, therefore, the number of particles, can be reduced, which decreases the required calculation time.

Embedded within the box the numerical sample was prepared for shearing. Therefore, the ‘sediment’ sample consisted of 3,895 perfectly idealized numerical ‘silt’ particles, which were randomly and loosely generated throughout the entire box during all 5 model runs. Clastic sediments such as sand, silt, clay commonly consist of a log-normal particle distribution [Spencer, 1963; Füchtbauer, 1988; Leeder, 1999]. We also adopt a log-normal distribution with a diameter range of  $5.6\ \mu\text{m} - 20\ \mu\text{m}$ , investigating the mechanical behavior of fine and medium ‘silt’ during failure. Assuming a Mohr-Coulomb rheology, we used the coefficient of friction, as well as the contact stiffnesses and density values, which have already been successfully used to simulate dry sediments [Morgan, 1999; Kock and Huhn, 2007a]. All significant model parameters for the 2D and 3D models are listed in Table 2-1.

**Table 2-1: Model configuration and fixed properties.**

<b>Properties:</b>	<b>2D</b>	<b>3D</b>
Normal stress $\sigma_N$ [Pa]	$5 \cdot 10^6$	
Shear rate $v_S$ [ $\mu\text{m/s}$ ]	1.0	
Particle number	3,895	(small) $\sim 50,000$ (tall) $\sim 180,000$
<b><u>Particle properties</u></b>		
Normal stiffness $k_N$ [N/m]	$1 \cdot 10^9$	
Shear stiffness $k_S$ [N/m]	$1 \cdot 10^9$	
Diameter [ $\mu\text{m}$ ]	5.6 - 20	
Particle coefficient of friction $\mu_{(p)}$	0.6	

Before initiation of the shearing process, the numerical samples were compressed to simulate the natural stress conditions of a buried sediment sample. In that respect, the top wall was moved in the negative y-direction acting as a servo-mechanism. This servo built up a constant confining normal stress ( $\sigma_N$ ) of 5 MPa calculated by the forces acting on the boundary particles generating conditions comparable to previous analogue and numerical studies [Hazzard and Mair, 2003; Anthony and Marone, 2005; Kock and Huhn, 2007a]. Subsequent to the vertical servo-mechanism, a constant horizontal shear velocity ( $v_S$ ) of 1  $\mu\text{m/s}$  was applied, in the positive x-direction, thus, inducing a shear stress on the top wall (Figure 2-1a). This is a common shear velocity used in numerical and laboratory shear tests [Morgan and Boettcher, 1999; Kopf and Brown, 2003; Saffer and Marone, 2003]. The shear process was carried out at least to 200 % strain, which was calculated via the ratio of the current x-displacement of top wall versus the initial box height.

### 3D

Based on this 2D shear box setting, the 3D shear experiments were developed. For that, the 2D box was extended into the third dimension to a depth of 800  $\mu\text{m}$  to create 3D shear experiments with a quadratic x-z-base (Figure 2-1b). The 3D boxes had either a height larger than the 2D model (790  $\mu\text{m}$ ; experiment 3D<sub>tall</sub>) or a reduced height (290  $\mu\text{m}$ ; experiment 3D<sub>small</sub>). The latter configuration was employed to reduce calculation time significantly by utilizing only 50,000 particles compared to the 180,000 particles of 3D<sub>tall</sub> experiment while simultaneously testing if a lower particle limit exists to simulate a natural deformation behavior and material properties. The 3D approach required that the top and bottom walls consisted of a double layer of single, uniform spheres positioned in a body-centered cubic pattern (Figure 2-1b). Furthermore, wall rotation, as well as wall bending was excluded in the 3D experiments, similar to the assumptions applied in laboratory tests. All side walls were defined as ‘periodic’ boundaries’ just like the 2D experiments. As all information, for example stresses, were transmitted through the periodic boundaries (see above 2D settings), the side-effects of frictionless wall, observed in previous studies [Hazzard and Mair, 2003; Abe and Mair, 2005; Mair and Abe, 2011] were reduced.

All further geometrical parameters and boundary conditions, e.g., particle size, confining stress, and shear velocity, as well as physical properties, such as density, stiffnesses, and friction, were identical to those of the 2D model set-up.

### 2.2.3 Measurement techniques

Based on the DEM model approach, particle positions, contact forces, and stresses were available for all particles at each time-step. In consideration of storage capacity, we analyzed all experimental runs after every 1 % and to the point of 200 % strain (experiments 3D<sub>tall</sub>:  $\varepsilon_{\max} = 600\%$ ). We focused on the evolution of macroscopic material properties, such as the coefficient of friction  $\mu$  porosity  $\eta$ , and box height  $H$ , as well as shear band localization and thickness, as functions of the experimental settings (2D vs. 3D<sub>small</sub>, 3D<sub>tall</sub>). The coefficient of friction  $\mu$  was calculated as the ratio of shear stress  $\tau$  and normal stress  $\sigma_N$ .

$$\mu = \frac{\tau}{\sigma_N} \quad (\text{Eq. 2-1})$$

All other investigated material properties were logged by the software package directly. The porosity is determined as follows:

$$\eta = \frac{V_{\text{void}}}{V_{\text{meas}}} = \frac{V_{\text{sphere}} - V_{\text{ball}}}{V_{\text{meas}}} = 1 - \frac{V_{\text{ball}}}{V_{\text{meas}}}. \quad (\text{Eq. 2-2})$$

Where  $V_{\text{meas}}$  is the volume of measured area,  $V_{\text{void}}$  the pore volume and  $V_{\text{ball}}$  the volume of spherical particles

$$V_{\text{ball}} = \sum_{N^P} (V^P) - V^{\text{overlap}} \quad (\text{Eq. 2-3})$$

$N^P$  is the number of particles;  $V^P$  is the volume of particles and  $V^{\text{overlap}}$  the overlapping volume at contacts. The coordination number  $C_N$  gives the number of neighbor particles and is calculated by the following formula:

$$C_N = \frac{\sum_{N_B} (n_C)^{(B)}}{N_B} \quad (\text{Eq. 2-4})$$

$N_B$  is the number of particles and  $n_C$  is the number of contacts per single particle. Through the built-in measurement functions, it was possible to calculate averaged parameters in specific areas of the sheared samples (Figure 2-1) (e.g., ‘measurement circles’ in 2D and ‘measurement spheres’ in 3D described in more detail by Potyondy and Cundall [2004]). These regions can envelop a) the central portion of the sample and/ or b) specific areas, such as the thin shear zones to gain a deeper insight into the physical properties, during failure on a grain scaled level. Taking advantage of this capability, we analyzed different horizontal layers in more detail in selected model runs (e.g., experiment 3D<sub>tall</sub> below).

Shear band detection and strain localization was obtained by calculation of the gradient of motion (norm of particle displacement vector) for each particle in 2D or 3D.

$$||d_p|| = \sqrt{(d_x^2 + d_y^2 + d_z^2)} \quad (\text{Eq. 2-5})$$

Before shearing, the initial displacement vector per particle was set to zero ( $d_p^{\text{ini}} = (0, 0, 0)$ ). For visualization of shear motion, the Generic Mapping Tool (GMT) [Wessel and Smith, 1991] was used to normalize the gradients and, consequently, to distinguish the shear motion and the resultant shear bands. The shear band thicknesses were determined from these images.

Comparison of the measured parameters to analogue experiments and other numerical studies allowed for validation of the modeled results.

## 2.3 Results

### 2.3.1 Overall sample analysis

For the investigation of the dimensionality effect we carried out a series of 5 iterations for the 2D and for each of the both 3D numerical shear box setups. This implies for each run a different initial configuration of the particle assembly.

The focus in these experiments was primarily on the physical properties of bulk coefficient of friction, porosity, and deformation behavior of the numerical ‘sediment’ during shear strain. The experimental findings and their variation in the physical properties are summarized in (Table 2-2).

**Table 2-2: Summarized results of all shear experiments and its variation. Bold marked results belong to the 3D<sub>tall</sub>\* exception where the shear zone developed at the fixed bottom.**

<b>Properties:</b>	<b>2D</b>	<b>3D<sub>small</sub></b>	<b>3D<sub>tall</sub></b>	
$\mu_{\text{peak}}$	$0.44 \pm 0.04$	$0.56 \pm 0.02$	0.57	
$\mu_{\text{crit}}$	$0.29 \pm 0.01$	$0.28 \pm 0.01$	$0.19 \pm 0.01$	<b>0.35</b>
$\mu_{\text{peak, layer}}$ (top, mid, bot)	-	$0.61 \pm 0.06$	$0.57 \pm 0.01$	<b>0.58</b>
		$0.62 \pm 0.06$	$0.58 \pm 0.01$	<b>0.58</b>
		$0.63 \pm 0.07$	$0.57 \pm 0.01$	<b>0.55</b>
$\eta$ ( $\varepsilon = 200\%$ )	$0.16 \pm 0.01$	0.38	0.35	<b>0.37</b>
$\eta_{\text{layer}}$ (top, mid, bot; $\varepsilon = 200\%$ )	-	$0.41 \pm 0.04$	$0.36 \pm 0.01$	<b>0.35</b>
		$0.37 \pm 0.02$	0.35	<b>0.35</b>
		$0.36 \pm 0.02$	$0.36 \pm 0.01$	<b>0.40</b>
Shear zone thickness [ $\mu\text{m}$ ]	$203 \pm 70$	$70 \pm 4$	$92 \pm 5$	<b>237</b>
Shear zone thickness (d50%)	$32 \pm 11$	$11 \pm 1$	$14 \pm 1$	<b>37</b>

Generally, all experimental setups showed that the analyses of the bulk friction coefficient during shearing revealed characteristic friction curve shapes. These started with an elastic linear increase and further grew by the period of strain hardening. Afterwards, with increasing strain, the peak friction  $\mu_{\text{peak}}$  developed and subsequently the decreasing friction coefficient was described by strain softening. After that process, the friction coefficient passed over into a critical state of stable friction  $\mu_{\text{crit}}$  in 2D and 3D<sub>small</sub> experiments (Figure 2-3a).



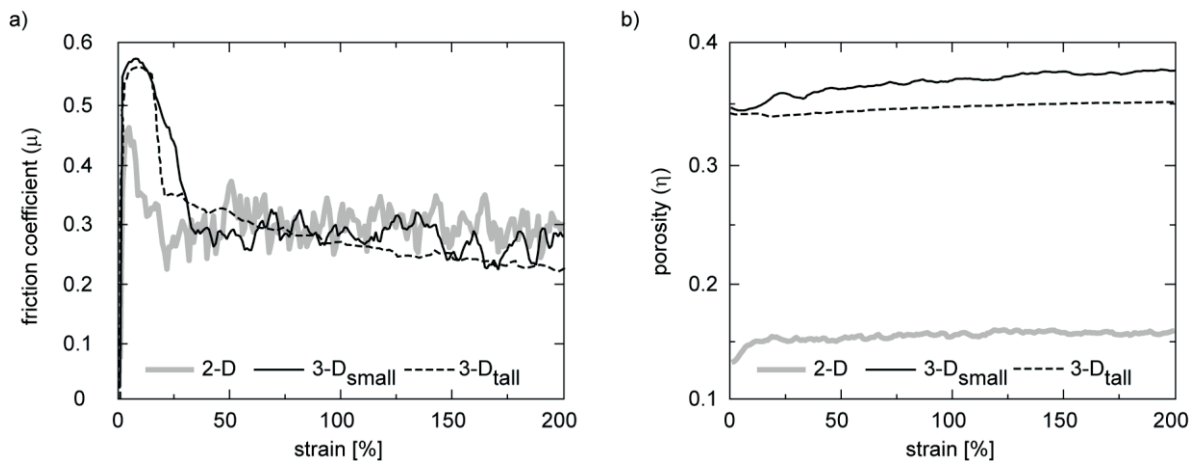


**Figure 2-3: Averaged material parameters measured for the entire sheared sample are shown. Friction (a) and porosity (b) versus overall shear strain is displayed for the 2D and 3D models.**

In the 2D experiments, the peak frictions occurred at the point of  $\mu_{\text{peak}} = 0.44 \pm 0.04$ . The hardening in advance and the softening part afterwards are characterized by strong increases and decreases, respectively. In contrast, the hardening and softening processes in the 3D experiments are not formed so steep. Thereby, both 3D experiments showed an equal peak friction coefficient in 3D<sub>small</sub> ( $\mu_{\text{peak}} = 0.56 \pm 0.02$ ) and 3D<sub>tall</sub> ( $\mu_{\text{peak}} = 0.57$ ) that obviously exceeded the mean peak value of the friction coefficient in 2D. After the strain softening, the 2D friction coefficient strongly fluctuated. This results in a mean critical state value that was the same  $\mu_{\text{crit}} \sim 0.3$  as for the 3D<sub>small</sub> experiment. Nonetheless, both critical state curves differ regarding the amplitude and frequency of the fluctuations. Thereby, noticeable stronger and more frequent fluctuations were observed for the 2D experiment. In comparison, the larger 3D<sub>tall</sub> series showed after the strong softening a second period of lower softening. For the large model setup no obvious fluctuations were observed during the entire shear deformation.

With progressed shear deformation we observed changes in the bulk porosity. In general, an increasing porosity was observed during the deformation. Thereby the initial porosity for the 2D setup was lower than for the 3D experiments. Even a comparison of all experiment series showed that the average 2D porosity for the point of  $\varepsilon = 200\%$  was significantly lower ( $\eta = 0.16 \pm 1$ ) than for the 3D<sub>small</sub> ( $\eta = 0.38$ ) and the 3D<sub>tall</sub> ( $\eta = 0.35$ ) experiments.

The relative particle motion, as an indicator for the failure plane evolution, revealed the influence of dimensionality on geometry and localization of the shear zones (Figure 2-4). Particularly, the shear band position inside the samples differed between 2D and 3D experiments. In the 2D experiments, all shear bands were located at the shear box bottom while in the 3D<sub>small</sub> experiments the upper sample portion failed just below the moved wall. In the 3D<sub>tall</sub> experiments the shear band was observed at the upper and lower part of the shear box. In the following, the 3D<sub>tall</sub> experiment where the shear band was formed close to the fix wall is termed as 3D<sub>tall</sub>\*.

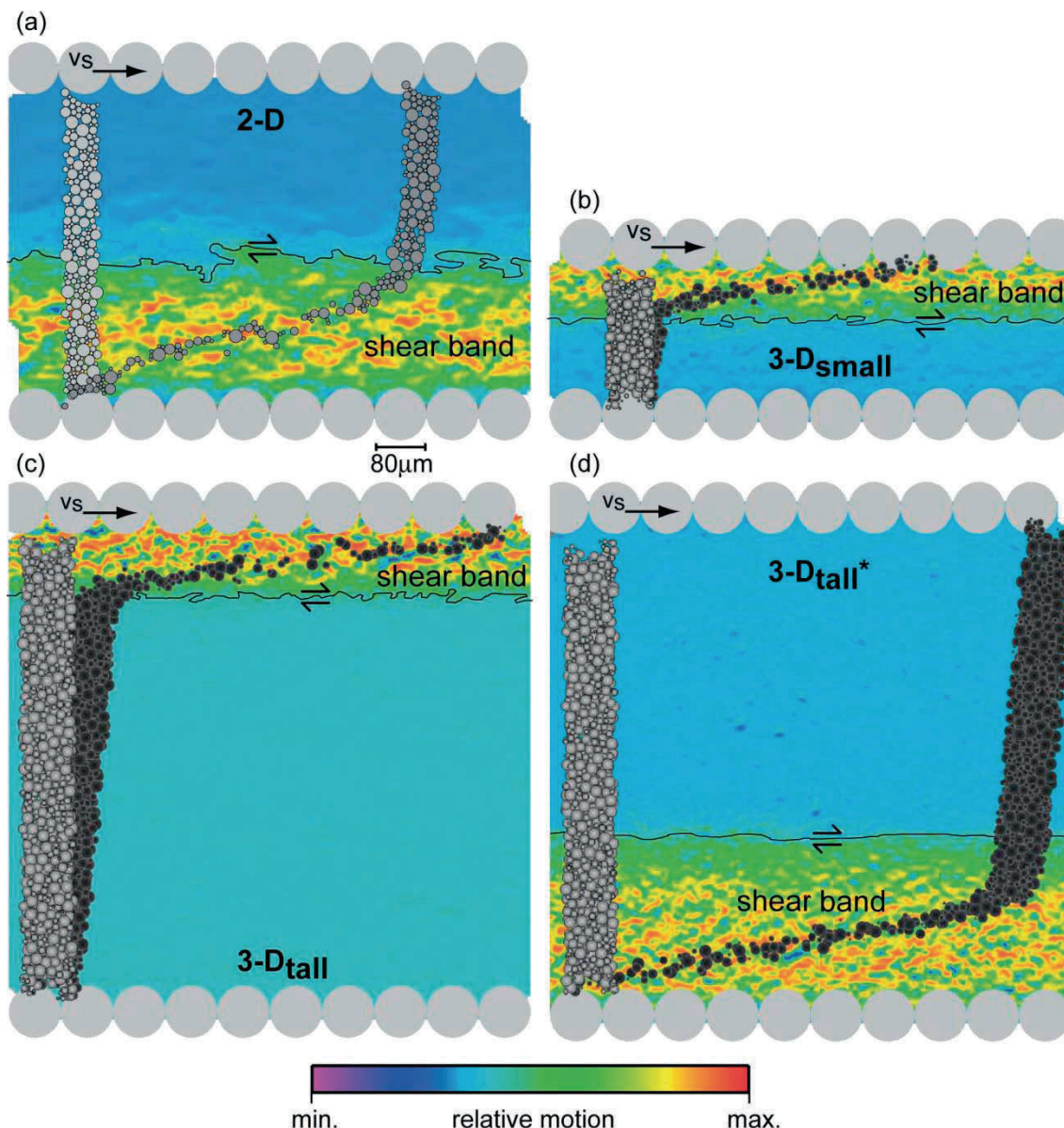


Figure 2-4: Normalized displacement gradient after 200 % shear strain is shown for the 2D experiment, as well as along vertical slices cutting through the central portion of the sheared sample in the 3D<sub>small</sub> and 3D<sub>tall</sub> models. Warm color tones signify high relative offset between neighboring particles, whereas cold tones signify low relative displacements.

A dimensionality effect on the shear band thickness had been observed in all experimental setups (Figure 2-4). Vertical aligned passive markers of grey-colored particles illustrated the internal sample deformation. At low strain rates before the peak is reached the entire samples were deformed. Simple shear dominated this time period. With the formation of the peak friction coefficients the shear zones developed. From now on the passive markers were characterized by a curved shape. While the shear zone was continuously stretched the remaining sample part was almost unaffected by the particle shear movement.

At the point of 200 % strain, stable, well-pronounced, and wide shear bands of  $203 \pm 70 \mu\text{m}$  thickness had been developed in the 2D experiments. That is equal to  $32 \pm 11$  particles of a mean diameter ( $32 \pm 11 d_{50\%}$ ). In contrast, the shear bands in the 3D experiments were significantly thinner. For the 3D<sub>small</sub> experiment, a stable shear band thickness of  $70 \pm 4 \mu\text{m}$

was determined and conformed to  $11 \pm 1 d_{50\%}$ . A mean shear band thickness of  $92 \pm 5 \mu\text{m}$  ( $14 \pm 1 d_{50\%}$ ) was observed for the  $3D_{\text{tall}}$  experiments.

### 2.3.2 Effect of the shear zone localization

Only in the  $3D_{\text{tall}}$  experiments including the case of  $3D_{\text{tall}}^*$  the shear bands occurred at the top and bottom part of the same shear box setup. In this study it is shown that for this case both types of top and bottom shear band localization in  $3D_{\text{tall}}$  underlie different physical response (Figure 2-5). In the  $3D_{\text{tall}}^*$  experiment no period of secondary strain softening was observed. Additionally, a larger stable critical state friction coefficient  $\mu_{\text{crit}}^* = 0.35$  was formed. Another variation was observed for the porosity in the  $3D_{\text{tall}}$  experiments (Figure 2-5). Instead of a curved parameter increase as it was observed for the  $3D_{\text{tall}}$  experiments the  $3D_{\text{tall}}^*$  experiment showed a linear increase in porosity.

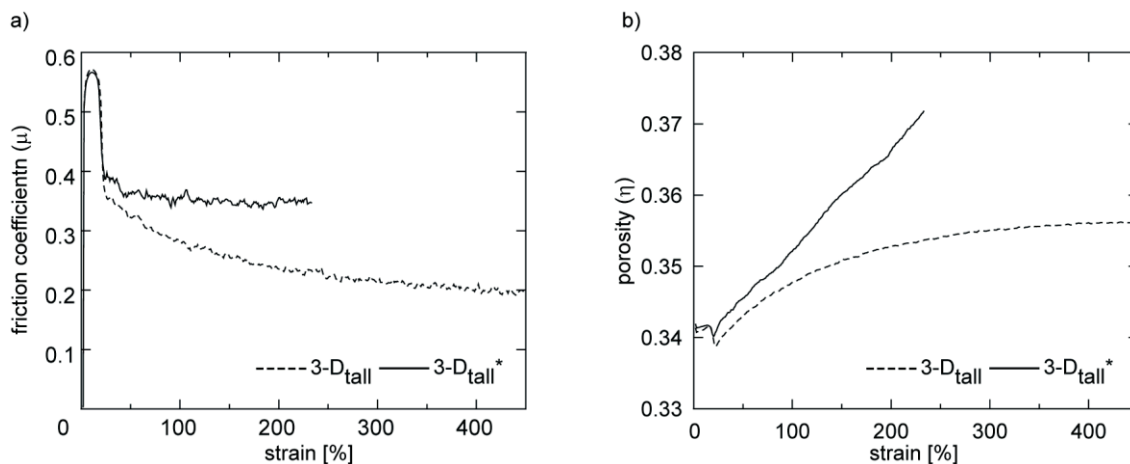


**Figure 2-5: Comparison of  $3D_{\text{tall}}$  vs.  $3D_{\text{tall}}^*$  experiments. The illustration shows the bulk friction coefficient (a) and the bulk porosity (b).**

More findings regarding the detailed vertical observation of the shear zone localization in the  $3D_{\text{tall}}$  experiments are shown in Figure 2-6. The subdivision of the sample into three horizontally aligned layers allowed for a more accurate shear zone investigation. For the  $3D_{\text{tall}}$  experiments the friction coefficient within the layers distinguished from each other in the second period of softening and in the amplitude of fluctuations. Thereby, the strongest softening effect was observed for the middle layer whereas the top layer containing the shear zone showed the lowest influence. Furthermore, the amount of fluctuations inside the layers decreased with the distance from the shear zone. At the top layer the largest fluctuations were observed and they were reduced in the middle part of the samples. For the bottom layer almost no fluctuations were found. In contrast, the layers of the  $3D_{\text{tall}}^*$  behaved all the same. No separation in the softening behavior has been observed. Nonetheless, the same amplitude in the fluctuations within the layers was detected. Altogether, the  $3D_{\text{tall}}^*$  experiment showed a more homogenous behavior regarding the friction coefficient in the different subdivisions whereas in the  $3D_{\text{tall}}$  experiments a separation of the friction coefficient was observed.

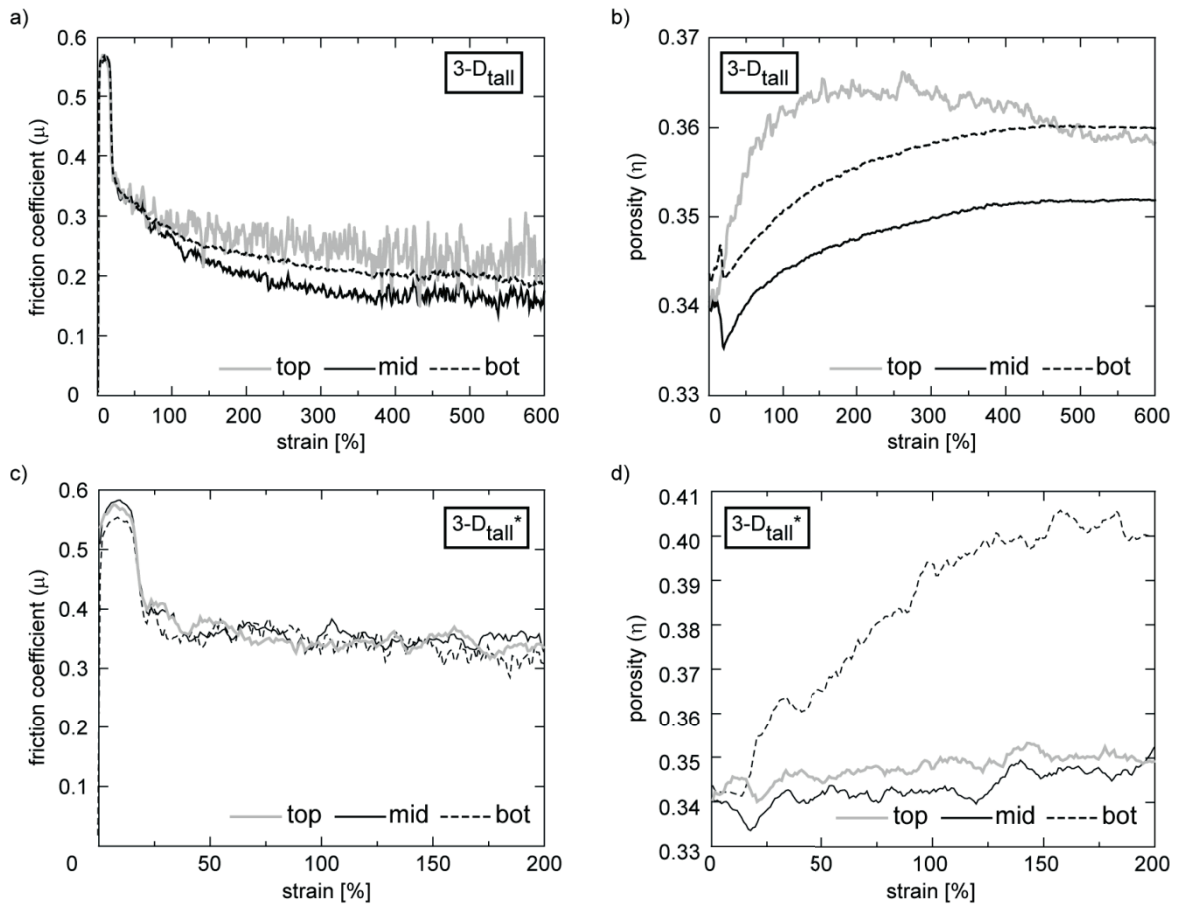


**Figure 2-6: A detailed illustration of horizontal layers outcomes regarding the coefficient of friction and the porosity of the  $3D_{tall}$  and  $3D_{tall}^*$  experiment.**

The consideration of the porosity within the layers also revealed strong variation between the behaviors of the different located shear zones (Figure 2-6). In both experiments the layers that contain the shear zone behaved different. The increase in porosity inside the shear zone layers was significantly larger than in the other layers. A comparison of both shear zone containing layers revealed that a larger porosity increase was detected for the  $3D_{tall}^*$  experiment. Nevertheless, further variations in the porosity behavior have been found in the layers without the shear zone. In the  $3D_{tall}$  experiment a smooth curve shape without fluctuations were found. Whereas in the  $3D_{tall}^*$  experiment all three layers signified fluctuations.

## 2.4 Discussion

### 2.4.1 General

In all experiments, a typical elasto-plastic material behavior and characteristic strain hardening/ softening effects were observed before and after peak friction. This behavior is typical for dense particle assemblies due to the irreversible deformation processes between single grains [Mitchell and Soga, 2005] and corresponds with observations from studies on sediments [e.g., Lohrmann et al., 2003]. However, the peak strength in the 3D numerical experiments was more pronounced compared to the 2D shear tests. Such an increase of the hardening and softening has also been observed with increasing packing density in lab shear tests [Lohrmann et al., 2003]. A similar increase in peak friction was found numerically by

Kock and Huhn [2007a] and Guo and Morgan [2004], who postulated that the important factor for peak strength was particle friction and particle shape. However, as such particle parameters and model boundary conditions were constant between our 2D and 3D experiments, the assumption can be made that particle packing could also be an important factor in controlling the peak friction [Thornton, 2000; Schöpfer et al., 2009]. The analysis of the coordination numbers (see the following section) showed an increase in the number of particle contacts, and hence, an increasing packing density in 3D, which was assumed as a controlling factor for hardening/ softening behavior. So, the initial porosity and the number of particle contacts were lower in 2D and resulted in a lower internal packing. Whereas in both 3D experiments, the internal packages were equal and lead to similar, but higher peak frictions (Figure 2-3a, 3b).

#### 2.4.2 Measured material properties as a function of dimensionality 2D vs. 3D

For natural quartz sand, the peak coefficient of friction ranges between 0.6 and 1.2 [Mitchell and Soga, 2005]. Our 2D experiment exhibited friction values that were out of this range and significantly lower. In contrast, those values of the 3D experiments were larger and closer to the lower end of this natural range. Similar relationships between dimensionality and material friction have been observed using laboratory [Frye and Marone, 2002; Mair et al., 2002] and numerical approaches [Morgan, 1999; Hazzard and Mair, 2003]. A potential explanation for this effect could be that material friction depends on particle shape and, subsequent, particle interlocking, as well as on the rolling and sliding effects [Mitchell and Soga, 2005]. The latter has already been evaluated by 2D numerical experiments, which revealed a decrease in peak friction with an increasing roll effect. Different approaches resulted in an increase in the rolling resistance by damping of the rotational velocities [Morgan, 1999], using non-spherical particles [Guo and Morgan, 2004], or modifying the contact law [Iwashita and Oda, 1998]. However, in the present study, as we utilized identical grain size distributions of ideal spherical particles in both 2D and 3D experiments, this effect was negligible. The model extension from 2D into the third dimension caused an increase in the mean particle contact numbers, 3.27 for 2D and 4.11 for 3D, which, increased the particle interlocking resulting in an increase in the averaged material friction. Therefore, the larger number of contacts in 3D, caused an increase in the interlocking of particles compared to 2D as previously suggested by Hazzard and Mair [2003]. The importance of particle interlocking for controlling the magnitude of peak friction or shear strength of the material has already been identified for natural dense sand [Mitchell and Soga, 2005].

Both  $3D_{\text{small}}$  and  $3D_{\text{tall}}$  experiments had the same sample settings and boundary conditions, which resulted in identical mean coordination numbers and stress conditions, as well as similar magnitudes of particle-interlocking. Consequently, the fact that the peak frictions were identical supports our hypothesis that this parameter is controlled by particle interlocking.

The critical state friction found in the 2D and  $3D_{\text{small}}$  experiments matches to previous studies [Morgan, 1999; Aharonov and Sparks, 2002; Kock and Huhn, 2007a]. Surprisingly, an increase in the particle number, and hence, in the shear box height had reduced the critical state friction in the  $3D_{\text{tall}}$  experiments (except of  $3D_{\text{tall}}^*$ ). Thereby, the critical state friction typically appear independent of the stress history and in particular of the initial microstructure due to the fact that the sample is destructured before the critical state is achieved [Mitchell and Soga, 2005]. For this reason the shearing resistance, and thus, the critical state friction generally depends on the sample composition and the effective stresses [Mitchell and Soga, 2005]. In the 2D and 3D experiments the sample composition and the effective stresses

should be identical due to the predefined particle size distribution and the same applied boundary forces.

Another concept to explain the critical state friction values concentrates on the particles participating in the shear process. While in the hardening process the passive strain markers showed simple shear behavior for the entire sample - subsequently with the peak friction the shear band was initiated and the passive markers bended. At this point the shear effect, which was applied with the moved wall, was only transferred to the particles inside the shear band. The remaining particles were not considered during the further deformation. For that reason the ratio of affected particles and non-affected particles is crucial. Consequently, the ratio of the shear band thickness and the sample thickness has to take into account to assess the critical state friction. In turn, the friction during the critical state gives the indication how many sample particles are involved in the shearing process and formed the shear band.

In these experiments the porosity observations showed a large deviation between the 2D and the 3D experiments (Figure 2-3). The main reason is the reduction of the dimensionality in 2D that regarded the particle assembly only on a plane state. Furthermore, the 2D and the 3D experimental setups are restricted in the volume dilation which is only allowed in the vertical direction perpendicular to the shearing. In dense granular material the formation of a shear band during the shearing process requires a loosening of the rigid contacts, and hence, a dilation of the sample volume to provide an increasing mobility regarding the shearing for single particles [Mitchell and Soga, 2005]. Thus, the microstructure of the particle assembly is changed in order to increase the particle mobility for shearing.

The applied particle properties derived from the round particle shape [Collins and McGown, 1974; Mitchell and Soga, 2005] and the log normal particle size distribution [Spencer, 1963; Füchtbauer, 1988; Leeder, 1999] observed for silty sediments simulated a 3D porosity similar to laboratory observations according to silt loaded with the same confining stress [Fawad et al., 2010]. In 2D the strong porosity increase at the beginning appeared from the shear zone development, and thus, from the according bulk particle dilation. In 3D an additional effect of a porosity decrease occurred during the friction softening. It is assumed that the shear band dilation required space that cannot enough provided by the servo-mechanism. For that reason the shear zone in the clamped sample is dilative and simultaneously behaves compressive to the remaining sample.

In Figure 2-3, a stronger increase in the porosity is shown for the 3D<sub>small</sub> experiment although the shear band thickness in the 3D<sub>tall</sub> experiment is larger. In general, the thicker the shear band the more additional pore space will be available during the formation of the shear band. The reason for this behavior lies in the observation of the entire initial sample height. That also implies the consideration of the particles out of the shear band. Because the proportion of the particles involved in the shear band relative to the remaining particles is larger for the 3D<sub>small</sub> experiment a stronger effect in the variation of the porosity was measured. Consequently, these values do not conform to the absolute values regarding the dilation of the upper wall.

### **2.4.3 Shear band localization and shear band thickness as a function of dimensionality 2D vs. 3D**

The position of shear bands within the DEM shear experiments and their thicknesses were different with dimensionality (Figure 2-4). However, the influences caused by particle shape

[Kock and Huhn, 2007b] and particle distribution [Saltzer and Pollard, 1992; Morgan and Boettcher, 1999], observed in prior numerical shear experiments, were neglected because we used identical grain size distributions and grain shapes in all of our 2D and 3D experiments.

The shear bands were formed at the shear box bottom, close to the fixed wall, in our 2D experiments. In contrast, most of the shear bands evolved close to the sheared wall in our 3D experiments. This is in accordance with both, laboratory ring shear tests on natural sands [Sadrekarimi and Olson, 2010], as well as in numerical shear tests [Mair and Abe, 2008]. The only exception was observed for the 3D<sub>tall</sub> setup. The fact that in the 3D<sub>tall</sub> series both cases of top and bottom shear zone formation occurred allowed us for the direct investigation of this effect. Both model iterations differed significantly in their physical behavior. When the shear zone was formed at the bottom the sample easier resist to the progressed shear deformation after the shear zone was formed. This is possibly supported by the circumstances that the distribution of the friction coefficient is homogenously inside the sample (Figure 2-6). In contrast the standard 3D<sub>tall</sub> experiments showed a vertical separation of the friction coefficient, and hence, local areas of lower strength. A potential reason for this special behavior can be assumed in the initial particle configuration that significantly determined the relation of initial and ongoing particle interlocking.

The strong relative particle movement within the shear zone led to a sample dilation. The explanation for this behavior is that densely packed particles require free spaces to move. We observed for the 3D<sub>tall</sub> experiments the larger the shear zone thickness the larger the porosity increase (Figure 2-5b). The large linear increase of experiment 3D<sub>tall</sub><sup>\*</sup> is the result of a continuously grew of the shear zone.

Laboratory measurements suggest that the shear zone thickness depends on the mean grain diameter [Vardoulakis *et al.*, 1978] which functioned as a scale parameter and allow for a comparison of the shear zone thickness that differ in size and dimensionality. Accordingly, the shear band thickness of our 2D experiment, which was  $32 \pm 11$  times the mean particle size. This value is a bit larger compared to other 2D DEM biaxial tests [Bardet and Proubet, 1991; Oda and Iwashita, 2000], which showed thicknesses of 15-20 times the mean particle diameter. Furthermore, laboratory tests showed a shear band formation with 7-15 times the mean grain diameter with simplified '2D' plane strain conditions [Vardoulakis, 1980; Oda *et al.*, 1998]. Our 3D experiments offered ratios that fitted into this range with values of  $11 \pm 1$  (3D<sub>small</sub>),  $14 \pm 1$  (3D<sub>tall</sub>). For the 3D<sub>tall</sub><sup>\*</sup> experiment a value of 37 (3D<sub>tall</sub><sup>\*</sup>) times the mean particle diameter was found that is very similar to the 2D experiments. It can be assumed that the localization of the shear zone also affected the geometry, and thus, the shear zone thickness. Unfortunately, no data from 3D lab experiments are available to quantify, compare, and evaluate these observations. Consequently, these parameters and correlations cannot be transferred to natural conditions, hence, we are not in a position to quantify the applicability of 2D vs. 3D experiments for investigation of shear zone thicknesses.

#### 2.4.4 Effects of model size or particle number on deformation behavior of granular materials 3D<sub>small</sub> vs. 3D<sub>tall</sub>

The comparison of our 3D shear box experiments revealed that model size or simulated particle number within the sheared sample controls the fluctuations in the measured material properties. A similar correlation between parameter fluctuation and the number of considered particles, as well as strain, has already been observed and shows that the higher the number of considered particles, the lower the fluctuation [Mitchell and Soga, 2005]. These authors

assumed that for natural granular materials the slip of single contacts is masked by the behavior of the mass as a whole. This correlates with observations from our experiment  $3D_{\text{tall}}$ . Additionally, erratic fluctuations were also observed for natural materials by Barton and Procter [1974], who initially showed that the erratic fluctuation behavior of displaced connected particle surfaces appears for individual contacts in mineral friction measurements.

Our more detailed analyses of single horizontal layers during shearing showed a distinct inhomogeneity of the material behavior, such as friction and porosity along the vertical axis between single layers. In both 3D experiments, the behavior of the layer, including the shear band and the failure plane, behaved in contrast to the remaining minor deformed layers. Additionally, upper layers, which exhibited the largest strain and localized deformation, showed the largest fluctuations in material parameters.

These facts showed that the investigation of the entire shear box offered only a mean value of the minor- and majorly -deformed volumes. For the detailed investigation of material decoupling, a separate consideration of minor- and majorly -deformed material behavior is necessary to determine the discrepancy, and hence, highlight the behavior on the shear plane.

The applied calculation of the average friction coefficient of particle stress tensors is an advantage of numerical simulation over laboratory measurements. Using the average friction coefficient allow for involving particles located in central and marginal shear box position whereas laboratory measurements are mean values and restricted on total shear stress at the boundary driving wall. This fact makes a direct one-to-one comparison of both systems impossible. Nevertheless the average friction coefficient gives a more accurate state of the inner stress than the boundary measurement approach of laboratory studies. This is supported by our observation of vertically varying friction coefficient of particle packing that exhibited the heterogeneous nature inside the sample. However, for a general rough comparison of the stress development within laboratory and numerical investigations the used approach is applicable.

## 2.5 Conclusion

In this study, the material response of identical 2D and 3D numerical DEM ring shear experiments is compared. It is demonstrated that with both dimensional settings an elasto-plastic material behavior with strain hardening and softening was simulated. Furthermore, this study exposed the effects of dimensionality on the physical material properties, such as the coefficient of friction, in particular, the peak friction and the critical state friction, as well as the porosity and the shear band localization. For the 2D experiments a lower peak friction was determined compared to the 3D experiments. Therefore, the dimensionality was identified as a factor influencing the peak friction. Nonetheless, the 3D experiments allowed the conclusion that the peak friction appeared independent of the model size ( $3D_{\text{small}}$ ,  $3D_{\text{tall}}$ ) and the shear zone localization ( $3D_{\text{tall}}$ ,  $3D_{\text{tall}}^*$ ). In contrast, the 3D experiments revealed a dependency of the critical state friction on the model size and the shear band localization. In the  $3D_{\text{tall}}$  experiments the ratios of the shear zone thickness to the sample thickness are lower than in 2D,  $3D_{\text{small}}$ , and  $3D_{\text{tall}}^*$ . We postulate that there exist a direct relation regarding the critical state of friction and the ratio of particles which participated at the shearing process and the particles that are not affected by the shearing.



In addition, we point out the controlling effect of dimensionality on the porosity. We found obviously lower porosity values in 2D. On the other side, the 3D porosity values fitted well to laboratory outcomes of laboratory studies.

## Acknowledgements

We wish to thank S. Abe for helpful discussions. We also wish to thank, L. Wenk, B. Flaim and L. Podszun for assistance. This work was funded through DFG-Research Center / Excellence Cluster “The Ocean in the Earth System”.

## References

- Abe, S., and K. Mair (2005), Grain fracture in 3D numerical simulations of granular shear, *Geophysical Research Letters*, 32(L05305), 1-4.
- Abe, S., and K. Mair (2009), Effects of gouge fragment shape on fault friction: New 3D modelling results, *Geophysical Research Letters*, 36(L23302), 1-4.
- Aharonov, E., and D. Sparks (1999), Rigidity Phase Transition in Granular Packings, *Physical Review E*, 60(6), 6890-6896.
- Aharonov, E., and D. Sparks (2002), Shear profiles and localization of granular materials, *Physical Review E*, 65(051302), 1 - 12.
- Anthony, J. L., and C. Marone (2005), Influence of particle characteristics on granular friction, *Journal of Geophysical Research*, 110(B08409), doi:10.1029/2004JB003399.
- Bardet, J. P., and J. Proubet (1991), A numerical investigation of the structure of persistent shear bands in granular media, *Geotechnique*, 41(4), 599-613.
- Biegel, R. L., C. G. Sammis, and J. H. Dieterich (1989), The frictional properties of a simulated fault gouge having a fractal particle size distribution, *Journal of Structural Geology*, 11(7), 827 - 846.
- Collins, K., and A. McGown (1974), The form and function of microfabric features in a variety of natural soils, *Geotechnique*, 24, 223-254.
- Cundall, P. A., and O. D. L. Strack (1978), BALL - A program to model granular media using the distinct element method, in *Technical Note, Advanced Technology Group*, edited, Dames and Moore, London.
- Cundall, P. A., and O. D. L. Strack (1979), A discrete numerical model for granular assemblies, *Geotechnique*, 29(1), 47-65.
- Fawad, M., N. H. Mondol, J. Jahren, and K. Bjørlykke (2010), Microfabric and rock properties of experimentally compressed silt-clay mixtures, *Mar Petrol Geol*, 27(8), 1698-1712.
- Frye, K. M., and C. Marone (2002), The effect of particle dimensionality on granular friction in laboratory shear zones, *Geophysical Research Letters*, 29(19), 1916-1919.

- Füchtbauer, H. (Ed.) (1988), *Sedimente- und Sedimentgesteine*, 1141 pp., E.Schweizbart'sche Verlagsbuchhandlung, Stuttgart.
- Guo, Y., and J. K. Morgan (2004), Influence of normal stress and grain shape on granular friction: Results of discrete element simulations, *Journal of Geophysical Research*, 109(B12305), 1-16.
- Guo, Y., and J. K. Morgan (2007), Fault gouge evolution and its dependence on normal stress and rock strength - results of discrete element simulations: Gouge zone properties, *Journal Of Geophysical Research*, 112(B10403), 1-17.
- Hazzard, J. F., and K. Mair (2003), The importance of the third dimension in granular shear, *Geophysical Research Letters*, 30(13), 1708-1711.
- Itasca (2004), PFC 2D 3.1 Manual, edited, Itasca Consulting Group, Inc., Minneapolis.
- Itasca (2005), PFC 3D 3.1 Manual, edited, Itasca Consulting Group, Inc., Minneapolis.
- Iwashita, and Oda (1998), Rolling Resistance at Contacts in Simulation of Shear Band Development by DEM, *Journal of Engineering Mechanics*, 124(3), 285-292.
- Kock, I., and K. Huhn (2007a), Influence of particle shape on the frictional strength of sediments - A numerical case study, *Sediment Geol*, 196(1-4), 217-233.
- Kock, I., and K. Huhn (2007b), Numerical investigation of localization and micromechanics in a stratified soil specimen, *Journal of Structural Geology*, 29(10), 1679 - 1694.
- Kopf, A., and K. M. Brown (2003), Friction experiments on saturated sediments and their implications for the stress state of the Nankai and Barbados subduction thrusts, *Mar Geol*, 202(3-4), 193-210.
- Kuhn, M. R. (2010), Micro-mechanics of fabric and failure in granular materials, *Mechanics of Materials*, 42(9), 827-840.
- Leeder, M. (1999), *Sedimentology and Sedimentary Basins - From turbulence to tectonics*, 608 pp., Blackwell Publishing, Oxford.
- Lohrmann, J., N. Kukowski, J. Adam, and O. Oncken (2003), The impact of analogue material properties on the geometry, kinematics, and dynamics of convergent sand wedges, *Journal of Structural Geology*, 25(10), 1691-1711.
- Mair, K., and C. Marone (1999), Friction of simulated fault gouge for a wide range of velocities and normal stresses, *J. Geophys. Res.*, 104(B12), 28899-28914.
- Mair, K., and J. F. Hazzard (2007), Nature of stress accommodation in sheared granular material: Insights from 3D numerical modeling, *Earth and Planetary Science Letters*, 259(3-4), 469-485
- Mair, K., and S. Abe (2008), 3D numerical simulation of fault gouge evolution during shear: Grain size reduction and strain localization, *Earth and Planetary Science Letters*, 274(1-2), 72-81.
- Mair, K., and S. Abe (2011), Breaking Up: Comminution Mechanisms in Sheared Simulated Fault Gouge, *Pure Appl. Geophys.*, 1-12.

- Mair, K., K. M. Frye, and C. Marone (2002), Influence of grain characteristics on the friction of granular shear zones, *Journal of Geophysical Research*, 107(B10), 2219-2227.
- Mandl, G. (1988), *Mechanics of Tectonic Faulting: Models and Basic Concepts*, Elsevier, Amsterdam.
- Marone, C., and C. H. Scholz (1989), Particle-size distribution and microstructures within simulated fault gouge, *Journal of Structural Geology*, 11(7), 799-814.
- Mitchell, J. K., and K. Soga (2005), *Fundamentals of Soil Behaviour*, 3rd ed., 577 pp., John Willey & Sons, Hoboken, New Jersey.
- Mora, P., and D. Place (1999), The Weakness of Earthquake Faults, *Geophysical Research Letters*, 26.
- Morgan, J. K. (1999), Numerical simulations of granular shear zones using the distinct element method 2. Effects of particle size distribution and interparticle friction on mechanical behavior *Journal of Geophysical Research*, 104(B2), 2721-2732.
- Morgan, J. K., and M. S. Boettcher (1999), Numerical simulations of granular shear zones using the distinct element method 1. Shear zone kinematics and the micromechanics of localization *Journal of Geophysical Research*, 104(B2), 2703-2719.
- Oda, M., and K. Iwashita (2000), Study on couple stress and shear band development in granular media based on numerical simulation analyses, *International Journal of Engineering Science*, 38(15), 1713-1740.
- Oda, M., H. Kazama, and J. Konishi (1998), Effects of induced anisotropy on the development of shear bands in granular materials, *Mechanics of Materials*, 28(1-4), 103-111.
- Place, D., and P. Mora (2000), Numerical Simulation of Localization Phenomena in a Fault Zone, *Pure Appl. Geophys.*, 157, 1821 - 1845.
- Potyondy, D. O., and P. A. Cundall (2004), A bonded-particle model for rock, *International Journal of Rock Mechanics & Mining Sciences*, 41, 1329-1364.
- Rechenmacher, A. L. (2006), Grain-scale processes governing shear band initiation and evolution in sands, *Journal of the Mechanics and Physics of Solids*, 54(1), 22-45.
- Sadrekarami, A., and S. M. Olson (2010), Shear Band Formation Observed in Ring Shear Tests on Sandy Soils, *Journal of Geotechnical and Geoenvironmental Engineering*, 136(2), 366-375.
- Saffer, D. M., and C. Marone (2003), Comparison of smectite- and illite-rich gouge frictional properties: application to the updip limit of the seismogenic zone along subduction megathrusts, *Earth and Planetary Science Letters*, 215(1-2), 219-235.
- Saltzer, S. D., and D. D. Pollard (1992), Distinct element modeling of structures formed in sedimentary overburden by extensional reactivation of basement normal faults, *Tectonics*, 11(1), 165-174.
- Schöpfer, M. P. J., S. Abe, C. Childs, and J. J. Walsh (2009), The impact of porosity and crack density on the elasticity, strength and friction of cohesive granular materials: Insights from DEM modelling, *International Journal of Rock Mechanics and Mining Sciences*, 46(2), 250-261.

- Spencer, D. W. (1963), The Interpretation of grain size distribution curves of clastic sediments, *Journal of Sedimentary Petrology*, 33(1), 11.
- Thornton, C. (2000), Numerical simulation of deviatoric shear deformation of granular media, *Geotechnique*, 50(1), 43-53.
- Vardoulakis, I. (1980), Shear band inclination and shear modulus of sand in biaxial tests, *International Journal for Numerical and Analytical Methods in Geomechanics*, 4(2), 103-119.
- Vardoulakis, I., M. Goldscheider, and G. Gudehus (1978), Formation of shear bands in sand bodies as a bifurcation problem, *International Journal for Numerical and Analytical Methods in Geomechanics*, 2(2), 99-128.
- Wessel, P., and W. H. F. Smith (1991), Free software helps map and display data, *EOS Trans. AGU*, 72, 441.

### 3 Chapter Three

#### (Manuscript 2)

Prepared to submit to

#### Geophysical Research Letters

## Strength analysis as a function of granular sediment fabrics

Lutz Torbahn<sup>1,\*</sup>, Katrin Huhn<sup>1</sup>

<sup>1</sup> MARUM – Center for Marine Environmental Sciences and Faculty of Geosciences, University of Bremen, Leobener Str., D-28359 Bremen, Germany

\* Corresponding author: Phone +49(0)421 218 65866 Fax +49(0)421 218 65872

E-mail: ltorbahn@marum.de

### Abstract

[1] We present a new numerical analysis procedure using the Discrete Element Method (DEM) for investigating the influence of grain shape and microstructure of grain-to-grain behavior on sediments strength. The DEM was used to construct a three-dimensional direct shear test to determine the frictional strength of three granular grain shape end-members, such as spheres, rods, and plates, that approximate numerical ‘silt’ and ‘clay’ on a micro-scale. It was shown that an increase in grain shape complexity caused an increase in frictional strength. In doing so, the frictional strength is based on the stresses at the particle contacts and the number and shape of grain-to-grain contacts which are most likely indicative of the contact area. By observing the contact area, a topological classification of the grain microstructure into point, edge and face contacts was possible. In this study, it was shown that the fundamental structure of contact types is essential for evaluating the frictional response.

**Keywords:** direct shear test, DEM, shear strength, grain shape, fabric, 3D modeling

### 3.1 Introduction

[2] The shear strength, as an elementary attribute of sedimentary systems, controls natural deformation processes, such as failure zones. Numerous studies suggest that the shear strength, particularly the coefficient of friction, is affected by the sediment composition and texture [Krantz, 1991; Marone, 1998; Saffer *et al.*, 2001; Kopf and Brown, 2003; Ask and

*Kopf*, 2004]. Generally, the frictional strength of sand is much stronger than the strength of the complex texture of clay-rich sediments [*Lupini et al.*, 1981; *Logan and Rauenzahn*, 1987; *Morrow et al.*, 1992; *Bos et al.*, 2000; *Morrow et al.*, 2000; *Saffer and Marone*, 2003]. The clay content has a significant effect on the sediment shear strength [*Saffer and Marone*, 2003; *Huhn et al.*, 2006]. As for instance, shear planes for gravitational mass flow processes were characterized by the presence of clay [*Hampton et al.*, 1996; *Kopf and Brown*, 2003; *Saffer and Marone*, 2003; *Ask and Kopf*, 2004].

[3] Analyses of deformed clay microstructures identified the tabular geometry of clay grains as one controlling factor for the mechanical behavior [*Bennett et al.*, 1991a]. This is supported by 2D numerical experiments that revealed the dependency of clay deformation and particle shape, which was primarily controlled by grain sphericity and roughness [*Kock and Huhn*, 2007b]. Furthermore, numerical investigations of non-spherical particles, which were signified by a decrease in sphericity, showed an increase in material strength [*Yan*, 2009; *Szarf et al.*, 2011].

[4] The relatively few studies on this subject were either 2D investigations that gave only indications of natural 3D behavior [*Kock and Huhn*, 2007b], or investigations that only examined the variation of sphericity simulating rod-like or triangular grain shapes [*Kock and Huhn*, 2007b; *Yan*, 2009; *Szarf et al.*, 2011]. It follows that the mechanical processes of tabular shape associated with clayey material is inadequately understood. We address this problem while undertaking a comparison of numerical experiments investigating the different grain shapes, such as spheres, rods, and plates. In this study, we will present our findings concerning the impact of grain shape complexity on sediment strength which contributed to improve the understanding of this geometrical factor.

### 3.2 Method

[5] The Discrete Element Method (DEM) is a state of the art tool for numerical investigations of granular processes with large strain [e.g. *Morgan*, 1999; *Hazzard and Mair*, 2003; *Abe and Mair*, 2005; 2009]. The fundamental characteristic of DEM simulations is the predefinition of particle- and contact-properties where the resulting overall material behavior ensures the comparability to laboratory outcomes. Detailed information about the functionality of DEM was described by many previous studies [e.g., *Cundall and Strack*, 1978; 1979; *Potyondy and Cundall*, 2004]. For our study we used a commercial three-dimensional DEM code (PFC3D) from Itasca Consulting Group, Inc. [*Itasca*, 2011].

[6] For model preparation, we constructed a numerical direct shear device (Figure 3-1) that was comparable to laboratory shear devices. Therein, we used a rectangular box with a square base (100  $\mu\text{m}$  x 100  $\mu\text{m}$ ) and a variable height which depended on the particle volume. The box boundary consisted of walls to prevent particle escape. All samples contained 120,000 spherical particles with an equal size (2  $\mu\text{m}$ ). Particle property of friction coefficient  $\mu_p = 0.6$  was applied. Additionally, the particle contact behavior was described by a linear contact law. For grain shape modification, single particles were combined using unbreakable bonds towards rod-like and tabular (quadratic shape) aggregates of more complexity (Figure 3-1). This means, aggregates were not allowed to change their outer shape and, neither abrasion with particle release, nor aggregate bending, was possible. The initial aggregate orientation and its spatial distribution inside the shear box were randomly

generated. The elastic sample response was achieved by certain particle stiffness parameters  $k_N = k_S = 10^9$  N/m.

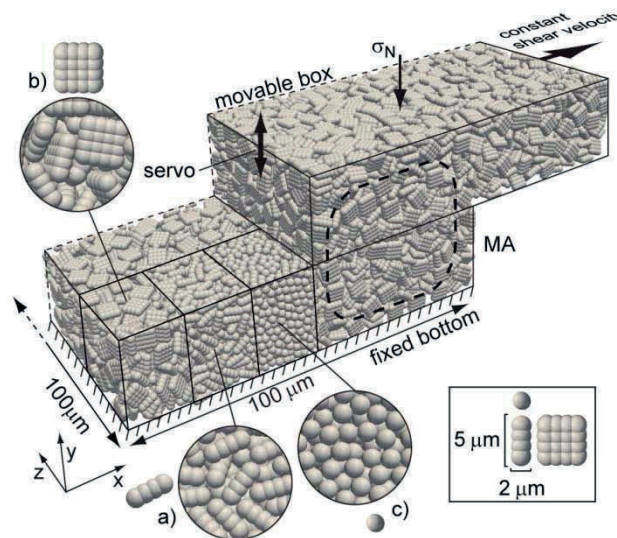


**Figure 3-1: Schematic illustration of the direct shear test and the applied boundary conditions for the three basic end-member grain shapes with the magnified micro-fabric for a) rods, b) plates, and c) spheres. MA indicates the measurement area for friction coefficient.**

[7] Preparing the shear process, the ‘sediment’ samples were compressed by a constant vertical downward load on the top wall, which acted during the entire experimental run. The shearing process was linked with the lateral movement of the upper shear box part. For this, a constant shear velocity of  $1 \mu\text{m/s}$  was used, which is consistent with previous analogue and numerical shear studies [Morgan, 1999; Saffer and Marone, 2003; Kock and Huhn, 2007b].

[8] For the interpretation of our experiments, two measurement routines were used. (1) The sediment strength is indicated by the material friction coefficient which is derived from the stress states of single particles within the measured volume (Figure 3-1). This stress tensor was necessary to calculate the frictional strength as the ratio of averaged shear and normal stresses ( $\mu = \tau / \sigma_N$ ).

The different states of strength (e.g. hardening, peak strength, softening, critical state) a sediment pass through during shear strain was well described for laboratory experiments by Lohrmann [2003]. With increasing shape complexity, it was possible that an aggregate had more than one contact to one neighboring aggregate. Due to this fact, the number of contacts between two aggregates varied. (2) We assumed that the contact number determined the contact size. This size parameter allowed for a topological classification into point-, edge-, and face-contacts (Figure 3-2), which was required for this new approach of fabric analyses. For the topological analysis we used the contact data from the entire model.

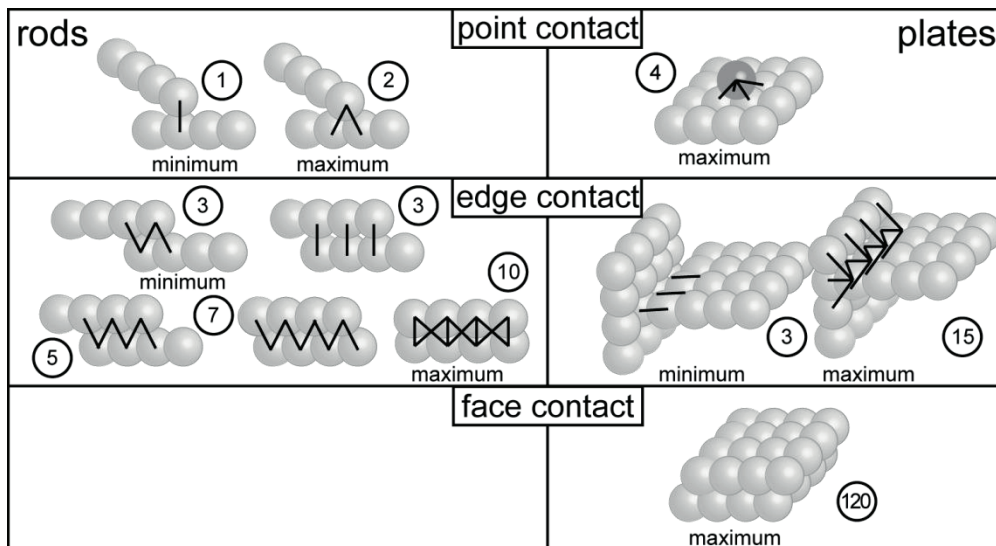


Figure 3-2: Classification of contact types and visualization of contact numbers for elongated particles (rods and plates). The encircled numerals represent the number of contacts indicating the contact size. Beams illustrate single contacts.

### 3.3 Results

[9] The material friction for the three grain shapes during the whole shear process is summarized in Figure 3-3. The uniform spheres showed an elastic-plastic material behavior with strain hardening and softening. The material friction initially increased to an obvious peak ( $\mu_{\text{peak}} = 0.36$ ,  $\varepsilon = 15 \mu\text{m}$ ) characterizing the strain hardening process and changed into strain softening which continued to the critical state ( $\mu_{\text{crit}} = 0.31$ ,  $\varepsilon > 20 \mu\text{m}$ ).

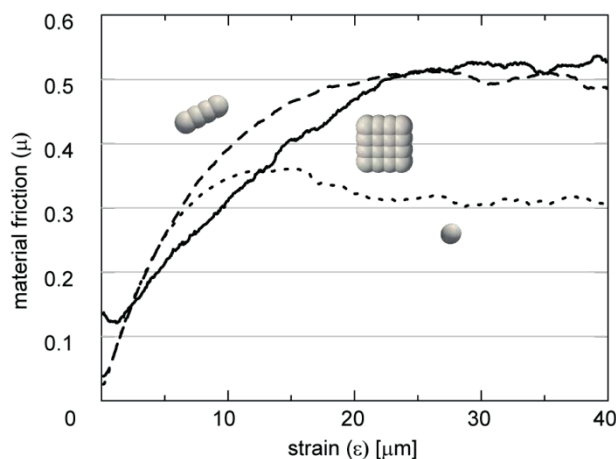


Figure 3-3: Characteristic curve shapes of material friction vs. strain for the three different grain shapes: spheres (pointed line), rods (dashed line), plates (line).

[10] In contrast, the frictional strength of the rod-like aggregates differed during shear deformation (Figure 3-3). Only at the initial  $5 \mu\text{m}$  strain did the curve shape conform to the behavior of spherical particles. With further strain, the material hardening increased continuously until the peak friction ( $\mu_{\text{peak}} = 0.5$ ,  $\varepsilon = 26 \mu\text{m}$ ) was reached. Therewith, the peak was larger and formed later than the spherical peak. After the peak, a slight trend to material softening with a decreasing curve behavior was observed until the end of shear deformation ( $\varepsilon_{\text{end}} = 40 \mu\text{m}$  strain).



[11] A further increase in shape complexity towards tabular aggregates resulted into more modification of the frictional response (Figure 3-3). For plates, a significant larger initial material friction ( $\mu_{\text{initial}} = 0.14$ ) was observed followed by a short softening event. Subsequently, a longer period of strain hardening was observed towards the point of peak friction ( $\mu_{\text{peak}} = 0.52$ ,  $\varepsilon = 30 \mu\text{m}$ ), which remained at the same level until  $\varepsilon_{\text{end}}$  was reached.

[12] These summarized general observations were made for an increase in aggregate shape complexity. The material friction at initial state became larger. The peak friction and, therewith, the deformation degree to achieve the peak increased.

### 3.4 Discussion

[13] The present study was designed to determine the effect of grain shape on the sediment strength and consequently on the material friction. For ideal spherical particles this investigation produced results (Figure 3-3) that correspond with the numerical experiments of Yan [2009] and Szarf et al. [2011] who also used spherical grain shapes. We found out that an increase in the shape complexity, towards rod-like aggregates, resulted in an increase in the material friction. This finding is in agreement with previous numerical studies using the DEM [Guo and Morgan, 2004; Yan, 2009; Szarf et al., 2011] that showed that an increase in the material friction was the consequence of the decreasing aggregate sphericity. This relationship is based on the fact that a deviation from the basic ideal spherical particle shapes resulted in restricted aggregate rotation, and hence, larger deformation resistance and material friction [Ting et al., 1993; Lin and Ng, 1997; Iwashita and Oda, 1998; Kock and Huhn, 2007b; Yan, 2009].

[14] We think that the material friction is fabric specific. As such, our findings support the hypothesis of increased complexity with further modifying of aggregates into tabular shape. This tabular material, as we assumed, showed larger frictional strength than rods and spheres (Figure 3-3). Surprisingly, only slight differences between rod-like and tabular aggregates were observed.

Nonetheless, the trend we found for the increasing material strength derived from the grain shape complexity is inversely to nature. As mentioned above, laboratory results show larger material strength for silt than for clayey material. One significant reason may be that in nature the aggregates have more options to change their shape by mechanical effect, e.g., abrasion of particles, disaggregation or particle deformation. In our simulations the aggregates were not able to decompose or change their shape by the use of bending. However, these findings of the stiff aggregates well show the dependency of material friction on pure grain shape without further deformation of the inner grain structure, but also suggested that there must be additional factors influencing the frictional response. For natural processes we can deduce the material strength, in case of stiff indestructible grains, that will increase with higher grain shape complexity during deformation. Due to the fact that the material friction is defined as the ratio of averaged stress tensor components at the aggregate contacts [Morgan, 1999], we further analyzed this contact behavior in more detail.

[15] A summary of the contact size distribution data versus the frequency per aggregate for the final deformation state is presented in Figure 3-4. Both curves showed out a similar shape that was characterized by a high frequency of small contacts. Further, with an increase in contact size a significant reduction of the frequency was observed. The two curve shapes approximated the characteristics of a power law. Due to the remarkable resemblance between both contact size distributions we considered this fact as a potential indicator for the

almost equal behavior of the material friction. We assumed that similar contact conditions between the rod-like and tabular aggregate fabrics were the reason for the slight variation in strength. In addition to several studies, which also observed an increase in material friction with grain shape complexity and justify this with a reduction in aggregate rotation, we contrary were in a position to attribute this influence to a dependency on the same contact size distribution. It does necessarily imply that for natural granular material the distribution of contact sizes is a meaningful factor influencing the frictional response. Unfortunately, laboratory methods are not able to detect the contact structure and sizes, and hence, no comparable data from real granular material is available to support these numerical results.

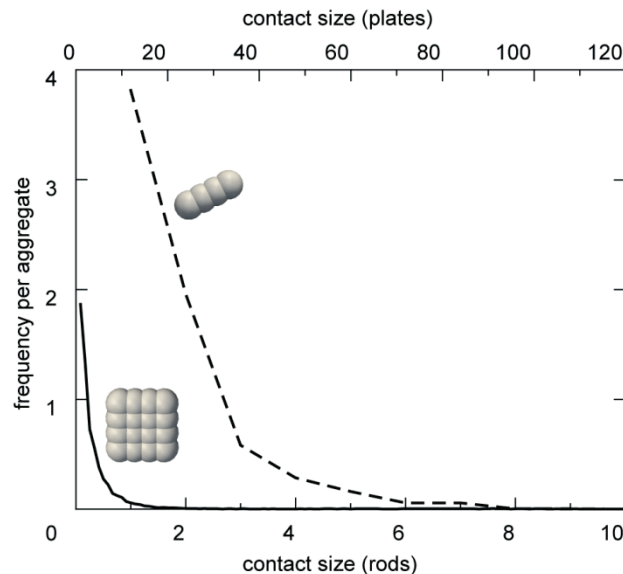


**Figure 3-4: Distribution of contact sizes for elongated particles after 40  $\mu\text{m}$  strain. Small contacts show the largest frequency. Both curve shapes are comparable to a power law distribution.**

[16] The contact size data was interpreted to obtain the topological classifications of aggregate fabric (Figure 3-5). A detailed consideration of the aggregate contact relations regarding the contact types of point, edge, and face contacts (Figure 3-2) showed almost equally distributed ratios for rods and plates. Summarizing the data of contact types for strain versus the normalized frequency ratio indicated that the micro-fabrics were dominated by point contacts (Figure 3-5). Thereby, the conversion of contact types of point into edge contacts during deformation within rod-like and tabular grain shape was almost identical. On the basis of this data which demonstrated the conversion of point into edge contacts showed that with progressive strain an increase in edge contacts correlated well with the development of material friction. This fact let us assume that with higher ratio of edge and face contacts the frictional response would increase. For natural granular material this changes within the topological microstructure towards higher order of contact sizes (edge and face contacts), which was caused by shear deformation, induced an increase in material friction.

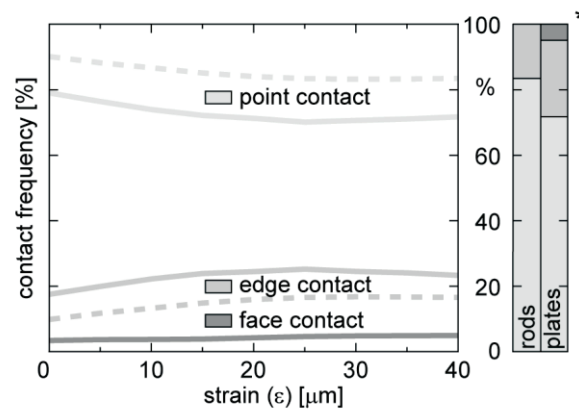


**Figure 3-5: Contact frequency vs. strain for elongated particles of rods (dashed lines) and plates (lines). For 40  $\mu\text{m}$  strain a direct comparison of parts per contact type are illustrated in the 100% stacked column chart (\*).**

### 3.5 Conclusion

[17] Our 3D numerical direct shear modeling revealed that the particle shape plays an important role in the sediment strength. We were able to show that a variation in grain shape complexity affects different aspects of the macroscopic frictional response such as 1) the initial frictional resistance, 2) the value of peak friction, and 3) the degree of deformation to achieve the state of peak friction. For the randomly aligned and elongated aggregates (rods and plates), we demonstrated a dependency of frictional strength on the topological microstructure of grain-to-grain contacts. The ability to study the topological characteristics of sediment microstructure provides new insights into the understanding of shear processes. Our method offers a large potential to investigate the rearrangement of contact related fabric during strain.

[18] Our focus in the next step will be to increase the shape complexity, to create mixtures of silt and clay compositions, to investigate the effect of pore volume changes, to define microstructures that substitute the fabric of clay- and ash-layers, and the implementation of fluids to test the effect of pore pressure. This will enable to reproduce more complex initial micro-fabric of predominated grain associations, such as book sheet, stair-step, card-house, or card-book.

### Acknowledgements

We wish to thank, L. Podszun, L. Wenk, and B. Flaim for assistance. This work was funded through DFG-Research Center / Excellence Cluster “The Ocean in the Earth System”.

### References

- Abe, S., and K. Mair (2005), Grain fracture in 3D numerical simulations of granular shear, *Geophysical Research Letters*, 32(L05305), 1-4.
- Abe, S., and K. Mair (2009), Effects of gouge fragment shape on fault friction: New 3D modelling results, *Geophysical Research Letters*, 36(L23302), 1-4.

- Ask, M. V. S., and A. Kopf (2004), Constraints on the state of in situ effective stress and the mechanical behaviour of ODP Leg 186 claystones in the Japan Trench forearc, *The Island Arc*, 13(1), 242-257.
- Bennett, R. H., N. R. O'Brien, and M. H. Hulbert (1991a), Determinants of Clay and Shale Microfabric Signatures: Processes and Mechanisms, in *Microstructure of Fine-Grained Sediments*, edited by R. H. Bennett, Bryant, W. R., Hulbert, M. H., p. 582, Springer-Verlag, New York.
- Bos, B., C. J. Peach, and C. J. Spiers (2000), Frictional-viscous flow of simulated fault gouge caused by the combined effects of phyllosilicates and pressure solution, *Tectonophysics*, 327(3-4), 173-194.
- Cundall, P. A., and O. D. L. Strack (1978), BALL - A program to model granular media using the distinct element method, in *Technical Note, Advanced Technology Group*, edited, Dames and Moore, London.
- Cundall, P. A., and O. D. L. Strack (1979), A discrete numerical model for granular assemblies, *Geotechnique*, 29(1), 47-65.
- Guo, Y., and J. K. Morgan (2004), Influence of normal stress and grain shape on granular friction: Results of discrete element simulations, *Journal of Geophysical Research*, 109(B12305), 1-16.
- Hampton, M. A., H. J. Lee, and J. Locat (1996), Submarine landslides, *Rev Geophys*, 34(1), 33-59.
- Hazzard, J. F., and K. Mair (2003), The importance of the third dimension in granular shear, *Geophysical Research Letters*, 30(13), 1708-1711.
- Huhn, K., I. Kock, and A. Kopf (2006), Comparative numerical and analogue shear box experiments and their implications for the mechanics along the failure plane of landslides, *Norwegian Journal of Geology*, 86(3), 209-220.
- Itasca (2011), PFC 3D 4.0 Manual, edited, Itasca Consulting Group, Inc., Minneapolis.
- Iwashita, and Oda (1998), Rolling Resistance at Contacts in Simulation of Shear Band Development by DEM, *Journal of Engineering Mechanics*, 124(3), 285-292.
- Kock, I., and K. Huhn (2007), Influence of particle shape on the frictional strength of sediments - A numerical case study, *Sediment Geol*, 196(1-4), 217-233.
- Kopf, A., and K. M. Brown (2003), Friction experiments on saturated sediments and their implications for the stress state of the Nankai and Barbados subduction thrusts, *Mar Geol*, 202(3-4), 193-210.
- Krantz, R. W. (1991), Measurements of friction coefficients and cohesion for faulting and fault reactivation in laboratory models using sand and sand mixtures, *Tectonophysics*, 188(1-2), 203-207.
- Lin, X., and T.-T. Ng (1997), A three-dimensional discrete element model using arrays of ellipsoids, *Geotechnique*, 47(No. 2), 319-329.

- Logan, J. M., and K. A. Rauenzahn (1987), Frictional dependence of gouge mixtures of quartz and montmorillonite on velocity, composition, and fabric, *Tectonophysics*, 144(1-3), 87-108.
- Lohrmann, J., N. Kukowski, J. Adam, and O. Oncken (2003), The impact of analogue material properties on the geometry, kinematics, and dynamics of convergent sand wedges, *Journal of Structural Geology*, 25(10), 1691-1711.
- Lupini, J. F., A. E. Skinner, and P. R. Vaughan (1981), The drained residual strength of cohesive soils, *Geotechnique*, 31(2), 181-213.
- Marone, C. (1998), Laboratory-derived friction laws and their application to seismic faulting, *Annual Review of Earth and Planetary Sciences*, 26, 643-696.
- Morgan, J. K. (1999), Numerical simulations of granular shear zones using the distinct element method 2. Effects of particle size distribution and interparticle friction on mechanical behavior *Journal of Geophysical Research*, 104(B2), 2721-2732.
- Morrow, C. A., B. Radney, and J. Byerlee (1992), Frictional Strength and the Effective Pressure Law of Montmorillonite and Illite Clays, in *Fault mechanics and transport properties of rocks; a festschrift in honor of W. F. Brace*, edited by B. a. W. Evans, T., p. 524, Academic Press, San Diego.
- Morrow, C. A., D. E. Moore, and D. A. Lockner (2000), The effect of mineral bond strength and adsorbed water on fault gouge frictional strength, *Geophysical Research Letters*, 27(6), 815-818.
- Potyondy, D. O., and P. A. Cundall (2004), A bonded-particle model for rock, *International Journal of Rock Mechanics & Mining Sciences*, 41, 1329-1364.
- Saffer, D. M., and C. Marone (2003), Comparison of smectite- and illite-rich gouge frictional properties: application to the updip limit of the seismogenic zone along subduction megathrusts, *Earth and Planetary Science Letters*, 215(1-2), 219-235.
- Saffer, D. M., K. M. Frye, C. Marone, and K. Mair (2001), Laboratory results indicating complex and potentially unstable frictional behavior of smectite clay, *Geophysical Research Letters*, 28(12), 2297-2300.
- Szarf, K., G. Combe, and P. Villard (2011), Polygons vs. clumps of discs: A numerical study of the influence of grain shape on the mechanical behaviour of granular materials, *Powder Technology*, 208(2), 279-288.
- Ting, J. M., M. Khwaja, L. R. Meachum, and J. D. Rowell (1993), An ellipse-based discrete element model for granular materials, *INTERNATIONAL JOURNAL FOR NUMERICAL AND ANALYTICAL METHODS IN GEOMECHANICS*, 17(9), 603-623.
- Yan, W. M. (2009), Fabric evolution in a numerical direct shear test, *Computers and Geotechnics*, 36(4), 597-603.



## 4 Chapter Four

### (Manuscript 3)

In press

Krastel et al. (eds.), *Submarine Mass Movements and Their Consequences, Advances in Natural and Technological Hazards Research 37*, DOI 10.1007/978-3-319-00972-8 8, © Springer International Publishing Switzerland 2014

## Interrelationship between sediment fabric, pore volume variations as indicator for pore pressure changes, and sediment shear strength

Lutz Torbahn, Katrin Huhn

MARUM – Center for Marine Environmental Sciences, University of Bremen, Leobener Str., D-28359 Bremen, Germany ([ltorbahn@marum.de](mailto:ltorbahn@marum.de) / Phone +49(0)421 218 65864

### Abstract

The physical characterization of sediments forms the basis for slope stability analysis. The shear strength of water-saturated sediments is a function of sediment properties and pore pressure conditions. A reduction in strength, e.g., as a result of transient pore pressure changes, can cause the collapse of the sediment matrix and subsequently slope sediment fails. As failure processes in the sediment elude from direct observation, matrix deformation processes, sediment grain interactions, and the associated stresses can be examined by numerical simulations. The major aim of this study was to evaluate the effects of varied sediment fabric on pore volume changes and sediment strength in sheared samples. For all sediment fabrics, an inversely proportional relationship between strength and porosity was observed. A controlling effect of grain shape on the maximum friction coefficient value was demonstrated.

**Keywords:** sediment strength, pore volume change, sediment fabric, failure mechanism, Discrete Element Method

### 4.1 Introduction

Numerous studies have shown that mineralogical composition and pore fluid pressure control the mechanical behaviour of water-saturated sediments [*Lambe and Whitman*, 1969; *Marone*, 1998], which can be described by the Mohr-Coulomb failure criterion [*Handin*, 1969; *Byerlee*, 1978]. If the pore pressure exceeds the characteristic material strength, the stress-imposed granular matrix will fail [*Mitchell and Soga*, 2005; *Goren et al.*, 2010]. Therefore, transient pore pressure changes are widely accepted as a potential trigger mechanism for landslides [e.g., *Hampton et al.*, 1996; *Locat and Lee*, 2002]. Various processes can cause

such transient pore pressure variations, e.g., sea level changes and gas hydrate dissolution. The latter will be of particular importance in the near future, especially in higher latitudes, because gas hydrate dissociation will be driven by global warming [Mienert *et al.*, 2010]. Accordingly, an improved understanding of the interplay between sediment fabric, pore pressure (or indicative pore volume variations), and sediment shear strength is of increasing importance to define the potential trigger mechanisms of submarine landslides.

To examine these processes occurring prior to and during failure of submarine slopes, which elude from direct observation, we developed a 3D numerical direct shear test based on the Discrete Element Method (DEM). With this the relationship between sediment fabric, pore volume variations, and shear strength was examined. In our simulations, the sheared samples represented the basal shear plane of submarine landslides, whereas the fixed part of the shear box represented the undisturbed slope sediment. The mobilized sediment of the landslide was represented by the movable part of the shear box. The shear plane evolved inside the sheared sample as the localized failure. This experimental setting allowed for investigation of failure initiation and failure evolution. Sediment fabrics were created based on idealized fundamental grain shapes of spheres and aggregates of rod-like and plate-like shape as numerical replacements for natural silt and clay grains. The simulations were designed to address the following key questions:

1. How is sediment strength linked to pore volume changes during failure?
2. Does sediment fabric or sediment-grain complexity control sediment shear strength and pore volume evolution during shearing?
3. Are there any local effects of pore volume changes during the evolution of failure planes?

### 4.2 Method

In recent years, numerical simulations using the DEM came into focus for investigation of physical aspects of grain interactions and localized deformation inside granular brittle materials [Morgan, 1999; Hazzard and Mair, 2003; Abe and Mair, 2009]. The principle functionality of the DEM [e.g., Cundall and Strack, 1978; Potyondy and Cundall, 2004] provided the framework for the current study in which the three-dimensional DEM code PFC3D (ITASCA©) was used.

We developed a numerical direct shear device (Figure 4-1) comparable in function to laboratory direct shear experiments. For each test, 120,000 spherical grains of uniform size (2  $\mu\text{m}$ ) filled a six-sided rectangular shear box (100  $\mu\text{m}$  x 100  $\mu\text{m}$ ). The spherical grains approximated the shape of natural rounded silt with a grain size equivalent to the transition from clay to silt. Frictionless walls were used to enable (i) comparable boundary conditions in all experiments and (ii) to exclude influences caused by the roughness of the driving plate on the friction coefficient and shear strain distribution, which has been observed in lab and numerical shear tests [Anthony and Marone, 2005; Abe and Mair, 2009].

In order to create naturally packed samples, grains were created inside a higher box and then compressed by a downward moving top wall until the packing conformed to natural sediment conditions [Hazzard and Mair, 2003; Abe and Mair, 2005]. A stable load on the top wall was maintained by a servo-mechanism throughout the entire shear process (Figure 4-1).



A constant shear velocity ( $1 \mu\text{m/s}$ ) (with no acceleration) was enacted on the upper wall of the shear box inducing shear deformation in the positive x-direction.

Increased grain complexity and, thus, sediment fabric, was achieved by aggregating single spherical particles using unbreakable bonds (Figure 4-1). The rod-like or plate-like shapes were stable throughout shear and were not susceptible to bending or abrasion. After aggregation, the aggregates were randomly oriented.

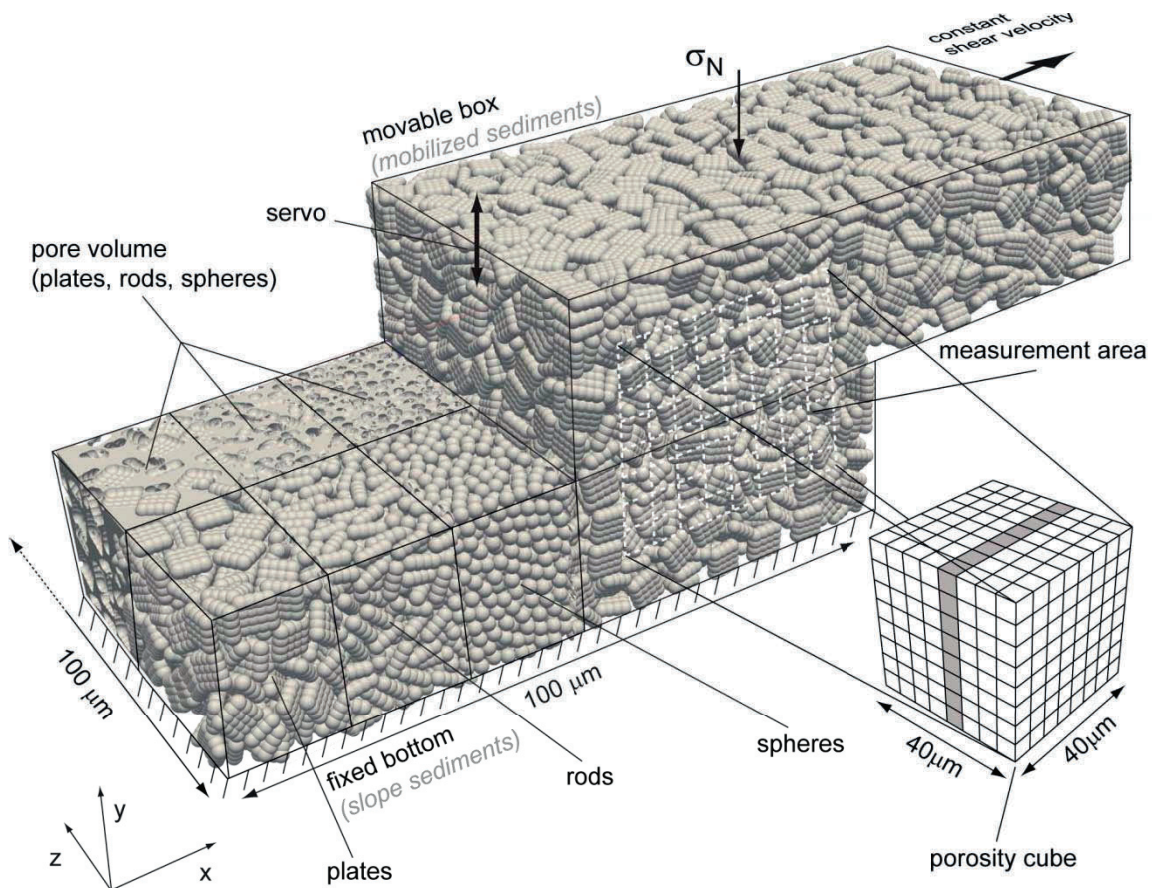


**Figure 4-1: Compilation of shear sample components including the realized fabrics of plate-like grains, rod-like grains, and spherical grains and visualization of pore volume for the three grain fabrics. The dashed white mesh shows the measurement area for material friction and porosity inside the sample. The cube and sub-cubes illustrate the measurement volume for porosity, whereas the grey sub-cubes indicate the layer of local pore volume investigation.**

To simulate natural slope sediments, e.g., silt and clay, numerical grain properties were defined as follows: the coefficient of particle friction ( $\mu_P$ ) = 0.6 and as we used a linear contact model, normal ( $k_N$ ) and shear ( $k_S$ ) grain stiffness were required: ( $k_N, k_S$ ) =  $10^9$  N/m. This friction coefficient and according stiffness values have previously been successfully used to simulate marine sediments [e.g., *Kock and Huhn, 2007b*]. Moreover, using the same particle properties for both numerical ‘clay’ and ‘silt’- shaped particles ensures fair comparison and focusses the study to the influences of the grain shape. An artificially large particle density was used to force quasi-static deformation conditions by using a density scaling method. Thus, a sequence of equilibrium states was simulated to ensure that dynamical features, such as masses and grain inertia were negligible. This method ensures that dry and water-saturated sands exhibit the same behaviour when using the same static properties [*Roux and Combe, 2002*].

Three measurement routines were used for the interpretation of model results: (1) The friction coefficient was calculated from the stress states at individual grain contacts using the Mohr-Coulomb failure criterion [e.g., *Potyondy and Cundall, 2004*], e.g., for dry and cohesionless material, such as that used here. Inside the sheared sample the measured friction coefficient varied. Therefore, we calculated the average friction coefficient in certain areas during shear deformation. (2) The norm of the particle movement vector was used to determine zones of small and large grain slip along vertical slices through the central part of the sheared sample. Areas of relatively large grain motion highlighted areas of localized slip or failure planes in the sediment [*Kock and Huhn, 2007a*]. (3) Porosity variations were calculated to quantify the influences of grain complexity on the pore volume evolution by:

$$\eta = V_{\text{pore volume}} / V_{\text{sample volume}} \quad (\text{Eq. 4-1})$$

We used the Visualization Toolkit (VTK) [*Schroeder et al., 2004*] which allowed for calculation and visualization of the 3D pore space. VTK generates a volume model for the inner part of the sheared sample (40  $\mu\text{m}$  x 30  $\mu\text{m}$  or 40  $\mu\text{m}$  x 40  $\mu\text{m}$ ) consisting of a Cartesian regular grid (Figure 4-2-I b, c). After the grain volumes were subtracted from the entire volume model (Figure 4-2-I d), a grid triangulation was necessary to calculate the pore volume [*Alyassin et al., 1994*].

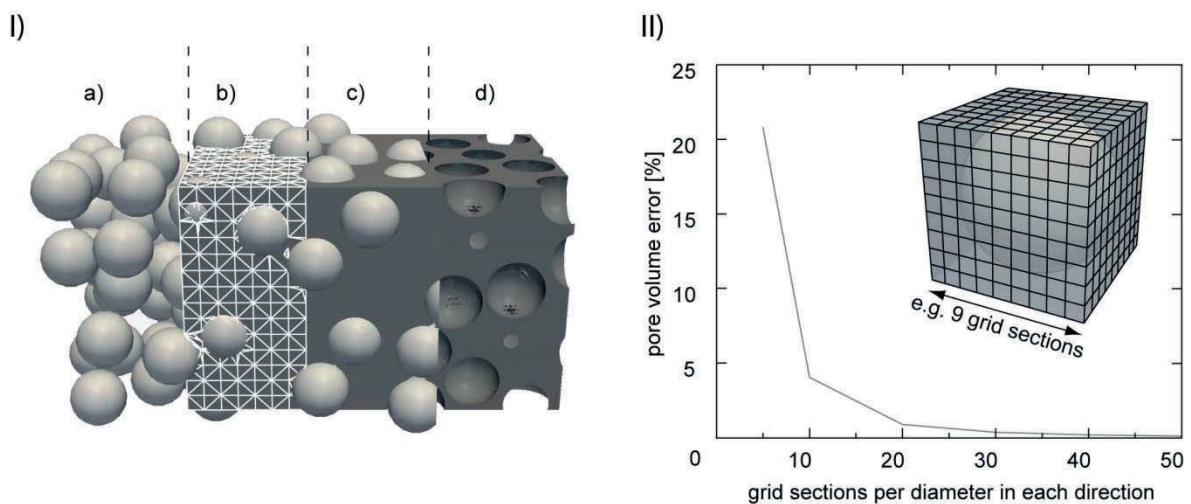


**Figure 4-2:** I) Schematic illustration of stepwise pore volume calculation: a) a loosely packed sediment grain assembly, b) a rough triangulated volume mesh, c) a pore volume mesh with sediment grains, and d) a pure mesh of pore volume. II) Pore volume error estimation for different numbers of sections per grain diameter. For the applied 30 grid sections per basic grain diameter a pore volume error lower than 1% occurred.

The pore volume error, therefore, depends on the number of grid sections per grain diameter (Figure 4-2). A benchmark (Figure 4-2-II) showed an acceptable pore volume error of 0.38% for 30 grid sections per diameter (2  $\mu\text{m}$ ). For the entire volume model (Figure 4-1), a total number of 600 x 600 x 600 grid sections were required to ensure volume accuracy.

### 4.3 Results

All numerical shear experiments revealed a direct influence of grain complexity, and hence, sediment fabric, on material behaviour (see results of measurement routines (1)-(3) below). In particular, the friction coefficient, as an indicator for the sediment strength (Figure 4-3) and the porosity changes as an indicator for pore pressure variations (Figure 4-4), showed direct relationships with grain complexity.

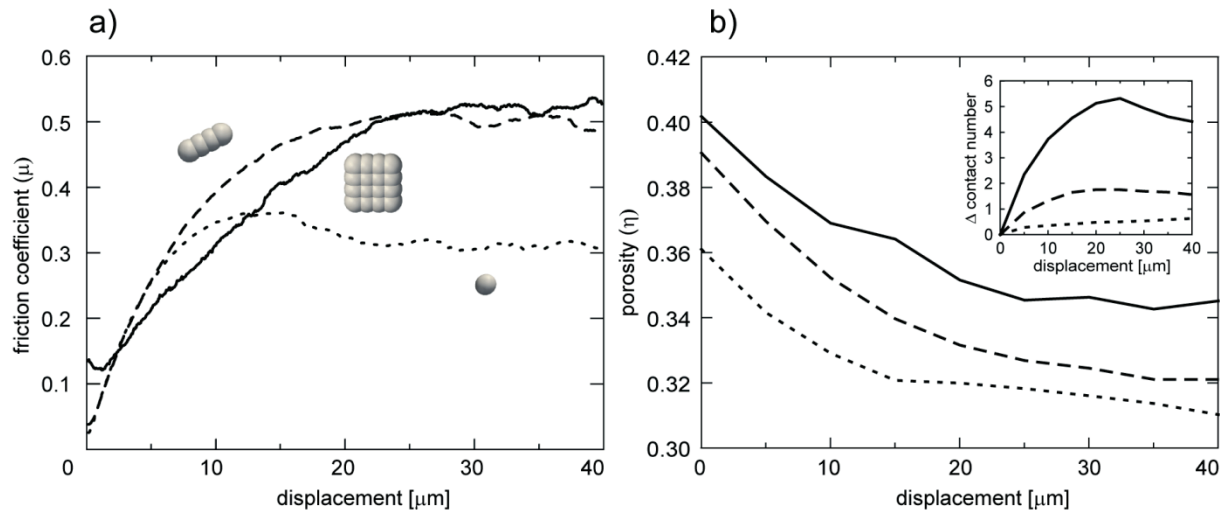


**Figure 4-3: Characteristic curve of a) friction coefficient and b) porosity vs. displacement for the three aggregates: sphere (dotted line), rod (dashed line), and plate (solid line).**

1) For all experiments, we observed - independent of grain shape - an increase of the friction coefficient and a corresponding decrease in the porosity (Figure 4-3). However, the curve shapes of the friction coefficient and porosity indicated specific distinctions in material behaviour that were influenced by the grain or, especially, aggregate shapes.

With increasing grain complexity, the friction coefficient at initial shear deformation increased (Figure 4-3a). The curves for spheres and rods were nearly identical before the curve bifurcated at 6  $\mu\text{m}$  displacement, whereas the curve for tabular aggregates differed at low strain.

Subsequent deformation was affected by material hardening as evidenced by an increase in the friction coefficient towards the peak friction for all grain types. A peak friction coefficient of 0.37, in case of spheres, and 0.51 for rods, was observed after  $\sim 14 \mu\text{m}$  and  $\sim 26 \mu\text{m}$  displacement, respectively (Figure 4-3a). Following peak friction, an overall material softening process was indicated by a decrease in the friction coefficient towards a steady or critical state. This phase of material softening and subsequent stable friction was only observed for spheres and rods. Furthermore, only the spherical particle experiments clearly attained a critical state. In contrast, even after 40  $\mu\text{m}$  displacement, peak friction was not attained during shearing of the plate-like aggregates. Instead, the friction coefficient continuously increased. For the same strain, the experiment with plate-like aggregates only achieved a pre-peak state.

Peak friction appears to depend on grain complexity. In fact, increasing grain shape complexity led to an increased peak friction coefficient. However, the friction coefficient curves of rods and plates showed very similar variations.

2) All pore volume curves exhibited different initial and final porosity values (Figure 4-3b). It was demonstrated that porosity increases with increasing grain shape complexity, but

decreases universally with increasing strain. The porosity gradient was also a function of grain complexity: the porosity magnitude decreased by 5.1% for spheres, 7% for rods, and 5.5% for plates during the 40  $\mu\text{m}$  displacement.

3) At 0 – 5  $\mu\text{m}$  displacement, the relative grain movements were identical for all sediment fabrics. No distinct failure planes were observed except in small areas at the side wall edges (Figure 4-4a). The sediment matrix was dominated by compression for spheres and rods, whereas plates showed a more balanced distribution between compression and extension.

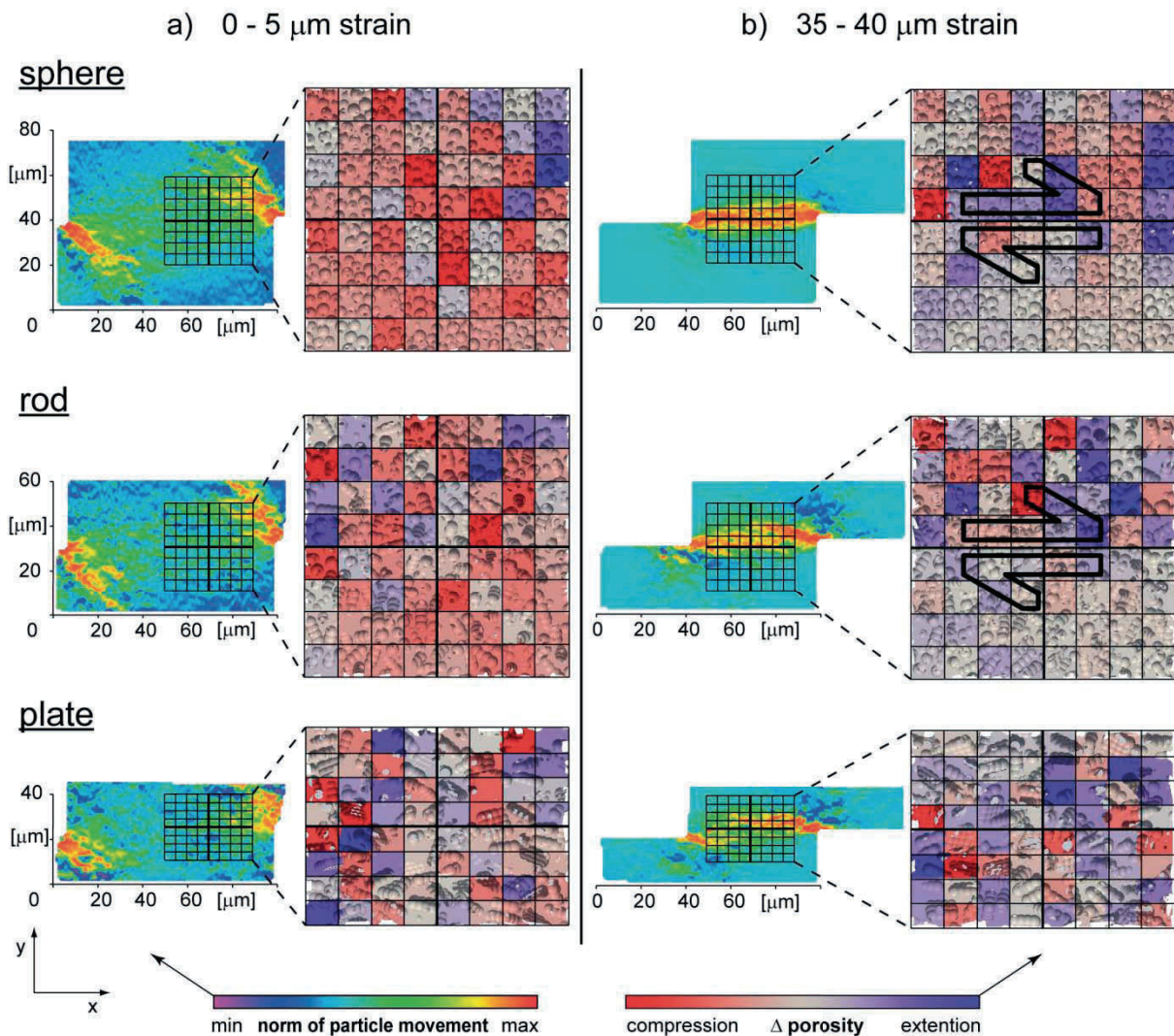


**Figure 4-4: Visualization of sediment slip behaviour derived from the particle movement as well as pore volume changes as an indicator for the pore pressure distribution within the initial and final 5  $\mu\text{m}$  displacement. Large arrows in the pore volume plot represent the position and orientation of the developed failure plane.**

In contrast, both grain movements and porosity changes showed different patterns for the different grain shapes from 35 – 40  $\mu\text{m}$  displacement (Figure 4-4b). For spheres and rods, a horizontally oriented zone of larger grain slip was observed. The most significant pore volume change occurred above this shear plane in the upper part of the shear box, while the

underlying part was unaffected. After failure, when the sediment matrix broke and a stable shear plane evolved, only the upper shear box part underwent progressive heterogeneous pore volume changes. This pattern clearly mirrored the location of the shear plane by separation of areas of low vs. high pore volume changes. In contrast, no distinct horizontal slip area of large grain motion was observed for plate-like grains (Figure 4-4b). Instead, two parallel areas of minor slip evolved shortly before development of a stable shear plane. At that time, the porosity changes were still randomly balanced and distributed throughout the entire sample.

## 4.4 Discussion

### 4.4.1 Interplay: sediment strength and pore volume changes

This study was designed to assess the relationship of sediment strength and pore volume changes during shearing. An increase in the friction coefficient and a corresponding decrease in porosity occurred with increasing shear strain in all experiments (Figure 4-3). Hence, the densification of the sediment matrix caused an increase in the number of grain contacts. This was directly associated with an increase in sediment shear strength because a larger number of contacts must break to generate a failure plane. This finding correlates with laboratory shear experiments, e.g., Lohrmann et al. [2003], where the initial sediment compaction and the respective porosity evolution was attributed to control the shear strength of granular materials.

#### Effect of grain shape complexity

Detailed analyses of the relationship of sediment strength and pore volume changes revealed a direct effect from fabric complexity. Generally, increasing grain complexity caused an increase in sediment strength and porosity (Figure 4-3) or an increase in particle contacts, particularly in case of plate-like grains (Figure 4-3b). With strain, the contact numbers and the homogeneity of the stress network increased which also caused a restricted grain motion. Moreover, the increase in porosity with increasing grain complexity likely resulted from the generation of heterogeneous aggregate structures of complex microfabric, which create additional pore volumes. These results are consistent with those of other studies and suggest that the growth in sediment strength is also attributable to the resistance of grain rotation [Iwashita and Oda, 1998; Yan, 2009].

Our simulations also showed that particle complexity affects the amplitude of the coefficient of friction as well as the critical strain rate required to reach the peak friction value. However, Moore and Lockner [2007] found similar shear strength values for more complex sediment textures, e.g., dry montmorillonite, and mostly rounded grains, e.g., sand and silt. These differences can be explained by the fact that natural aggregates break down during heavy loading. As a predefined boundary condition, however, our aggregates were not able to disaggregate. Therefore, a low confining pressure regime was simulated resulting in a breakdown of only the fabric structure. The collapse of the different fabric structures was, nonetheless, sufficient ( $\Delta\eta > 5\%$ ) to cause specific compaction rates.

In summary, a more complex grain shape or sediment fabric caused an increase in pore volume and an increase in sediment strength. This observation correlates to natural materials with respect to porosities. However, natural wet clays typically have much lower strength values compared to silt and sand. This aspect cannot be simulated with our

modelling approach because fluids or fluid effects and cohesive forces have been excluded so that the focus is only on microfabric effects [Lupini *et al.*, 1981; Saffer and Marone, 2003].

Based on the general assumption that a reduction in pore volume resulted in a pore pressure increase [Goren *et al.*, 2010], all fabrics displayed different increases in the potential pore pressures caused by pore volume reduction during densification (Figure 4-3). The failure of a simple grain shape occurred at lower porosity changes indicating that less complex grains, e.g., non-cohesive sands or silts, more readily react to pore pressure changes compared to more complex sediment textures. Hence, our results confirm that non-cohesive slopes will fail in the case of lower transient pore pressure changes compared to cohesive slopes.

### 4.4.2 Local pore volume changes

After the initial deformation, the pore volume change for the spherical fabric was dominated by compression (Figure 4-4a). With increasing grain shape complexity, a more heterogeneous distribution of porosity changes was observed. This effect was a result of grain motion and rotation during shearing, which destroyed the initial grain microfabric and re-oriented the elongated grains of higher shape complexity. In contrast, the lowest compaction rate and most homogeneous porosity change were observed for the spherical grain fabric, which allowed an ideal packing scenario.

At the final deformation stage from 35 – 40  $\mu\text{m}$  displacement, particle re-arrangement was finished for spheres and rods. Constant porosities evolved in the lower part of the shear box, whereas the upper part was still dominated by compression and extension. In both experiments, stable friction after peak was achieved and a shear plane developed at the transition from homogenous to heterogeneous pore volume changes. In contrast, pore volume changes were still homogeneously distributed through the sheared sample and no shear plane was observed for plate-like grains. This finding indicates that the pore volume below a landslide failure plane is not significantly changed after plane initiation, while pore volume changes above the shear plane continue.

## 4.5 Conclusion

The aim of this study was to assess the effect of grain shape and pore volume changes on sediment strength. The following general conclusions can be drawn:

- For increasing shear deformation, we observed an increase in the friction coefficient and a simultaneous decrease in porosity. Thereby, the reduction in porosity (matrix densification) caused an increase in the grain contact number which resulted in an increase in the coefficient of friction. In addition, increasing grain shape complexity caused a further increase in sediment strength and porosity as a consequence of a non-ideal packing and the associated grain rotation restriction. The breakdown of the microfabrics in the case of more complex textures resulted in a reduction of porosity and a significant increase in grain contacts, which again caused an increase in the friction coefficient.
- Non-cohesive slopes exhibit lower porosities and densifications prior to failure and are more prone to lower transient pore pressure changes compared to cohesive slopes, hence failing under lower triggers.
- This new approach indicates the evolution of domains of compressional and extensional behaviour during the evolution of the failure plane. The underlying undisturbed sediments below the failure plane show no pore volume changes, while the upper part exhibits

significant porosity fluctuations. Hence, high resolution porosity analyses should allow for the identification of the basal failure planes of landslides.

## Acknowledgements

We wish to thank, S. Abe and I. Görz for very constructive reviews and M. Stipp. Further we thank L. Podszun, L. Wenk, B. Flaim, G. Bartzke, J. Kuhlmann and Y. Hellmann for assistance. This work was funded through the DFG-Research Center / Excellence Cluster MARUM "The Ocean in the Earth System".

## References

- Abe S and Mair K (2009) Effects of gouge fragment shape on fault friction: New 3D modelling results. *Geophysical Research Letters* 36, 1-4.
- Abe S and Mair K (2005) Grain fracture in 3D numerical simulations of granular shear. *Geophysical Research Letters* 32, 1-4.
- Alyassin AM, Lancaster JL, Downs JH, and Fox PT (1994) Evaluation of new algorithms for the interactive measurement of surface area and volume. *Medical Physics* 21, 741-52.
- Anthony JL and Marone C (2005) Influence of particle characteristics on granular friction. *Journal of Geophysical Research* 110, doi:10.1029/2004JB003399.
- Byerlee JD (1978) Friction of Rocks. *Pure and Applied Geophysics* 116, 615 - 25.
- Cundall PA and Strack ODL (1978) BALL - A program to model granular media using the distinct element method. Dames and Moore, London.
- Goren L, Aharonov E, Sparks D, and Toussaint R (2010) Pore Pressure Evolution in Deforming Granular Material: A General Formulation and the Infinitely Stiff Approximation. *Journal of Geophysical Research* 115,
- Hampton MA, Lee HJ, and Locat J (1996) Submarine landslides. *Reviews of Geophysics* 34, 33-59.
- Handin J (1969) On the Coulomb-Mohr failure criterion. *Journal of Geophysical Research* 74, 5343-8.
- Hazzard JF and Mair K (2003) The importance of the third dimension in granular shear. *Geophysical Research Letters* 30, 1708-11.
- Iwashita and Oda (1998) Rolling Resistance at Contacts in Simulation of Shear Band Development by DEM. *Journal of Engineering Mechanics* 124, 285-92.
- Kock I and Huhn K (2007) Numerical investigation of localization and micromechanics in a stratified soil specimen. *Journal of Structural Geology* 29, 1679 - 94.
- Kopf A and Brown KM (2003) Friction experiments on saturated sediments and their implications for the stress state of the Nankai and Barbados subduction thrusts. *Marine Geology* 202, 193-210.
- Kosoglu LM, Bickmore BR, Filz GM, and Madden AS (2010) Atomic Force Microscopy Method for Measuring Smectite Coefficients of Friction. *Clays and Clay Minerals* 58, 813-20.

- Lambe TW and Whitmann RV (1979) In Soil Mechanics. Vol. pp. John Wiley & Sons, Singapore.
- Locat J and Lee HJ (2002) Submarine landslides: advances and challenges. Canadian Geotechnical Journal 39, 193-212.
- Lohrmann J, Kukowski N, Adam J, and Oncken O (2003) The impact of analogue material properties on the geometry, kinematics, and dynamics of convergent sand wedges. Journal of Structural Geology 25, 1691-711.
- Lupini JF, Skinner AE, and Vaughan PR (1981) The drained residual strength of cohesive soils. Geotechnique 31, 181-213.
- Marone C (1998) Laboratory-derived friction laws and their application to seismic faulting. Annual Review of Earth and Planetary Sciences 26, 643-96.
- Mienert J, Vanneste M, Haflidason H, and Bünz S (2010) Norwegian margin outer shelf cracking: a consequence of climate-induced gas hydrate dissociation? International Journal of Earth Sciences 99, 207-25.
- Mitchell JK and Soga K (2005) In Fundamentals of Soil Behaviour. 3rd (ed.), Vol. pp. John Wiley & Sons, Hoboken, New Jersey.
- Moore DE and Lockner DA (2007) Friction of the Smectite Clay Montmorillonite. In The Seismogenic Zone of Subduction thrust Faults. T. Dixon CM (ed.), Vol. pp. 317-45. Columbia University Press,
- Morgan JK (1999) Numerical simulations of granular shear zones using the distinct element method 2. Effects of particle size distribution and interparticle friction on mechanical behavior Journal of Geophysical Research 104, 2721-32.
- Potyondy DO and Cundall PA (2004) A bonded-particle model for rock. International Journal of Rock Mechanics & Mining Sciences 41, 1329-64.
- Roux J-N and Combe G (2002) Quasistatic rheology and the origins of strain. Comptes Rendus Physique 3, 131-40.
- Saffer DM and Marone C (2003) Comparison of smectite- and illite-rich gouge frictional properties: application to the updip limit of the seismogenic zone along subduction megathrusts. Earth and Planetary Science Letters 215, 219-35.
- Schroeder W, Martin K, and Lorensen B (2004) In The Visualization Toolkit, Third Edition.
- Yan WM (2009) Fabric evolution in a numerical direct shear test. Computers and Geotechnics 36, 597-603.



## 5 Chapter Five Summary

The outcomes from the three manuscripts point out many particle features. Apart from the particle characteristics that are partly observable in laboratory studies, such as dimensionality, friction coefficient, and porosity, there are some features only observable using the numerical approach during shear deformation, such as particle motion inside the sample, local pore volume evolution of clay and silt, and the detailed contact configuration of arbitrary shaped particles. The experiments performed in this study provide a valuable insight into the complicated micromechanical processes. Concerning the scientific relevance with respect to natural conditions and laboratory experiments, it was shown that dimensionality, and especially the factor of grain shape, noticeably affect the deformation behavior of granular matter. The initial research questions could be answered within this study.

### 5.1 Concluding remarks and perspectives

#### 5.1.1 Conclusions

This study illustrates that individual features on a grain scale influence the bulk behavior of many grains. The dependence of the macroscopic behavior on microscopic features is highlighted within this work especially for the friction coefficient and the porosity.

(1) Here, the influence of the dimensionality is described in Chapter 2. The material behavior for both dimensional approaches showed elasto-plastic behavior with pronounced strain hardening and softening. Further, the 3D environment directly affected the deformation behavior and the microfabric while raising the peak friction coefficient and porosity. Within identical particle sizes and distribution, different relations of the particle neighborhood led to different microfabrics, and hence, to variation in the particle interlocking. A consequence of the dimensionality was also found regarding the porosity, as the additional degree of freedom ensures that more space is available for the 3D particle arrangement.

The factor of dimensionality also influenced the localization of the failure plane. A minor dimensionality developed failure planes at the fixed wall and a rigid block was moved above the failure plane, which is initiated by the moving boundary wall. For the three-dimensional approach, the particle interlocking of the sample led to a failure plane development almost at the movable sheared wall. Depending on the localization, the failure zone thickness varies. While the thickness is lower if it is formed close to the moving wall, a broader failure zone developed in the case of the two-dimensional failure plane, which occurred close to the fixed wall.

(2) The modification of the grain shape easily showed how important this geometrical feature is. In Chapter 3, it was demonstrated that the influence of the grain shape changes with respect to the frictional strength. Thereby, the elongated shapes (rod-like and plate-like) evolve to have a larger frictional strength than the standard ideal spherical particles.

A reason for this is the changes in the microfabric caused by the elongation of the particle shapes. This is also reflected by the grain contact configurations. The numerical approach allowed for the determination of the grain-to-grain contact properties. The frequency of the contact sizes is equal to a power law for rod-like and plate-like shapes. This similarity in the contact microfabric regarding the similar friction coefficient is additionally supported by the observation that the predominant types of contacts of rod-like and plate-like shapes are the point contacts that also define the frictional behavior of the ideal spherical particles. In addition, larger contact types of edge contacts and face contacts for plate-like shapes

occurred at a lower frequency. However, this change in the microfabric also changes the frictional strength. The low number of edge and face contacts reflect the high potential of the microfabric to change towards a uniformly aligned and parallel oriented arrangement with appropriate differing frictional responses. Unfortunately, that kind of contact analysis is not verifiable in laboratory experiments.

(3) Besides the contact configuration, the changes in the microfabric caused by the grain shape also affected the development of the pore volume. The Chapter 4 described in more detail the effect of grain shape on the pore volume evolution during the shear process. The study showed inversely proportional behavior regarding frictional strength and the pore volume. Thereby, the frictional strength increases simultaneously to a pore volume decrease. The alignment of particles during shear, which is responsible for the volume reduction and causes the breakdown of the microfabric, led to an increase in frictional strength.

The detailed observation of local pore volume changes within the sheared sample allowed for the investigation of pore spaces in high resolution during the shear process. This analyzing method also allows for visualizing of the local pore spaces and is, therefore, suitable for the visualization of the microfabric. A local reduction in pore volume can be associated with an increase in a potential pore pressure for saturated sediments or fault gouges. At the beginning of the shear process the sample is dominated by a reduction in the pore volume, which conforms to an increase in the pore pressure. After a failure plane evolved, changes in the pore volume only occurred above the shear zone. That means that the development of the shear zone changed the internal microfabric and affected the changes in the frictional behavior and the pore volume development.

### 5.1.2 Perspectives

Research in the future should focus more on the variability of the microfabrics in all its facets. Stronger flocculated particle domains intrinsically may have a higher potential of volume strain if the particle microstructure breaks down. Such consequences also affect the frictional behavior of the material. For this, it is necessary to use the method used in this study to determine the contacts and contact types of arbitrary shaped particles to describe microfabric changes and apply this to the frictional material behavior. This would allow for more accurate numerical descriptions of the granular behavior of, e.g., marine clays, ashes, or biological material in sediments. Moreover, the implementation of different grain shapes in a ring shear device would improve the investigations with regard to large strain rates. Especially for clayey material large strain behavior is important.

Further, it is preferable to implement some kind of fluid dynamics into an existing 3D numerical ring shear environment, such as that used in this study. This would allow for the investigation of pore pressures that is essentially required for stability analysis of marine sediments and can significantly contribute to slope stability analysis.

Additionally, the insights of the micromechanics and microstructure should be used to design a macroscopic numerical model to investigate the macroscopic dynamics, such as that of landslides, which may help to assess landslide behavior and the investigation of potential trigger-mechanisms.

## References

- Abe, S., and K. Mair (2005), Grain fracture in 3D numerical simulations of granular shear, *Geophysical Research Letters*, 32(L05305), 1-4.
- Abe, S., and K. Mair (2009), Effects of gouge fragment shape on fault friction: New 3D modelling results, *Geophysical Research Letters*, 36(L23302), 1-4.
- Abe, S., J. H. Dieterich, P. Mora, and D. Place (2002), Simulation of the Influence of Rate- and State-dependent Friction on the Macroscopic Behaviour of Complex Fault Zones with the Lattice Solid Model, *Pure and Applied Geophysics*, 159(9), 1967 - 1983.
- Aharonov, E., and D. Sparks (1999), Rigidity Phase Transition in Granular Packings, *Physical Review E*, 60(6), 6890-6896.
- Aharonov, E., and D. Sparks (2002), Shear profiles and localization of granular materials, *Physical Review E*, 65(051302), 1 - 12.
- Alyassin, A. M., J. L. Lancaster, J. H. Downs Iii, and P. T. Fox (1994), Evaluation of new algorithms for the interactive measurement of surface area and volume, *Medical Physics*, 21(6), 741-752.
- Amontons, G. (1699), Mémoires de l'Académie Royale A, 257-282.
- Andrade, J. E., C. F. Avila, S. A. Hall, N. Lenoir, and G. Viggiani (2011), Multiscale modeling and characterization of granular matter: From grain kinematics to continuum mechanics, *Journal of the Mechanics and Physics of Solids*, 59(2), 237-250.
- Anthony, J. L., and C. Marone (2005), Influence of particle characteristics on granular friction, *Journal of Geophysical Research*, 110(B08409), doi:10.1029/2004JB003399.
- Ask, M. V. S., and A. Kopf (2004), Constraints on the state of in situ effective stress and the mechanical behaviour of ODP Leg 186 claystones in the Japan Trench forearc, *The Island Arc*, 13(1), 242-257.
- Atkinson, J. (2007), *The mechanics of soils and foundations*, Taylor & Francis, London, [Angleterre].
- Ausloos, M., R. Lambiotte, K. Trojan, Z. Koza, and M. Pe, kala (2005), Granular matter: A wonderful world of clusters in far-from-equilibrium systems, *Physica A: Statistical Mechanics and its Applications*, 357(2), 337-349.
- Aylmore, L. A. G., and J. P. Quirk (1960), Domain or Turbostratic Structure of Clays, *Nature*, 187(4742), 1046-1048.
- Bardet, J. P., and J. Proubet (1991), A numerical investigation of the structure of persistent shear bands in granular media, *Geotechnique*, 41(4), 599-613.
- Beeler, N. M., T. E. Tullis, M. L. Blanpied, and J. D. Weeks (1996), Frictional behaviour of large displacement experimental faults, *Journal of Geophysical Research*, 101(B4), 8697-8715.
- Belheine, N., J. P. Plassiard, F. V. Donzé, F. Darve, and A. Seridi (2009), Numerical simulation of drained triaxial test using 3D discrete element modeling, *Computers and Geotechnics*, 36(1-2), 320-331.
- Bennett, W. R. Bryant, and G. H. Keller (1981), Clay fabric of selected submarine sediments; fundamental properties and models, *Journal of Sedimentary Research* 51(1), 217-232.
- Bennett, N. R. O'Brien, and M. H. Hulbert (1991a), Determinants of Clay and Shale Microfabric Signatures: Processes and Mechanisms, in *Microstructure of Fine-Grained Sediments*, edited by R. H. Bennett, Bryant, W. R., Hulbert, M. H., p. 582, Springer-Verlag, New York.
- Bennett, W. R. Bryant, and M. H. Hulbert (Eds.) (1991b), *Microstructure of Fine-Grained Sediments*, 582 pp., Springer-Verlag, New York.
- Biegel, R. L., C. G. Sammis, and J. H. Dieterich (1989), The frictional properties of a simulated fault gouge having a fractal particle size distribution, *Journal of Structural Geology*, 11(7), 827 - 846.
- Bos, B., C. J. Peach, and C. J. Spiers (2000), Frictional-viscous flow of simulated fault gouge caused by the combined effects of phyllosilicates and pressure solution, *Tectonophysics*, 327(3-4), 173-194.
- Bryn, P. (2005), Explaining the Storegga Slide, *Marine and Petroleum Geology*, 22, 11-19.
- Byerlee, J. D. (1978), Friction of Rocks, *Pure and Applied Geophysics*, 116, 615 - 625.
- Campbell, C. S. (1990), Rapid Granular Flows, *Annual Review of Fluid Mechanics*, 22, 57-90.

- Canals, M., et al. (2004), Slope failure dynamics and impacts from seafloor and shallow sub-seafloor geophysical data: case studies from the COSTA project, *Marine Geology*, 213(1-4), 9-72.
- Collins, K., and A. McGown (1974), The form and function of microfabric features in a variety of natural soils, *Geotechnique*, 24, 223-254.
- Cundall, P. A., and O. D. L. Strack (1978), BALL - A program to model granular media using the distinct element method, in *Technical Note, Advanced Technology Group*, edited, Dames and Moore, London.
- Cundall, P. A., and O. D. L. Strack (1979), A discrete numerical model for granular assemblies, *Géotechnique*, 29(1), 47-65.
- de Gennes, P. G. (1999), Granular matter: a tentative view, *Reviews of Modern Physics*, 71(2), S374-S382.
- Engelhardt, W., and K. H. Gaida (1963), Concentration changes of pore solutions during compaction of clay sediments, *Journal of Sedimentary Research* 33(4), 919-930.
- Farrow, G. E., J. P. M. Syvitski, and V. Tunnicliffe (1983), Suspended Particulate Loading on the Macrobenthos in a Highly Turbid Fjord: Knigh Inlet, British Columbia, *Canadian Journal of Fishing and aquatic science*, 40(1), 273-288.
- Fawad, M., N. H. Mondol, J. Jahren, and K. Bjørlykke (2010), Microfabric and rock properties of experimentally compressed silt-clay mixtures, *Marine and Petroleum Geology*, 27(8), 1698-1712.
- Fine, I. V., A. B. Rabinovich, B. D. Bornhold, R. E. Thomson, and E. A. Kulikov (2005), The Grand Banks landslide-generated tsunami of November 18, 1929: preliminary analysis and numerical modeling, *Marine Geology*, 215(1-2), 45-57.
- Forterre, Y., and O. Pouliquen (2008), Flows of Dense Granular Media, *Annual Review of Fluid Mechanics*, 40(1), 1-24.
- Frye, K. M., and C. Marone (2002), The effect of particle dimensionality on granular friction in laboratory shear zones, *Geophysical Research Letters*, 29(19), 1916-1919.
- Füchtbauer, H. (Ed.) (1988), *Sedimente- und Sedimentgesteine*, 1141 pp., E.Schweizbart'sche Verlagsbuchhandlung, Stuttgart.
- Gao, J., D. Luedtke, D. Gourdon, M. Ruths, J. Israelachvilli, and U. Landman (2004), Frictional Forces and Amontons' Law: From the Molecular to the Macroscopic Scale, *Journal of Physical Chemistry B*, 108, 3410 - 3425.
- Goren, L., E. Aharonov, D. Sparks, and R. Toussaint (2010), Pore Pressure Evolution in Deforming Granular Material: A General Formulation and the Infinitely Stiff Approximation, *Journal of Geophysical Research*, 115.
- Graton, L. C., and Fraser (1935), Systematic packing of spheres - with particular relation to porosity and permeability, *Journal of geology*, XLIII(8), 785-909.
- Guo, Y., and J. K. Morgan (2004), Influence of normal stress and grain shape on granular friction: Results of discrete element simulations, *Journal of Geophysical Research*, 109(B12305), 1-16.
- Guo, Y., and J. K. Morgan (2007), Fault gouge evolution and its dependence on normal stress and rock strength - results of discrete element simulations: Gouge zone properties, *Journal Of Geophysical Research*, 112(B10403), 1-17.
- Haflidason, H., H. P. Sejrup, A. Nygard, J. Mienert, P. Bryn, R. Lien, C. F. Forsberg, K. Berg, and D. Masson (2004), The Storegga Slide: architecture, geometry and slide development, *Marine Geology*, 213(1-4), 201-234.
- Hampton, H. J. Lee, and J. Locat (1996), Submarine landslides, *Reviews of Geophysics*, 34(1), 33-59.
- Hampton, A. H. Bouma, P. R. Carlson, B. F. Molnia, E. C. Clukey, and D. A. Sangrey (1978), Quantitative study of slope instability in the Gulf of Alaska., paper presented at Offshore Technology Conference.
- Handin, J. (1969), On the Coulomb-Mohr failure criterion, *Journal of Geophysical Research*, 74(22), 5343-5348.
- Härtl, J., and J. Y. Ooi (2011), Numerical investigation of particle shape and particle friction on limiting bulk friction in direct shear tests and comparison with experiments, *Powder Technology*, 212(1), 231-239.
- Hazzard, J. F., and K. Mair (2003), The importance of the third dimension in granular shear, *Geophysical Research Letters*, 30(13), 1708-1711.

- Herrmann, H. J. (2002), Granular matter, *Physica A: Statistical Mechanics and its Applications*, 313(1-2), 188-210.
- Heyman, J. (1972), *Coulomb's memoir on statics: An essay in the history of civil engineering.*, University Press, Cambridge [Eng.].
- Huhn, K., I. Kock, and A. Kopf (2006), Comparative numerical and analogue shear box experiments and their implications for the mechanics along the failure plane of landslides, *Norwegian Journal of Geology*, 86(3), 209-220.
- Itasca (2004), PFC 2D 3.1 Manual, edited, Itasca Consulting Group, Inc., Minneapolis.
- Itasca (2005), PFC 3D 3.1 Manual, edited, Itasca Consulting Group, Inc., Minneapolis.
- Itasca (2011), PFC 3D 4.0 Manual, edited, Itasca Consulting Group, Inc., Minneapolis.
- Iverson, N. R., J. E. Mann, and R. M. Iverson (2010), Effects of soil aggregates on debris-flow mobilization: Results from ring-shear experiments, *Engineering Geology*, 114(1-2), 84-92.
- Iwashita, and Oda (1998), Rolling Resistance at Contacts in Simulation of Shear Band Development by DEM, *Journal of Engineering Mechanics*, 124(3), 285-292.
- Jaeger, H. M., and S. R. Nagel (1992), Physics of the Granular State, *Science*, 255(5051), 1523-1531.
- Jaeger, H. M., S. R. Nagel, and R. P. Behringer (1996), Granular solids, liquids and gases, *Reviews of Modern Physics*, 68(4), 1259-1273.
- Jensen, R. P., P. J. Bosscher, M. E. Plesha, and T. B. Edil (1999), DEM Simulation of granular media - structure interface: effects of surface roughness and particle shape, *International Journal for Numerical and Analytical Methods in Geomechanics*, 23(6), 531-547.
- Kock, I., and K. Huhn (2007a), Numerical investigation of localization and micromechanics in a stratified soil specimen, *Journal of Structural Geology*, 29(10), 1679 - 1694.
- Kock, I., and K. Huhn (2007b), Influence of particle shape on the frictional strength of sediments - A numerical case study, *Sedimentary Geology*, 196(1-4), 217-233.
- Kopf, A., and K. M. Brown (2003), Friction experiments on saturated sediments and their implications for the stress state of the Nankai and Barbados subduction thrusts, *Marine Geology*, 202(3-4), 193-210.
- Krantz, R. W. (1991), Measurements of friction coefficients and cohesion for faulting and fault reactivation in laboratory models using sand and sand mixtures, *Tectonophysics*, 188(1-2), 203-207.
- Krumbein, W. C. (1941), Measurement and geological significance of shape and roundness of sedimentary particles, *Journal of Sedimentary Research*, 11(2), 64-72.
- Kuhn, M. R. (2010), Micro-mechanics of fabric and failure in granular materials, *Mechanics of Materials*, 42(9), 827-840.
- Kvalstad, T. J., L. Andresen, C. F. Forsberg, K. Berg, P. Bryn, and M. Wangen (2005), The Storegga slide: evaluation of triggering sources and slide mechanics, *Marine and Petroleum Geology*
- Ormen Lange - an integrated study for the safe development of a deep-water gas field within the Storegga Slide Complex, NE Atlantic continental margin*, 22(1-2), 245-256.
- Laberg, J. S., and T. O. Vorren (2000), The Traenadjupet Slide, offshore Norway - morphology, evacuation and triggering mechanisms, *Marine Geology*, 171(1-4), 95-114.
- Lafeber, D. (1966), Soil structural concepts, *Engineering Geology*, 1(4), 261-290.
- Lambe, and R. V. Whitman (1969), *Soil mechanics*, edited, Wiley, New York.
- Leeder, M. (1999), *Sedimentology and Sedimentary Basins - From turbulence to tectonics*, 608 pp., Blackwell Publishing, Oxford.
- Lin, X., and T.-T. Ng (1997), A three-dimensional discrete element model using arrays of ellipsoids, *Géotechnique*, 47(No. 2), 319-329.
- Locat, J., and H. J. Lee (2002), Submarine landslides: advances and challenges, *Canadian Geotechnical Journal*, 39(1), 193-212.
- Lockner, D. A., and N. M. Beeler (2002), Rock failure and Earthquakes, in *International handbook of earthquake and engineering seismology*, edited by W. Lee, Kanamori, H., Jennings, P., Kisslinger, C., p. 1200, Elsevier.
- Logan, J. M., and K. A. Rauenzahn (1987), Frictional dependence of gouge mixtures of quartz and montmorillonite on velocity, composition, and fabric, *Tectonophysics*, 144(1-3), 87-108.

- Lohrmann, J., N. Kukowski, J. Adam, and O. Oncken (2003), The impact of analogue material properties on the geometry, kinematics, and dynamics of convergent sand wedges, *Journal of Structural Geology*, 25(10), 1691-1711.
- Lupini, J. F., A. E. Skinner, and P. R. Vaughan (1981), The drained residual strength of cohesive soils, *Geotechnique*, 31(2), 181-213.
- Mahmood, A., and J. K. Mitchell (1974), Fabric property relationships in fine granular materials, *Clays and Clay Minerals*, 22, 397-408.
- Mair, K., and C. Marone (1999), Friction of simulated fault gouge for a wide range of velocities and normal stresses, *J. Geophys. Res.*, 104(B12), 28899-28914.
- Mair, K., and J. F. Hazzard (2007), Nature of stress accommodation in sheared granular material: Insights from 3D numerical modeling, *Earth and Planetary Science Letters*, 259(3-4), 469-485.
- Mair, K., and S. Abe (2008), 3D numerical simulation of fault gouge evolution during shear: Grain size reduction and strain localization, *Earth and Planetary Science Letters*, 274(1-2), 72-81.
- Mair, K., and S. Abe (2011), Breaking Up: Comminution Mechanisms in Sheared Simulated Fault Gouge, *Pure and Applied Geophysics*, 1-12.
- Mair, K., K. M. Frye, and C. Marone (2002), Influence of grain characteristics on the friction of granular shear zones, *Journal of Geophysical Research*, 107(B10), 2219-2227.
- Mandl, G. (1988), *Mechanics of Tectonic Faulting: Models and Basic Concepts*, Elsevier, Amsterdam.
- Marone, C. (1998), Laboratory-derived friction laws and their application to seismic faulting, *Annual Review of Earth and Planetary Sciences*, 26, 643-696.
- Marone, C., and C. H. Scholz (1989), Particle-size distribution and microstructures within simulated fault gouge, *Journal of Structural Geology*, 11(7), 799-814.
- Masson, M. Canals, B. Alonso, R. Urgeles, and V. Huhnerbach (1998), The Canary Debris Flow: source area morphology and failure mechanisms, *Sedimentology*, 45(2), 411-432.
- Masson, C. B. Harbitz, R. B. Wynn, G. Pedersen, and F. Løvholt (2006), Submarine landslides: processes, triggers and hazard prediction, *Philosophical Transactions of the Royal Society A: Mathematical, Physical and Engineering Sciences*, 364(1845), 2009-2039.
- McAdoo, B. G., L. F. Pratson, and D. L. Orange (2000), Submarine landslide geomorphology, US continental slope, *Marine Geology*, 169(1-2), 103-136.
- McAdoo, B. G., M. K. Capone, and J. Minder (2004), Seafloor geomorphology of convergent margins: Implications for Cascadia seismic hazard, *Tectonics*, 23(6).
- Mienert (2005), Ocean warming and gas hydrate stability on the mid-Norwegian margin at the Storegga Slide, *Marine and Petroleum Geology*, 22, 233-244.
- Mienert, M. Vanneste, H. Haflidason, and S. Bünz (2010), Norwegian margin outer shelf cracking: a consequence of climate-induced gas hydrate dissociation?, *International Journal of Earth Sciences*, 99(1), 207-225.
- Mitchell, J. K. (1976), *Fundamentals of Soil Behavior*.
- Mitchell, J. K., and K. Soga (2005), *Fundamentals of Soil Behaviour*, 3rd ed., 577 pp., John Wiley & Sons, Hoboken, New Jersey.
- Moon, C. F. (1972), The microstructure of clay sediments, *Earth-Science Reviews*, 8(3), 303-321.
- Moon, C. F., and C. W. Hurst (1984), Fabric of muds and shales: an overview, *Geological Society, London, Special Publications*, 15(1), 579-593.
- Moore, W. R. Normark, and R. T. Holcomb (1994), Giant Hawaiian Landslides, *Annual Review of Earth and Planetary Sciences*, 22(1), 119-144.
- Moore, D. E., and D. A. Lockner (2007), Friction of the Smectite Clay Montmorillonite, in *The Seismogenic Zone of Subduction thrust Faults*, edited by C. M. T. Dixon, pp. 317-345, Columbia University Press.
- Mora, P., and D. Place (1999), The Weakness of Earthquake Faults, *Geophysical Research Letters*, 26.
- Morgan, J. K. (1999), Numerical simulations of granular shear zones using the distinct element method 2. Effects of particle size distribution and interparticle friction on mechanical behavior *Journal of Geophysical Research*, 104(B2), 2721-2732.
- Morgan, J. K., and M. S. Boettcher (1999), Numerical simulations of granular shear zones using the distinct element method 1. Shear zone kinematics and the micromechanics of localization *Journal of Geophysical Research*, 104(B2), 2703-2719.

- Morgenstern (1967), Submarine slumping and the initiation of turbidity currents, in *Marine Geotechnique UP*, edited by A. F. Richards, pp. 189-220, Urbana, IL.
- Morgenstern, and J. S. Tchalenko (1967), The Optical Determination of Preferred Orientation in Clays and Its Application to the Study of Microstructure in Consolidated Kaolin. II, *Proceedings of the Royal Society of London. Series A. Mathematical and Physical Sciences*, 300(1461), 235-250.
- Morrow, C. A., B. Radney, and J. Byerlee (1992), Frictional Strength and the Effective Pressure Law of Montmorillonite and Illite Clays, in *Fault mechanics and transport properties of rocks; a festschrift in honor of W. F. Brace*, edited by B. a. W. Evans, T., p. 524, Academic Press, San Diego.
- Morrow, C. A., D. E. Moore, and D. A. Lockner (2000), The effect of mineral bond strength and adsorbed water on fault gouge frictional strength, *Geophysical Research Letters*, 27(6), 815-818.
- Nicot, F., F. Darve, R. G. N. Hazards, and S. Vulnerability of (2005), A multi-scale approach to granular materials, *Mechanics of Materials*, 37(9), 980-1006.
- Oakley, D. M., and B.-R. Jennings (1982), Clay Particle Sizing by Electrically-Induced Birefringence, *Clay Minerals*, 17, 313-325.
- Oda, M. (1972), Initial fabrics and their relations to mechanical properties of granular materials, *Soils and Foundation*, 1(12), 17-36.
- Oda, M., and K. Iwashita (2000), Study on couple stress and shear band development in granular media based on numerical simulation analyses, *International Journal of Engineering Science*, 38(15), 1713-1740.
- Oda, M., H. Kazama, and J. Konishi (1998), Effects of induced anisotropy on the development of shear bands in granular materials, *Mechanics of Materials*, 28(1-4), 103-111.
- Olsen, H. W. (1960), Hydraulic Flow Through Saturated Clays, *Clays and Clay Minerals*, 9(1), 131-161.
- Panayiotopoulos, K. P. (1989), Packing of sands—A review, *Soil and Tillage Research*, 13(2), 101-121.
- Place, D., and P. Mora (2000), Numerical Simulation of Localization Phenomena in a Fault Zone, *Pure and Applied Geophysics*, 157, 1821 - 1845.
- Pohlman, N. A., B. L. Severson, J. M. Ottino, and R. M. Lueptow (2006), Surface roughness effects in granular matter: Influence on angle of repose and the absence of segregation, *Physical Review E*, 73(3), 031304.
- Pöschel, T. (2000), *Dynamik granularer systeme : Theorie, Experimente und numerische Experimente*, Logos Verlag, Berlin.
- Potyondy, D. O., and P. A. Cundall (2004), A bonded-particle model for rock, *International Journal of Rock Mechanics & Mining Sciences*, 41, 1329-1364.
- Pouliquen, O., and F. Chevoir (2002), Dense flows of dry granular material, *Comptes Rendus Physique*, 3(2), 163-175.
- Powers, M. C. (1953), A new roundness scale for sedimentary particles, *Journal of Sediment. Petrology*, 23(2), 117-119.
- Rechenmacher, A. L. (2006), Grain-scale processes governing shear band initiation and evolution in sands, *Journal of the Mechanics and Physics of Solids*, 54(1), 22-45.
- Rietema, K. (1991), *The Dynamics of Fine Powders*, edited, Springer Netherlands, Dordrecht.
- Ristow, G. H. (2000), *Pattern formation in granular materials*, Springer, Berlin [etc.].
- Roux, J.-N., and G. Combe (2002), Quasistatic rheology and the origins of strain, *Comptes Rendus Physique*, 3(2), 131-140.
- Sadrekarami, A., and S. M. Olson (2010), Shear Band Formation Observed in Ring Shear Tests on Sandy Soils, *Journal of Geotechnical and Geoenvironmental Engineering*, 136(2), 366-375.
- Saffer, D. M., and C. Marone (2003), Comparison of smectite- and illite-rich gouge frictional properties: application to the updip limit of the seismogenic zone along subduction megathrusts, *Earth and Planetary Science Letters*, 215(1-2), 219-235.



- Saffer, D. M., K. M. Frye, C. Marone, and K. Mair (2001), Laboratory results indicating complex and potentially unstable frictional behavior of smectite clay, *Geophysical Research Letters*, 28(12), 2297-2300.
- Saltzer, S. D., and D. D. Pollard (1992), Distinct element modeling of structures formed in sedimentary overburden by extensional reactivation of basement normal faults, *Tectonics*, 11(1), 165-174.
- Schöpfer, M. P. J., S. Abe, C. Childs, and J. J. Walsh (2009), The impact of porosity and crack density on the elasticity, strength and friction of cohesive granular materials: Insights from DEM modelling, *International Journal of Rock Mechanics and Mining Sciences*, 46(2), 250-261.
- Schroeder, W., K. Martin, and B. Lorensen (2004), *The Visualization Toolkit, Third Edition*, {Kitware Inc.}.
- Schulze, D. (2009), *Pulver und Schüttgüter : Fliesseigenschaften und Handhabung*, Springer, Berlin; Heidelberg.
- Sloane, R. L., and T. R. Kell (1966), The Fabric of Mechanically Compacted Kaolin, *Clays and Clay Minerals*, 14, 289-296.
- Smalley, I. J., and J. G. Cabrera (1969), Particle Association in Compacted Kaolinite, *Nature*, 222(5188), 80-81.
- Smith, G. N. S. I. G. N. (1998), *Elements of soil mechanics*, Blackwell Science, Oxford; Malden, MA.
- Spencer, D. W. (1963), The Interpretation of grain size distribution curves of clastic sediments, *Journal of Sedimentary Petrology*, 33(1), 11.
- Strozyk (2009), Submarine landslides in active margin environments - Slope stability vs. neotectonic activity on the northeastern margin of Crete, eastern Mediterranean, PhD thesis, 138 pp, University of Bremen, Bremen.
- Strozyk, K. Huhn, M. Strasser, S. Krastel, I. Kock, and A. Kopf (2009), New evidence for massive gravitational mass-transport deposits in the southern Cretan Sea, eastern Mediterranean, *Marine Geology*, 263(1-4), 97-107.
- Sultan, N., P. Cochonat, M. Canals, A. Cattaneo, B. Dennielou, H. Haflidason, J. S. Laberg, D. Long, J. Mienert, and F. Trincardi (2004), Triggering mechanisms of slope instability processes and sediment failures on continental margins: a geotechnical approach, *Marine Geology*, 213(1-4), 291-321.
- Sun, Q., G. Wang, and K. Hu (2009), Some open problems in granular matter mechanics, *Progress in Natural Science*, 19(5), 523-529.
- Szarf, K., G. Combe, and P. Villard (2011), Polygons vs. clumps of discs: A numerical study of the influence of grain shape on the mechanical behaviour of granular materials, *Powder Technology*, 208(2), 279-288.
- Tchalenko, J. S. (1970), Similarities between Shear Zones of Different Magnitudes, *Geological Society of America Bulletin*, 81(6), 1625-1640.
- Terzaghi, K. (1925), *Erdbaumechanik*, 339 pp., Deuticke, Wien.
- Tessier, D., A. Lajudie, and J. C. Petit (1992), Relation between the macroscopic behavior of clays and their microstructural properties, *Applied Geochemistry*, 7, Supplement 1(0), 151-161.
- Thornton, C. (2000), Numerical simulation of deviatoric shear deformation of granular media, *Geotechnique*, 50(1), 43-53.
- Ting, J. M., M. Khwaja, L. R. Meachum, and J. D. Rowell (1993), An ellipse-based discrete element model for granular materials, *INTERNATIONAL JOURNAL FOR NUMERICAL AND ANALYTICAL METHODS IN GEOMECHANICS*, 17(9), 603-623.
- Trincardi, F., A. Cattaneo, A. Correggiari, and D. Ridente (2004), Evidence of soft sediment deformation, fluid escape, sediment failure and regional weak layers within the late Quaternary mud deposits of the Adriatic Sea, *Marine Geology*, 213(1-4), 91-119.
- Tucker, M. E. (1981), *Sedimentary Petrology*, 252 pp., Blackwell Scientific Publications, Oxford.
- Tucker, M. E. (1991), *Sedimentary Petrology An Introduction to the Origin of Sedimentary Rocks*, Blackwell Science, Oxford.
- Urgeles, R., M. Canals, and J. Roberts (1999), Fluid flow from pore pressure measurements off La Palma, Canary Islands, *Journal of Volcanology and Geothermal Research*, 94(1-4), 305-321.
- Urgeles, R., M. Canals, J. Baraza, B. Alonso, and D. Masson (1997), The most recent megalandslides of the Canary Islands: El Golfo debris avalanche and Canary debris flow, west El Hierro island, *Journal of Geophysical Research-Solid Earth*, 102(B9), 20305-20323.

- van Olphen, H. (1977), *An introduction to clay colloid chemistry for clay technologists, geologists, and soil scientists*, Wiley, New York [u.a.].
- Vardoulakis, I. (1980), Shear band inclination and shear modulus of sand in biaxial tests, *International Journal for Numerical and Analytical Methods in Geomechanics*, 4(2), 103-119.
- Vardoulakis, I., M. Goldscheider, and G. Gudehus (1978), Formation of shear bands in sand bodies as a bifurcation problem, *International Journal for Numerical and Analytical Methods in Geomechanics*, 2(2), 99-128.
- Watts, A. B., and D. G. Masson (1995), A giant landslide on the north flank of Tenerife, Canary Islands, *Journal of Geophysical Research, B, Solid Earth and Planets*, 100(12), 24,487-424,498.
- Wen, B. P., and A. Aydin (2003), Microstructural study of a natural slip zone: quantification and deformation history, *Engineering Geology*, 68(3-4), 289-317.
- Wessel, P., and W. H. F. Smith (1991), Free software helps map and display data, *EOS Trans. AGU*, 72, 441.
- Yan, W. M. (2009), Fabric evolution in a numerical direct shear test, *Computers and Geotechnics*, 36(4), 597-603.

## Danksagung

Die letzten vier Jahre waren für mich überaus lehrreich, interessant und zugleich herausfordernd. Dabei wurde ich stets von einer Vielzahl von Menschen unterstützt und begleitet die mich direkt und indirekt prägten.

In besonderem Maße möchte ich mich bei Prof. Dr. Katrin Huhn bedanken, die mir die Möglichkeit eröffnete wissenschaftliche Fragestellungen in Form einer Promotion am MARUM nachzugehen und mich dabei zu jeder Zeit unterstützte. Zudem ermöglichte sie es mir wichtige und prägende Erfahrungen als Expeditionsteilnehmer auf der MS Merian zu sammeln.

Bedanken möchte ich mich ebenfalls bei Prof. Dr. Tobias Mörz dafür, dass er sich des Gutachtens meiner Promotionsschrift angenommen hat.

Außerdem danke ich Dr. Steffen Abe und Dr. Ines Görz für ihre Unterstützung.

Ebenfalls bedanke ich mich bei Dr. Ingo Kock, der jederzeit für Fragen hilfreich zur Verfügung stand und mir gerade in der Anfangszeit mit seiner Arbeit und seinem Wissen eine große Hilfe war.

Des Weiteren bedanke ich mich bei Prof. Michael Strasser für hilfreiche fachliche Diskussionen und für spannende Schlagabtausche beim Tischtennis auf der Ausfahrt MSM 15/3.

Ein großer Dank geht an die Arbeitsgruppe SEDMOD mit Linda, Bryna, Lina, Gerhard, Jannis, Arzu, Franziska, Gesa, Frank, Xin, Melanie, Ella, Sarah und Nicole, die größtenteils mein Uni-Leben prägten.

Darüber hinaus danke ich wichtigen Freunden wie Miriam, Janna, Agnes und Paul mit denen ich eine sehr angenehme Zeit sowohl an der Uni als auch fern ab der Uni verbringen konnte.

In gleicher Weise möchte ich mich bei den vielen Freunden bedanken die ich beim Uni-Handball kennengelernt habe und die mir den sportlichen Ausgleich zum Uni-Alltag ermöglichten. Insbesondere danke ich Darius, Yvonne, Anke, Christine, Hasso, Frank, Gaby, Katja, Ina, dem „kleinen“ Nils, Kai, Albertina, Carola, Olan, Romina, Tatjana, Henning, Thorsten, Dimitri, Hendrik und dem „großem“ Nils.

Auch möchte ich mich bei meiner Werder-Handball-Mannschaft bedanken die auch mal ein Auge zugedrückt hat, wenn ich mal keine Zeit zum Trainieren hatte.

Ein besonderer Dank geht auch an Bianca, Bernd, Ines, Friederike, Tino, Sabine und Erich.

Und schließlich möchte ich mich bei meiner Familie bedanken die immer für mich da war und mich gerade auch in energieraubenden Zeiten immer wieder mit frischer Energie versorgte und unterstützte.





## Erklärung

Name: Lutz Torbahn

Datum: 24.09.2013

Anschrift: Am Rüten 31a, 28355, Bremen

## Erklärung

Hiermit versichere ich, dass ich

1. die Arbeit ohne unerlaubte fremde Hilfe angefertigt habe,
2. keine anderen als die von mir angegebenen Quellen und Hilfsmittel benutzt habe und
3. die den benutzten Werken wörtlich oder inhaltlich entnommen Stellen als solche kenntlich gemacht habe.

Bremen , den 24.09.2013

---

Unterschrift